MICROCOPY RESOLUTION TEST CHART

NATIONAL BUREAU OF STANDARDS-1963-A

LEVEL

INVENTORY

AD A139275

DTIC ACCESSION NUMBER
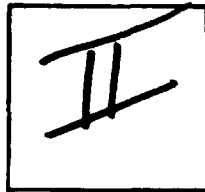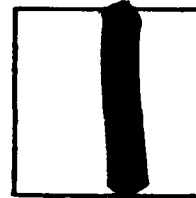
A Cerenkov-Raman Maser

Busby, Kenneth O. DOCUMENT IDENTIFICATION

Contract N00014-79-C-0760

May '80

DISTRIBUTION STATEMENT A
Approved for public release;
Distribution Unlimited

DISTRIBUTION STATEMENT

ACCESSION FOR

NTIS	GRA&I	☒
DTIC	TAB	☐
UNANNOUNCED		☐
JUSTIFICATION		

BY Per Ltr. on File

DISTRIBUTION /
AVAILABILITY CODES

DIST	AVAIL AND/OR SPECIAL
A/1	

DISTRIBUTION STAMP

DTIC
SELECTED
MAR 22 1984
D

DATE ACCESSIONED

83 10 07 065

DATE RECEIVED IN DTIC

DOCUMENT PROCESSING SHEET

DTIC FORM 70A
OCT 79

A CERENKOV-RAMAN MASER

A Thesis

Submitted to the Faculty

in partial fulfillment of the requirements for the

degree of

Doctor of Philosophy

by

Kenneth O. Busby
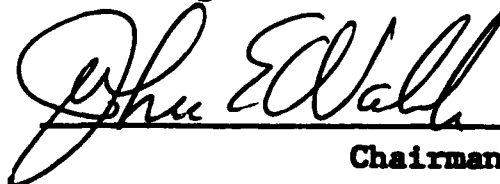
DARTMOUTH COLLEGE

Hanover, New Hampshire

May, 1980

Contract N00014-79-C-0760

Examining Committee:

_____
Chairman

Dean of Graduate Studies

ABSTRACT

The first observations of coherent microwave radiation resulting from Cerenkov-Raman backscattering have been made and are reported. An extensive experimental investigation of vacuum Raman backscattering has also been made. Theoretical models are presented to calculate the frequency and the gain at interaction for both the Raman and the Cerenkov-Raman backscattering interactions. Experimental data are compared to theoretical predictions.

ACKNOWLEDGEMENTS

TABLE OF CONTENTS

v

LIST OF TABLES

LIST OF ILLUSTRATIONS

A4 DIAGRAM OF THE ELECTRON BEAM SCALLOPS, WHICH LEAD TO CURRENT DENSITY MODULATIONS.

CHAPTER 1

INTRODUCTION

The objective of the experiment was to build a radiation source in the millimeter range that did not require the high accelerating voltages typical of devices such as the Cerenkov maser and the free electron laser. We have chosen an interaction in which the electron beam is coupled to a dielectric resonator via a rippled magnetic pump field, such that microwave radiation of a desired frequency is produced. This interaction is stimulated Raman scattering[1] in the presence of a dielectric material. We shall call this new interaction stimulated Cerenkov-Raman scattering.

The Raman interaction is depicted in figure 1.1. A single particle interaction is assumed. (E_0, P_0) and (E, P) are the electron energy and momentum before and after the scattering event, respectively. (ω_p, k_p) and (ω_s, k_s) are the frequency and wavenumber of the pump and scattered photons, respectively. We assume that the scattering event occurs within a medium of index of refraction n. Conservation of energy and momentum then requires:

$$E + \hbar \omega_p = E + \hbar \omega_s \qquad (1.1)$$
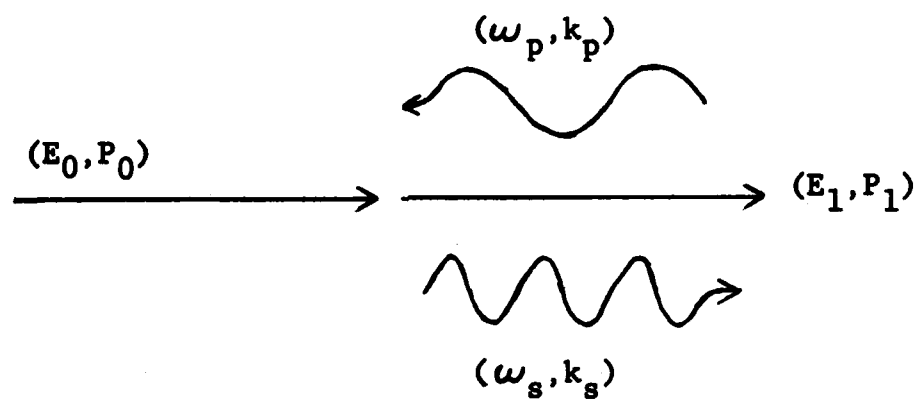
FIGURE 1.1 SINGLE PARTICLE RAMAN OR COMPTON SCATTERING

$$P_0 - \hbar k_p = P + \hbar k_s \tag{1.2}$$

Assuming that the photon energies and momentums are much smaller than the energy and momentum of the electron, and keeping only the lowest order terms, we find[2]:

$$\frac{\omega_s}{\omega_p} = \frac{1 + \beta n}{|1 - \beta n|} \tag{1.3}$$

where β is the electron velocity divided by the speed of light. As βn approaches 1, the frequency upshift becomes large. Thus, by choosing an index of refraction n large enough, it is possible to obtain a large frequency upshift with modest electron beam voltages.

The earliest work on stimulated Compton scattering was done by Kapitza and Dirac[3] in 1933. They concluded that it was barely possible to detect electrons deflected by a beam of light. The next important work was that of Ginzburg and Frank[4] who did the theory on the Doppler shifted frequencies of oscillators traveling in a medium. Ginzburg[5] noted that electron bunching would be needed to obtain large microwave powers. In 1951, Motz[6] published his calculations for the emission of microwaves when an electron beam is passed through an undulator. An undulator or wiggler is an electric or a magnetic field which forces a transverse oscillation on the electron beam. Futher theoretical work

has been done by Manheimer and Ott[7], Pantell[8], Hasegawa[9], and Colson[10].

The first practical device for the amplification of microwaves from an undulating electron beam was developed by Phillips[11]. With the development of relativistic, high current electron beams, many researchers became interested in microwave production. Many did research on Cerenkov masers and gyrotrons, and some worked on Raman masers. At present, only four other experimental groups in the United States, besides ourselves, work on Raman masers. They are the Bekefi[12] group at MIT, the Naval Research Laboratory group headed by Granatstein and Sprangle[13], the Schlesinger[14] group at Columbia, and the TRW[15] group in California. We are the only group working with dielectric loaded waveguides. Nation[16] has also made experimental contributions. The short wavelength record is held by Deacon, Elias, et al.[17], who produced 3.4 micrometer radiation with a magnetic wiggler and the electron beam of a linear accelerator.

In the following text, chapter 2 presents a kinematic theory for the prediction of the frequencies of microwave production. A derivation of the dynamic theory of the Raman and the Cerenkov-Raman interactions is given in chapter 3. Chapter 4 is a description of the experimental device, and the experimental results are compared to the theoretical predictions in chapter 5. The conclusions are made in

chapter 6.

CHAPTER 2

A KINEMATIC THEORY TO PREDICT THE FREQUENCY AT SYNCHRONISM

When a set of waves interact, the laws of energy and
momentum conservation must be satisfied. Given a wave
excitation, we can determine the allowed processes for
energy transfer from the excitation to the remaining waves.
An aim of our experiments is to identify the possibilities
which are the most attractive for the production of high
frequency radiation.

Raman or Cerenkov-Raman backscattering is a two wave
interaction resulting in a scattered wave. Thus, the the
theory must include three different waves that are coupled
to one another. The first wave is that of an electron beam
mode. The electron beam is assumed to be relativistic and
traveling parallel to a guiding longitudinal magnetic field.
The wave is imposed upon the electron beam and it can be
either a cyclotron wave or a plasma wave. Both the fast and
the slow electron beam modes need to be considered.

The pump wave is a magnetostatic wave produced by a
magnetic wiggler or an undulator. The magnetic wiggler
induces a sinusoidal ripple in the longitudinal direction of
the guiding magnetic field. From the electron beam frame of
reference, this ripple appears as an equivalent

6

electromagnetic wave.

The scattered wave is the observed microwave output. Since the interaction occurs within a waveguide, the scattered wave must have the dispersion relation of a waveguide mode.

The method for calculating the interaction frequency is to require the phase velocity of the electron beam mode and the pump wave, combined, be equal to the phase velocity of the scattered wave, as shown in figure 2.1A. Equivalently, we could require that the phase velocities of the scattered wave and the pump wave, combined, be equal to the phase velocity of the electron beam mode, as shown in figure 2.1B. Either way, the electron beam mode is coupled to the scattered microwaves via the pump wave. The point on the waveguide dispersion at which the phase velocities match up is called synchronism. The Raman interaction occurs at synchronism and the frequency at synchronism is the frequency of the scattered microwaves.

The negative energy electron beam dispersion relation is given by either

$$\omega = -\Omega + k V_0 \qquad (2.1A)$$

or

$$\omega = -\omega_{plasma} + k V_0 \qquad (2.1B)$$
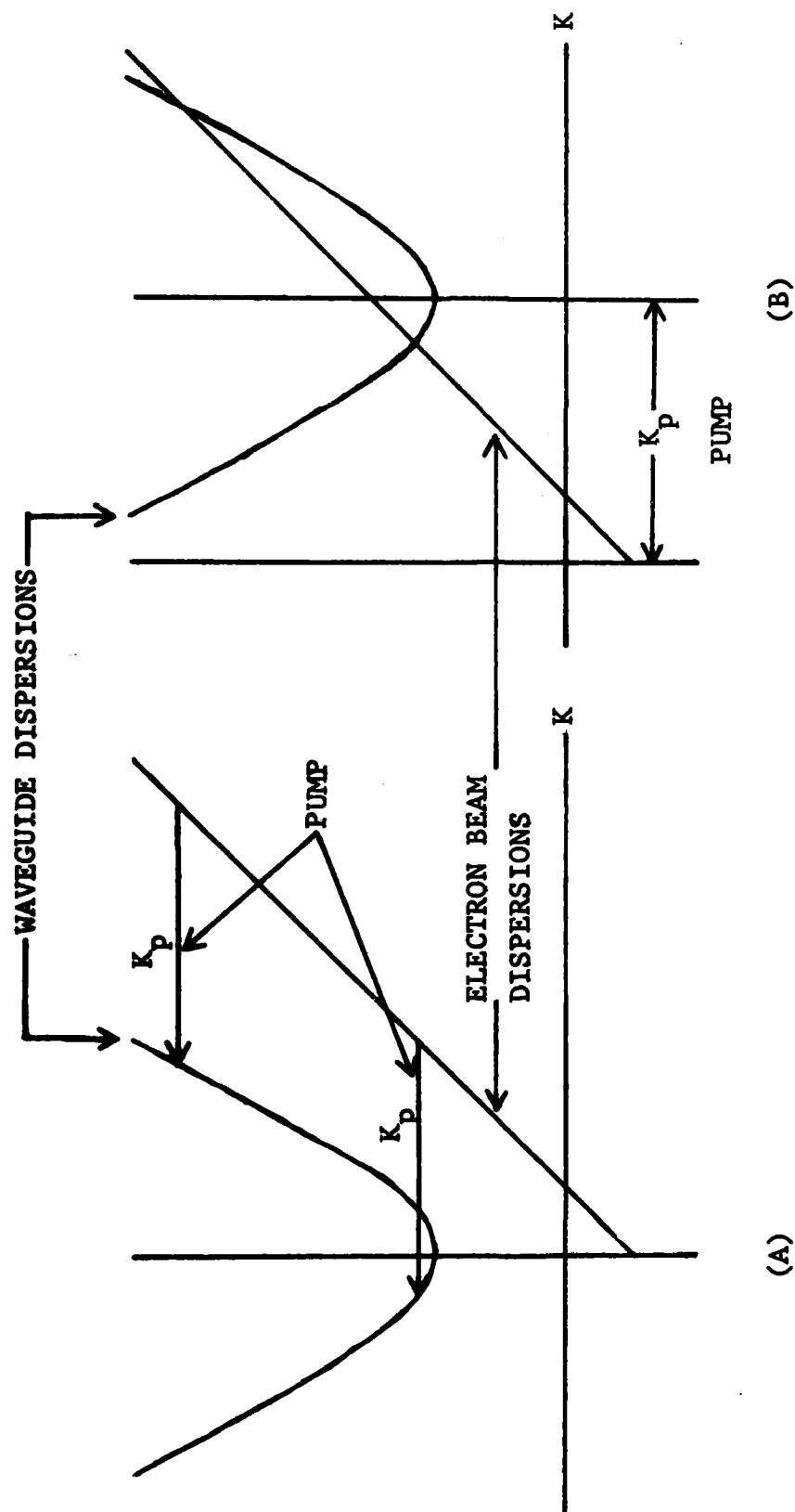
FIGURE 2.1 EQUIVALENT DISPERSION DIAGRAMS FOR THE RAMAN BACKSCATTERING INTERACTION. SYNCHRONISM OCCURS ON THE WAVEGUIDE DISPERSIONS EITHER WHERE THE PUMP DISPERSION POINTS TO, IN (A), OR WHERE THE ELECTRON BEAM DISPERSION INTERSECTS, IN (B).

where $\Omega = eB/\gamma_o mc$ is the electron beam cyclotron frequency and $\omega_{plasma} = (4\pi ne^2/\gamma_o^3 m)^{1/2}$ is the electron beam plasma frequency. γ_o is the relativistic factor $(1 - v_0^2/c^2)^{-1/2}$. v_0 is the electron velocity and c is the speed of light.

The pump wave due to the magnetic wiggler is modeled by by a wave with

$$k_p = 2\pi/\lambda_p , \quad \omega_p = 0. \tag{2.2}$$

λ_p is the wavelength of the longitudinal magnetic field ripple. Since the pump wave is at rest in the lab frame, the phase velocity, ω_p/k_p , must be equal to zero. Therefore, $k_p \neq 0$ requires that $\omega_p = 0$.

The waveguide dispersion relation is:

$$\epsilon \omega^2 = \omega_{co}^2 + k^2 c^2 \tag{2.3}$$

ω_{co} is the cutoff frequency of the unfilled waveguide, and ϵ is the dielectric constant of the medium within the waveguide. In equation (2.3), it is assumed that the waveguide is either completely filled or completely empty. If $\epsilon = 1$, then we have Raman backscattering, but if $\epsilon > 1$, then we have Cerenkov-Raman backscattering. It is apparent from either figure 2.1A or figure 2.1B, that at too low an electron beam velocity, no interaction can exist because the slope of the electron beam dispersion relation is too small.

As the electron velocity is raised higher, we reach the first point of synchronism. As the electron velocity is increased still further, the interaction splits into two frequency branches; one branch tending towards high frequency and the other branch tending towards the waveguide cutoff.

Actual computer calculations for unfilled and fully-filled waveguides are shown in figures 2.2 and 2.3. In this computer program, for a given electron beam energy and a given magnetic field for the cyclotron idler, the frequencies of interaction are calculated. The derivation of the equations is given below.

For partially filled waveguides, the waveguide dispersion is more complicated than that of equation (2.3) and is most easily solved numerically. In this case, it is advantageous to work backwards from a given (ω, k) of the waveguide dispersion relation and a given magnetic field for the cyclotron idler and then solve for the electron energy at interaction. A Scattered Wave Frequency vs. Electron Beam Voltage calculation for the partially filled case is shown in figure 2.4[18].

The calculation of the interaction frequencies for the unfilled waveguide and the fully filled waveguide is straight forward. Referring to figure 2 1B, the waveguide dispersion relation is shifted by k_p. Therefore, the waveguide dispersion relation becomes:
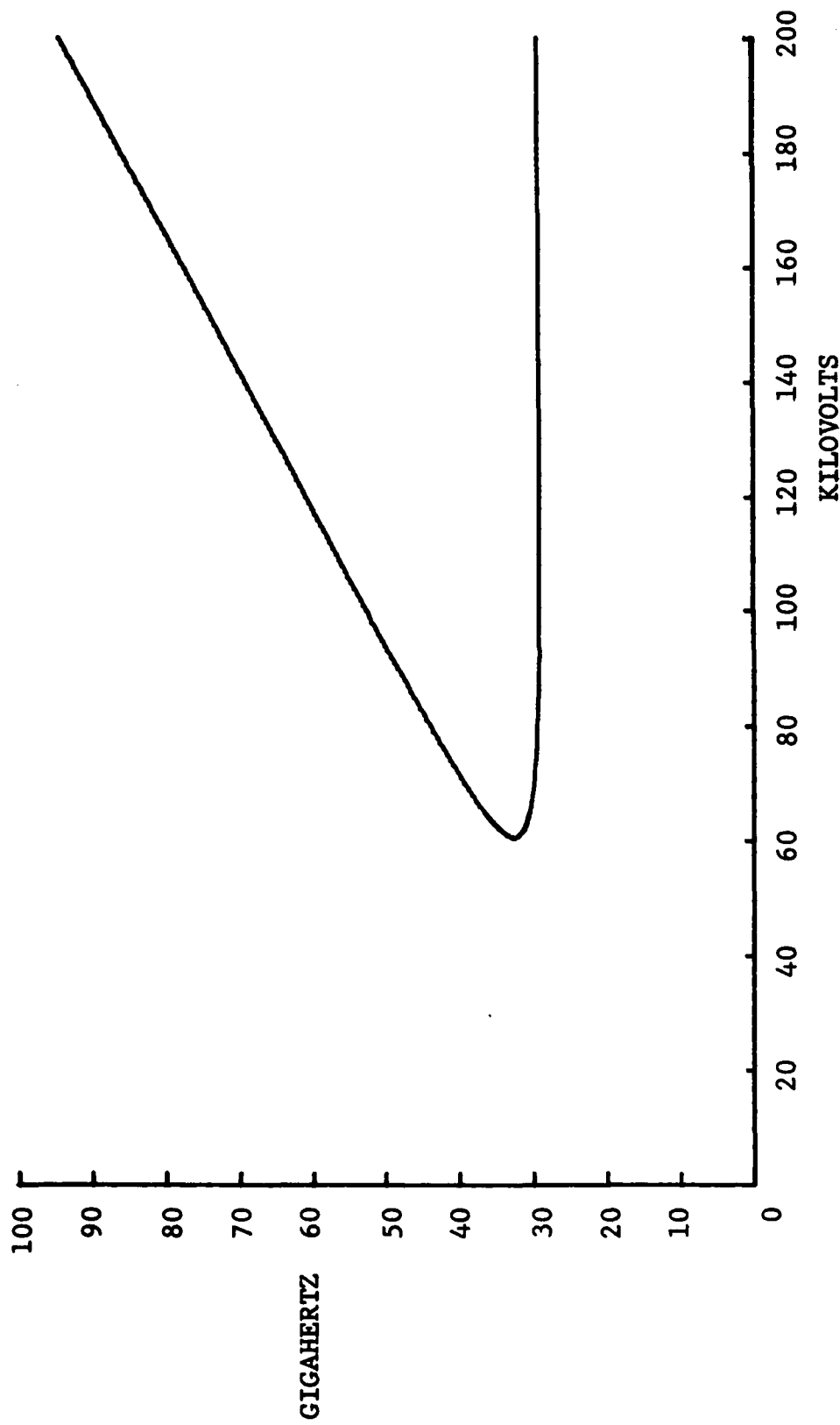
FIGURE 2.2 MICROWAVE FREQUENCY VS. ELECTRON BEAM ACCELERATING VOLTAGE FOR THE FAST ELECTRON CYCLOTRON MODE IN AN UNFILLED WAVEGUIDE. THE PUMP WAVELENGTH IS .91 CENTIMETERS, THE MAGNETIC FIELD IS 4500 GAUSS, AND THE WAVEGUIDE MODE IS TE_{01}. THE SLOW ELECTRON CYCLOTRON SOLUTION DOES NOT EXIST.
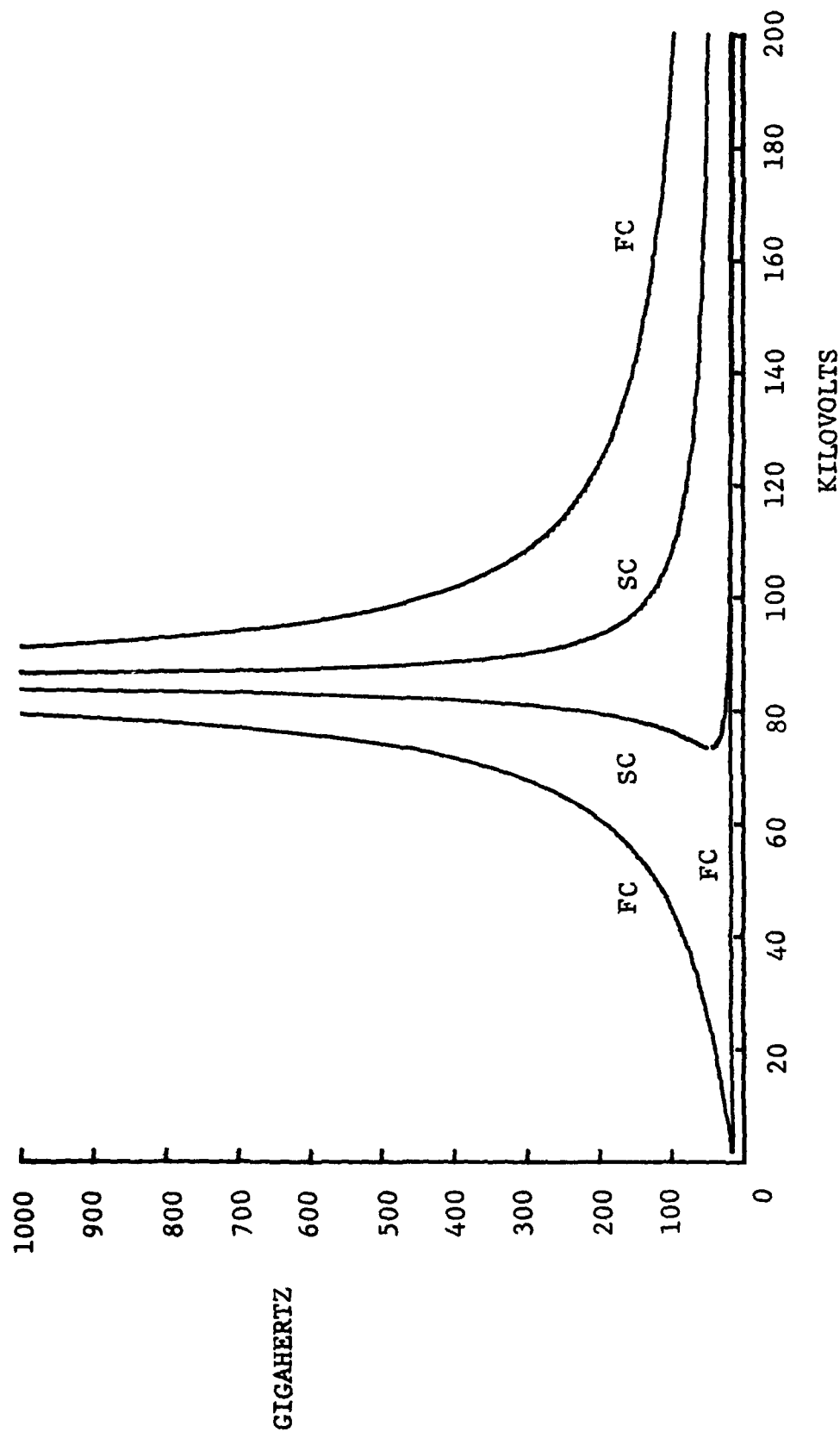
FIGURE 2.3 MICROWAVE FREQUENCY VS. ELECTRON BEAM ACCELERATING VOLTAGE FOR THE FAST AND SLOW ELECTRON CYCLOTRON MODES IN A FULLY FILLED WAVEGUIDE. THE PUMP WAVELENGTH IS .91 CENTIMETERS, AND THE MAGNETIC FIELD IS 4500 GAUSS. THE WAVEGUIDE MODE IS TE_{01}, AND THE DIELECTRIC CONSTANT OF THE FILLER IS 3.78.

12

13
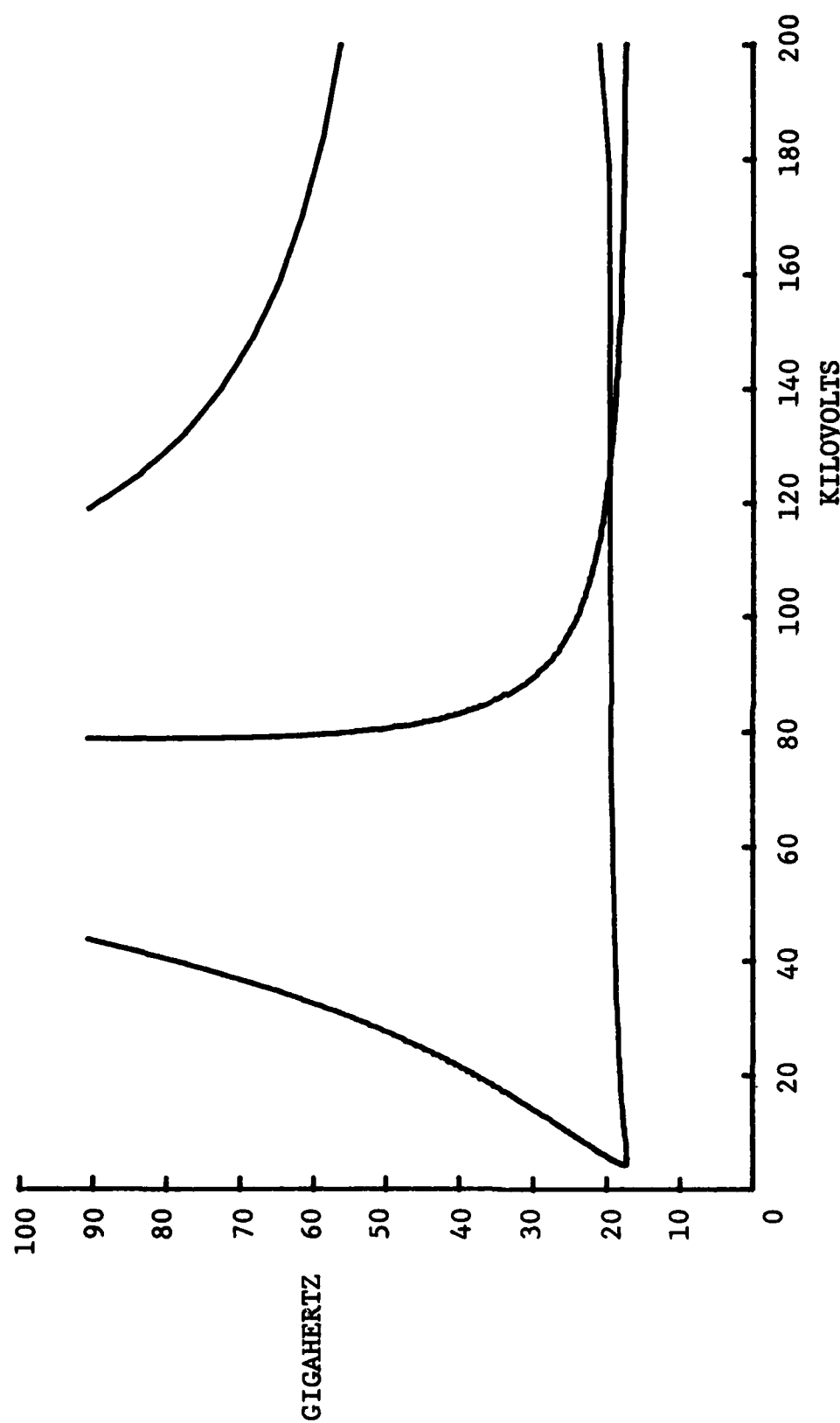
FIGURE 2.4 MICROWAVE FREQUENCY VS. ELECTRON BEAM ACCELERATING VOLTAGE FOR THE FAST AND SLOW ELECTRON CYCLOTRON MODES IN A PARTIALLY FILLED WAVEGUIDE. ALL PARAMETERS ARE THE SAME AS BEFORE, EXCEPT THE INNER RADIUS IS .125 INCHES, THE RATIO OF THE OUTER TO INNER RADIUS IS 1.98, AND THE DIELECTIC CONSTANT OF THE FILLER IS 3.78./8

$$(k-k_p)^2 c^2 = \epsilon \omega^2 - \omega_{co}^2 \qquad (2.4)$$

The dispersion relation for the slow electron beam mode, (2.1), can be written as:

$$k = \frac{1}{v_0}(\omega + W) \qquad (2.5)$$

Here, W is either the electron cyclotron frequency or the electron plasma frequency. For fast waves, we just let W be negative.

Substituting (2.5) for k into (2.4), we find:

$$(\omega + W)^2 - 2k_p v_0(\omega + W) + k_p^2 v_0^2$$
$$= (\epsilon \omega^2 - \omega_{co}^2)\frac{v_0^2}{c^2} \qquad (2.6)$$

Collecting terms with respect to the powers of , we find

$$\omega = \frac{1}{(1-\epsilon \frac{v_0^2}{c^2})}\left[(k_p v_0 - W) \\ \pm \sqrt{\epsilon}\,\frac{v_0}{c}\sqrt{(k_p v_0 - W)^2 - \frac{\omega_{co}^2}{\epsilon}(1-\epsilon\frac{v_0^2}{c^2})}\,\right] \qquad (2.7)$$

It is easy to see that for the upper (+) branch, that as $\sqrt{\epsilon}\,v_0/c$ approaches 1, ω becomes extremely large. For the lower (-) branch, as $\sqrt{\epsilon}\,v_0/c$ becomes arbitrarily close to 1, the ω_{co}^2 term in the square root becomes unimportant and the resulting $(1 - \sqrt{\epsilon}\,v_0/c)$ term in the numerator cancels with the same factor in the denominator, thus keeping finite. Equation (2.7) is used to do the frequency calculations for the graphs in figures 2.2 and 2.3.

The most important observation from the two graphs in figures 2.2 and 2.3 is that there are two branches of the interaction. The lower frequency branch is due to the nonlinear dispersion of the waveguide near cutoff. The upper frequency branch is similar to free space Raman or Cerenkov-Raman backscattering.

Referring to (2.7), we see that

$$\omega_{upper \atop branch} \approx \left| \frac{k_0 v_0 - w}{1 - \sqrt{\epsilon} \frac{v_0}{c}} \right| , \quad \sqrt{\epsilon} \frac{v_0}{c} \approx 1 \tag{2.8}$$

The absolute value of the quantity on the right hand side of (2.8) is due to the requirement that the interaction occur within the first quadrant of figure 2.1B.

By the dependence of the interaction upon the magnetic field, one can easily determine, experimentally, whether a fast or a slow electron cyclotron beam mode exists. For a fast cyclotron beam mode, a lower magnetic field requires a higher beam velocity to achieve synchronism. This behavior is due to the electron cyclotron frequency being directly proportional to the magnetic field. Thus, for a given velocity $v_0 < c$, a minimum magnetic field threshold can exist such that no synchronism is possible if the guiding magnetic field is below this magnetic field threshold. For a slow cyclotron beam mode, a higher magnetic field requires a higher beam velocity to achieve synchronism. Thus, for a given electron beam velocity $v_0 < c$, there exists

a maximum magnetic field limit such that no synchronism can occur if the guiding magnetic field exceeds this maximum magnetic field limit. These trends can be easily seen in figure 2.1 by adjusting the y-intercept, which is $\pm \Omega$.

For fast and slow plasma modes, a similar analogy can be made for the electron density, instead of the magnetic field. Since we do not have nearly as wide a range of electron plasma frequencies as we do with electron cyclotron frequencies, the experimental determination of fast and slow electron plasma modes is difficult.

A simple magnetic field-velocity relation can be obtained from figure 2.1B. The asymptotic slope of the waveguide dispersion is c/n, where n is the index of refraction. For interaction at $\omega = +\infty$ and $\beta n = 1$, it is required that

$$\Omega = \frac{eB}{\gamma_0 mc} = \frac{k_0 c}{n} , \quad v_0 = \frac{c}{n} \tag{2.9}$$

Therefore, for interaction at subluminal electron beam velocities ($\beta n < 1$), the magnetic field field intensity must be less than B_{max}, where

$$B_{max} = \frac{k_p}{\sqrt{n^2 - 1}} \left(\frac{mc^2}{e} \right) , \quad n > 1 \tag{2.10}$$

For $v_e < c$, B_{max} can become arbitrarily large as v becomes close to c, as long as B_{max} increases no faster than

$$\gamma_0 = (1 - v_0^2/c^2)^{-1/2}.$$

From figure 2.1, the minimum electron beam energy requirement for a vacuum TE_{01} mode for a 0.5 inch diameter waveguide, a magnetic field strength of 6 kilogauss and a $k_p = (2\pi)$ cm^{-1} is approximately 50 KeV. These parameters are well within our experimental capabilities, and we should expect to see interactions for both $n = 1$ and $n > 1$.

The major deficiency of the kinematic theory is that it does not predict the magnitude of the gain. However, the theory is a convenient way to calculate the possible scattered microwave frequencies. Provided the gain is sufficient to overcome the losses, these frequencies will appear in the output spectrum. An extension of the theory suitable to calculate the gain will be presented in the next chapter.

CHAPTER 3

THE CALCULATION OF GAIN FOR RAMAN AND CERENKOV-RAMAN BACKSCATTERING

In this chapter, we will calculate the gain per centimeter of the scattered wave due to an electron beam passing through the center of a magnetic wiggler and a cylindrical waveguide. This calculation will take the experimental conditions into account. The calculation will be done with cylindrical boundary conditions, and the magnetic wiggler will be modeled as a zero frequency pump.

All calculations are done in the laboratory frame of reference. First, the equation of motion, $F = dP/dt$, must be simplified because the full use of cylindrical coordinates in a relativistic problem would become intractable. Next we consider the modeling of the wave fields. We choose the beam mode so as to have longitudinal bunching of the electron beam. The pump wave is the sinusoidal magnetic field ripple due to the magnetic wiggler. The scattered wave is chosen to be in a TE mode, as is indicated by the experimental results. Since no Raman interaction is present until second order, all velocities, electron densities, and currents must be calculated through second order. Next, the wave equation, with the effects of electron density and electron

18

current included, is introduced. This wave equation is complex. One method of solution is to break the wave equation up into a real, normal mode part and an imaginary gain or loss part. The final result will appear similar to the parametric equations:

$$\frac{\partial}{\partial z} E_b = A_1 B_p E_s \tag{3.1A}$$

$$\frac{\partial}{\partial z} B_p = A_2 E_b E_s \tag{3.1B}$$

$$\frac{\partial}{\partial z} E_s = A_3 E_b B_p \tag{3.1C}$$

E_b, B_p, and E_s represent the electric or the magnetic field amplitudes of the beam mode, the pump wave, and the scattered wave, respectively. A_1, A_2, and A_3 are coefficients. The z direction is parallel to the initial electron beam velocity and the longitudinal guiding magnetic field.

Equations (3.1) are manifestly nonlinear. The goal of all the calculations is essentially to determine the coefficients A_1, A_2, and A_3. Since B_p is the magnitude of the magnetic wiggler field, it remains constant. Setting the coefficient A_2 in (3.1B) equal to zero, we can estimate the gain of the scattered wave. Solving for E_s, we find

$$E_s = (E_s)_0 \, e^{\chi z} \tag{3.2}$$

where $\qquad X = \sqrt{A_1 A_3}\ B_\rho$

and $(E_s)_0$ is a constant.

The gain is proportional to B_p. As one would expect, as the pump field increases, the gain increases. The coefficients, A_1 and A_3, are functions of the frequency. Therefore, the gain is a function of the frequency.

Although there is no direct experimental measurement of gain, it is easy to calculate a reasonable gain. Suppose the thermal noise due to the electron beam corresponds to an energy of 100 eV. The kinetic energy of the electrons is typically 50 KeV, and the thermal noise is due to a 0.2 percent spread in the electron velocities. If this thermal noise is coupled into the microwave fields, the available power to initiate the Raman interaction is[19]:

$$P = k_B T \Delta f \qquad\qquad (3.3)$$

where k_B is Boltzman's constant, T is the temperature, and Δf is the interaction bandwidth. Assuming $\Delta f = 1$ gigahertz, we find that the thermal noise power IS 1.6×10^{-8} watts.[20] To amplify the noise up to a signal of 100 watts requires an amplification of 98 decibels. The interaction length inside the magnetic wiggler is typically 17 centimeters long. Therefore, a gain per unit length is 6

decibels per centimeter. No consideration for signal saturation is taken into account because the scattered microwave power is much smaller than the pump wave power. The pump wave power is at least in the megawatt range.

From my own pulse CO_2 laser experience[21], I estimate the gain per unit length as .06 decibels per centimeter for a 25 megawatt laser pulse. This gain is calculated using an initial noise power of 10^{-13} watts[22] and a 40 pass build-up time, 91.6 centimeters per pass. We see that the gain from the Raman backscattering interaction is enormous compared to the gain of a medium sized pulse CO_2 laser.

The following calculation is a more realistic version of the Raman backscattering calculations done by Crewe[23]. We will find that solving the problem with cylindrical boundary conditions does make the solution more complicated.

3.1 THE DERIVATION OF THE SIMPLIFIED RELATIVISTIC FORCE EQUATION

When written out in cylindrical coordinates, the relativistic force equation

$$\underset{\sim}{F} = \frac{d}{dt}(\gamma m \underset{\sim}{v}) \tag{3.4}$$

has many terms in each directional component. We need to

choose a frame of reference in which all perturbation velocities are small in magnitude compared to some single characteristic velocity of the electron beam. In the electron beam frame of reference, there is no single large characteristic velocity, and the perturbation velocities in the radial, azimuthal, and longitudinal directions are all approximately of the same amplitude. Thus, in this frame, no simplifications, due to magnitude ordering, are applicable to the force equation.

But, if we transfer the calculations into the laboratory frame of reference, the characteristic velocity is the electron beam velocity, v_0. For the perturbation velocities to be much smaller than v_0, we must require that the perturbation electric and magnetic fields to be much less than the accelerating field in the electron gun. A typical accelerating voltage is approximately 80 kilovolts for a $\beta_0 = v_0/c = 1/2$, where c is the speed of light. Therefore,

$$E_{perturbation} \ll 80\ KV \simeq 250\ statvolts \tag{3.5A}$$

Since $\beta_0 B$ can result in as large a velocity perturbation as an electric field, an additional requirement is

$$B_\perp \ll 500\ gauss \tag{3.5B}$$

The equation of force, (3.4), must be simplified to remove the relativistic factor γ outside of the time derivative. We know that[24]:

$$\frac{d}{dt}(\gamma \underset{\sim}{v}) = \frac{\partial}{\partial t}(\gamma \underset{\sim}{v}) + \underset{\sim}{v} \cdot \nabla(\gamma \underset{\sim}{v}) \tag{3.6}$$

$$= \underset{\sim}{v}\frac{\partial \gamma}{\partial t} + \gamma\frac{\partial \underset{\sim}{v}}{\partial t} + \gamma \underset{\sim}{v} \cdot \nabla \underset{\sim}{v} + \underset{\sim}{v}(\underset{\sim}{v} \cdot \nabla \gamma) \tag{3.7}$$

Since $\quad \gamma = \dfrac{1}{\sqrt{1 - \dfrac{\underset{\sim}{v} \cdot \underset{\sim}{v}}{c^2}}}$ $\qquad\qquad$ (3.8)

then

$$\frac{\partial \gamma}{\partial t} = \gamma^3 \frac{\underset{\sim}{v}}{c^2} \cdot \frac{\partial \underset{\sim}{v}}{\partial t} \tag{3.9A}$$

and

$$\nabla \gamma = \gamma^3 \nabla \underset{\sim}{v} \cdot \frac{\underset{\sim}{v}}{c^2} \tag{3.9B}$$

Collecting all the terms, we have:

$$\frac{d}{dt}(\gamma \underset{\sim}{v}) = \gamma\frac{\partial \underset{\sim}{v}}{\partial t} + \frac{\gamma^3}{c^2}\underset{\sim}{v}\left(\underset{\sim}{v} \cdot \frac{\partial \underset{\sim}{v}}{\partial t}\right) \tag{3.10}$$

$$+ \gamma \underset{\sim}{v} \cdot \nabla \underset{\sim}{v} + \frac{\gamma^3}{c^2}\underset{\sim}{v}(\underset{\sim}{v} \cdot \nabla \underset{\sim}{v} \cdot \underset{\sim}{v})$$

Letting:

$$\underset{\sim}{v} = v_r \underset{\sim}{e}_r + v_\theta \underset{\sim}{e}_\theta + (v_0 + v_z)\underset{\sim}{e}_z \tag{3.11}$$

where $\underset{\sim}{e}_r$, $\underset{\sim}{e}_\theta$, and $\underset{\sim}{e}_z$ are unit vectors, we find that, to

first order, each directional component[25] of (3.10) reduces to:

$$\left(\frac{d}{dt}(\gamma \underset{\sim}{v})\right)_r \approx \gamma_0 \left(\frac{\partial v_r}{\partial t} + v_0 \frac{\partial v_r}{\partial z}\right) \tag{3.12A}$$

$$\left(\frac{d}{dt}(\gamma \underset{\sim}{v})\right)_\theta \approx \gamma_0 \left(\frac{\partial v_\theta}{\partial t} + v_0 \frac{\partial v_\theta}{\partial z}\right) \tag{3.12B}$$

$$\left(\frac{d}{dt}(\gamma \underset{\sim}{v})\right)_z \approx \gamma_0^3 \left(\frac{\partial v_z}{\partial t} + v_0 \frac{\partial v_z}{\partial z}\right) \tag{3.12C}$$

The definition of γ_0 is:

$$\gamma_0 = \gamma(\underset{\sim}{v} = \underset{\sim}{v_0}) = \frac{1}{\sqrt{1 - \frac{v_0^2}{c^2}}} \tag{3.13}$$

Setting $\underset{\sim}{F}$ equal to the Lorentz force,

$$\underset{\sim}{F} = -e\left(\underset{\sim}{E} + \frac{\underset{\sim}{v}}{c} \times \underset{\sim}{B}\right) \tag{3.14}$$

The zeroth order equation of motion is:

$$\underset{\sim}{F} = 0 \tag{3.15}$$

The first order equations of motion are:

$$\frac{\partial v_r}{\partial t} + v_0 \frac{\partial v_r}{\partial z} = -\frac{e}{\gamma_0 m}\left(E_r - \frac{v_0}{c}B_\theta + \frac{v_\theta}{c}B_0\right) \tag{3.16A}$$

$$\frac{\partial v_\theta}{\partial t} + v_0 \frac{\partial v_\theta}{\partial z} = -\frac{e}{\gamma_0 m}\left(E_\theta + \frac{v_0}{c}B_r - \frac{v_r}{c}B_0\right) \tag{3.16B}$$

$$\frac{\partial V_z}{\partial t} + V_0 \frac{\partial V_z}{\partial z} = -\frac{e}{\gamma_0^3 m}(E_z) \qquad (3.16C)$$

-e and m are the charge and mass of an electron. The E's and B's are the electric and magnetic fields of the electron beam mode, the pump wave, and the scattered wave. All the perturbation velocities are due to the wave fields interacting with the electrons. B_0 is the strong longitudinal guiding magnetic field in the z direction. B_0 is much larger than any of the wave field components.

Equations (3.16A) and (3.16B) are coupled to each other via the $v_\theta B_0/c$ and $v_r B_0/c$ terms on the right hand sides. This coupling is important, as it can lead to resonance effects. From (3.16) and the equation of continuity, we will derive a complete set of perturbation velocities and densities due to each wave.

3.2 THE WAVE FIELDS

There are three waves; the incident wave or the electron beam mode, the pump wave or the magnetic wiggler wave, and the scattered wave or the emitted microwaves. For the production of high power, coherent microwaves, it is necessary that the electron beam be bunched in the z direction. Therefore, only $E_z^b \neq 0$ is needed and all other electron beam mode fields are set to zero. Since the electron beam is nonneutral, there exists a radial electric

field due to the electrons' mutual repulsion. But this radial electric field crossed into the guiding magnetic field gives an asimuthal drift of electrons that is on a time scale that is slow compared to both the frequency of the scattered microwaves and the electron cyclotron frequency. Therefore, this radial electric field is not included.

A frequency, ω_b, a wavenumber, k_b. and a phase, ϕ_b, are associated with the electron beam mode. We will assume that the electron beam mode is an electron plasma mode. The electron beam is assumed to be perfectly cold as it enters the interaction region. The electrons can have velocity components in all three directions, but all electrons have the same velocities. The beam mode is modeled as :

$$\underset{\sim}{E_b} = E_z^b \, \underset{\sim}{e_z} \, e^{i(k_b z - \omega_b t + \phi_b)} + c.c. \qquad (3.17)$$

where c.c. stands for complex conjugate.

The fields of the pump wave are those appropriate for the interior of a magnetic wiggler immersed within an uniform longitudinal magnetic field. Referring to figure 3.1, we see that the magnetic wiggler is a series of circular disks. Every other disk is made of iron, which tends to pull the magnetic field lines towards itself. The remaining disks are made of aluminum, which are non-
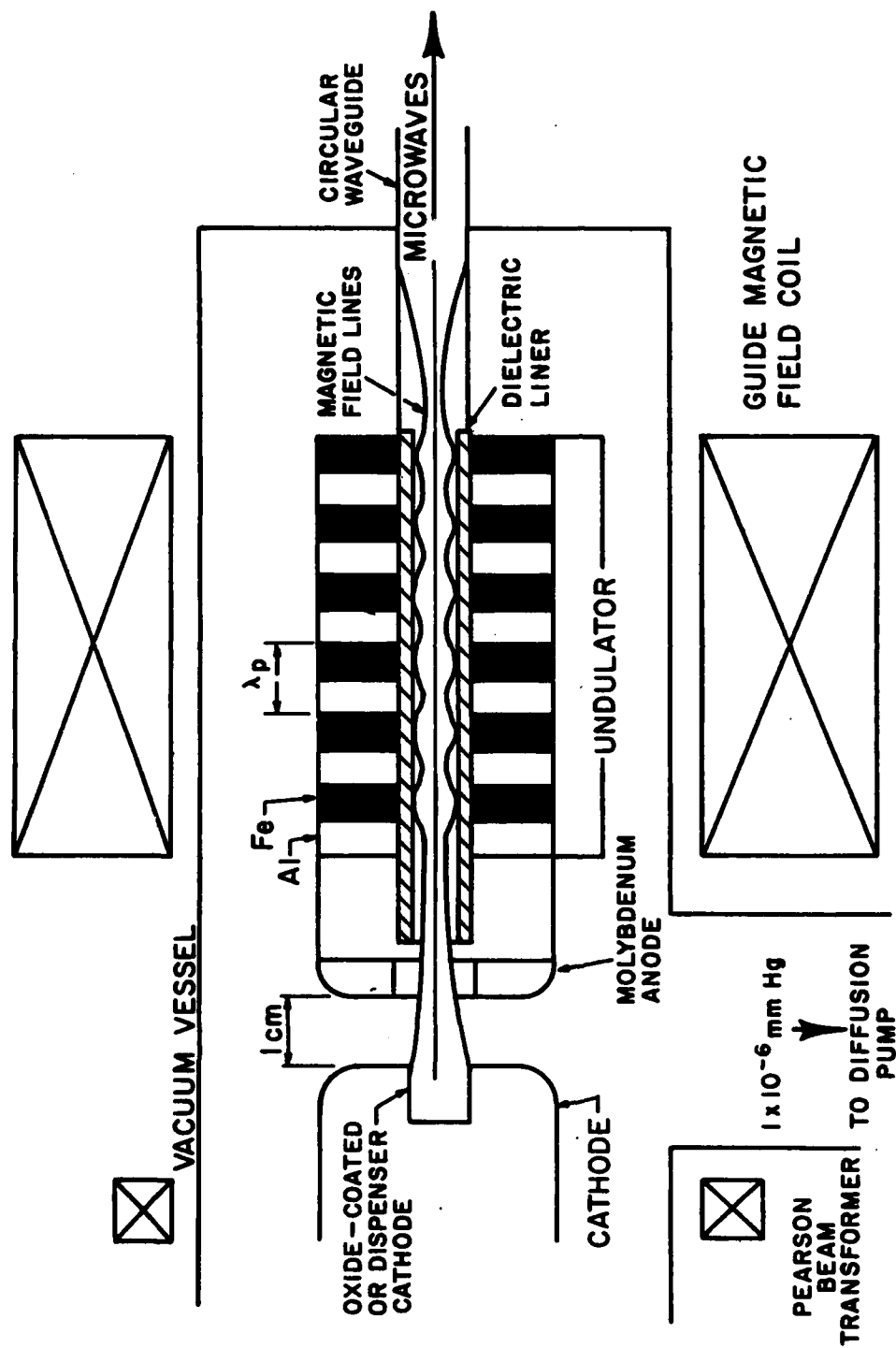
FIGURE 3.1 THE UNDULATOR AND THE RESONATOR STRUCTURE [26]

magnetic. Since there are no currents or displacement currents[27], we have

$$\nabla \times B = 0 \tag{3.18}$$

Therefore, B can be represented as the negative of the gradient of a scalar field, Φ_M.

$$B = -\nabla \Phi_M \tag{3.19}$$

Since $\nabla \cdot B = 0$, we have:

$$\nabla^2 \Phi_M = 0 \tag{3.20}$$

From figure 3.1, we see that Φ_M must be evaluated within a cylindrical coordinate system. Assuming no θ dependence, we have a solution[28] of the form:

$$\Phi_M = \alpha I_1(k_p r) e^{i(k_p z + \phi_p)} + C.C. \tag{3.21}$$

λ_p is defined as the wavelength of the static magnetic field within the wiggler. k_p is defined as:

$$k_p = \frac{2\pi}{\lambda_p} \tag{3.22A}$$

ϕ_p is a phase constant. The phase velocity, ω_p/k_p is zero

because the magnetic field is static in the laboratory frame of reference. Since k_p is nonzero, the pump frequency, ω_p, must equal zero.

$$\omega_p = 0 \qquad (3.22B)$$

Referring to (3.19), we find:

$$\mathcal{B} = -\alpha k_p \left(\frac{\partial I_1(k_p r)}{\partial (k_p r)} \underset{\sim}{e}_r + i I_1(k_p r) \underset{\sim}{e}_z \right) e^{i(k_p z + \phi_p)} \qquad (3.23)$$
$$+ C.C.$$

To avoid unnecessary complication with modified Bessel functions at this time, the magnetic pump field will be defined as:

$$\underset{\sim}{\mathcal{B}}_p = \left(\mathcal{B}_r^p \underset{\sim}{e}_r + i \mathcal{B}_z^p \underset{\sim}{e}_z \right) e^{i(k_p z + \phi_p)} + C.C. \qquad (3.24)$$

where

$$\mathcal{B}_r^p = -\alpha k_p \frac{\partial I_1(k_p r)}{\partial (k_p r)} \qquad (3.25A)$$

and

$$\mathcal{B}_z^p = -\alpha k_p I_1(k_p r) \qquad (3.25B)$$

One important point to note is that only the fundamental wavelength, λ_p, is used in the derivation.

Since the magnetic wiggler in figure 3.1 appears approximately as a square wave near the inside edge of the magnetic wiggler, we should have used a Fourier expansion for the z dependence of Φ_M. Only the odd harmonics need to be included. The higher harmonics are obviously much weaker in amplitude than the fundamental, but, experimentally, they turn out to be important. We will use only one Fourier component in the remainder of this chapter. Higher harmonics are easily accounted for by setting:[29,30,31]

$$k_p = \left(\frac{2\pi}{\lambda_p}\right)\left(\frac{1}{h}\right) \qquad h = 3, 5, 7, \cdots \qquad (3.26)$$

The remaining wave to be considered is the scattered wave. From the experiment, we have observed that the emitted microwaves have a lower frequency bound corresponding to the TE_{01} mode cutoff. Therefore, to simplify the following analysis, the scattered wave will be assumed to be in a TE mode. From Jackson[32], we find that the general form of the TE mode is

$$\underset{\sim}{E}_s = E_\theta^s \, \underset{\sim}{e}_\theta \, e^{i(k_s z - \omega_s t + \beta_s)} + c.c. \qquad (3.27A)$$

and

$$\underset{\sim}{B}_s = \left(B_r^s \, \underset{\sim}{e}_r + i B_z^s \, \underset{\sim}{e}_z\right) e^{i(k_s z - \omega_s t + \beta_s)} + c.c. \qquad (3.27B)$$

where

$$B_r^s = \frac{k_s}{\eta_s^2} \frac{\partial B_z^s}{\partial r} \tag{3.28A}$$

$$E_\theta^s = -\frac{\omega_s}{c k_s} B_r^s \tag{3.28B}$$

and

$$\eta_s^2 = \mu\epsilon \frac{\omega_s^2}{c^2} - k_s^2 \tag{3.28C}$$

3.3   THE VELOCITIES, ELECTRON DENSITIES, AND CURRENT DENSITIES

The equations of motion will be broken up into three separate sets; one set for each wave. The superscripts or subscripts p,b,s represent the pump wave, the electron beam mode, and the scattered wave, respectively.

Raman backscattering is a second order process driven by a nonlinear current consisting of density flucuations,created by one wave, and of velocity flucuations, created by another wave. There will also be second order corrections to the velocities, the electron densities, and the currents due to wave mixing. The definitions are stated as follows:

$$\underset{\sim}{V} = \underset{\sim}{V_0} + \underset{\sim}{V_p} + \underset{\sim}{V_b} + \underset{\sim}{V_s} + (\underset{\sim}{V_p})^{(2)} + (\underset{\sim}{V_b})^{(2)} + (\underset{\sim}{V_s})^{(2)} + c.c. \qquad (3.29)$$

where

$$\underset{\sim}{V_0} = V_0 \underset{\sim}{e_z} \qquad (3.30A)$$

$$\underset{\sim}{V_p} = (V_r^p \underset{\sim}{e_r} + V_\theta^p \underset{\sim}{e_\theta} + V_z^p \underset{\sim}{e_z}) e^{i(k_p z + \phi_p)} + c.c. \qquad (3.30B)$$

$$\underset{\sim}{V_b} = (V_r^b \underset{\sim}{e_r} + V_\theta^b \underset{\sim}{e_\theta} + V_z^b \underset{\sim}{e_z}) e^{i(k_b z - \omega_b t + \phi_b)} + c.c. \qquad (3.30C)$$

$$\underset{\sim}{V_s} = (V_r^s e_r + V_\theta^s \underset{\sim}{e_\theta} + V_z^s \underset{\sim}{e_z}) e^{i(k_s z - \omega_s t + \phi_s)} + c.c. \qquad (3.30D)$$

$$(\underset{\sim}{V_p})^{(2)} = ((V_r^p)^{(2)} \underset{\sim}{e_r} + (V_\theta^p)^{(2)} \underset{\sim}{e_\theta} + (V_z^p)^{(2)} \underset{\sim}{e_z}) e^{i(k_p z + \phi_p)} + c.c. \qquad (3.30E)$$

$$(\underset{\sim}{V_b})^{(2)} = ((V_r^b)^{(2)} \underset{\sim}{e_r} + (V_\theta^b)^{(2)} \underset{\sim}{e_\theta} + (V_z^b)^{(2)} \underset{\sim}{e_z}) e^{i(k_b z - \omega_b t + \phi_b)} + c.c. \qquad (3.30F)$$

$$(\underset{\sim}{V_s})^{(2)} = ((V_r^s)^{(2)} \underset{\sim}{e_r} + (V_\theta^s)^{(2)} \underset{\sim}{e_\theta} + (V_z^s)^{(2)} \underset{\sim}{e_z}) e^{i(k_s z - \omega_s t + \phi_s)} + c.c. \qquad (3.30G)$$

v_0 is the zeroth order velocity, the v's are the first order velocities, and the $(v)^{(2)}$'s are the second order velocities.

The definitions for the electron densities follow the same pattern as the velocities do.

$$n = n_0 + n_p e^{i(k_p z + \phi_p)} + n_b e^{i(k_b z - \omega_b t + \phi_b)}$$
$$+ n_s e^{i(k_s z - \omega_s t + \phi_s)} + (n_p)^{(2)} e^{i(k_p z - \omega_p t + \phi_p)} \quad (3.31)$$
$$+ (n_b)^{(2)} e^{i(k_b z - \omega_b t + \phi_b)} + (n_s)^{(2)} e^{i(k_s z - \omega_s t + \phi_s)} + c.c.$$

where n_0 is the unperturbed electron beam density.

The current densities are defined as follows:

$$\underset{\sim}{J} = \underset{\sim}{J_0} + \underset{\sim}{J_p} + \underset{\sim}{J_b} + \underset{\sim}{J_s} + (\underset{\sim}{J_p})^{(2)} + (\underset{\sim}{J_b})^{(2)} + (\underset{\sim}{J_s})^{(2)} + c.c. \quad (3.32)$$

where

$$\underset{\sim}{J_0} = -n_0 e \underset{\sim}{v_0} \quad (3.33A)$$

$$\underset{\sim}{J_p} = -n_p e \underset{\sim}{v_0} - n_0 e \underset{\sim}{v_p} \quad (3.33B)$$

$$\underset{\sim}{J_b} = -n_b e \underset{\sim}{v_0} - n_0 e \underset{\sim}{v_b} \quad (3.33C)$$

$$\underset{\sim}{J_s} = -n_s e \underset{\sim}{v_0} - n_0 e \underset{\sim}{v_s} \quad (3.33D)$$

The second order current densities are more difficult to determine.

$$(\underset{\sim}{J_p})^{(2)} = -e n_0 (\underset{\sim}{v_p})^{(2)} - e (n_b)^{(j)} (\underset{\sim}{v_s})^{(j)} - e (n_s)^{(j)} (\underset{\sim}{v_b})^{(j)} - e (n_p)^{(2)} \underset{\sim}{v_0} \quad (3.34A)$$

$$(\underset{\sim}{J}_b)^{(2)} = -en_0(\underset{\sim}{v}_b)^{(2)} - e(n_p)^{(j)}\underset{\sim}{v}_s - en_s(\underset{\sim}{v}_p)^{(j)} - e(n_b)^{(2)}\underset{\sim}{v}_0 \qquad (3.34B)$$

$$(\underset{\sim}{J}_s)^{(2)} = -en_0(\underset{\sim}{v}_s)^{(2)} - en_b(\underset{\sim}{v}_p)^{(-j)} - e(n_p)^{(-j)}\underset{\sim}{v}_b - e(n_s)^{(2)}\underset{\sim}{v}_0 \qquad (3.34C)$$

where we define:

$$(A)^{(j)} = \begin{cases} A & \text{if } j=1 \\ A^* & \text{if } j=-1 \end{cases}$$

and A is an arbitrary complex quantity.

The complex conjugations in equations (3.34) arise naturally from the frequency and wavenumber relationships among the pump, beam, and scattered waves. Consider the wave relationships as shown in figure 3.2. We define:

$$\omega_s = \omega_b \; , \quad \omega_p = 0 \qquad (3.35A)$$

and

$$k_s = k_b - s(j)k_p \; , \quad j = \pm 1 \qquad (3.35B)$$

Then, we have:

$$k_p z = -s(j)(k_s z - \omega_s t) + s(j)(k_b z - \omega_b t) \qquad (3.36A)$$

$$k_b z - \omega_b t = (k_s z - \omega_s t) + s(j)k_p z \qquad (3.36B)$$

$$k_s z - \omega_s t = (k_b z - \omega_b t) - s(j)k_p z \qquad (3.36C)$$
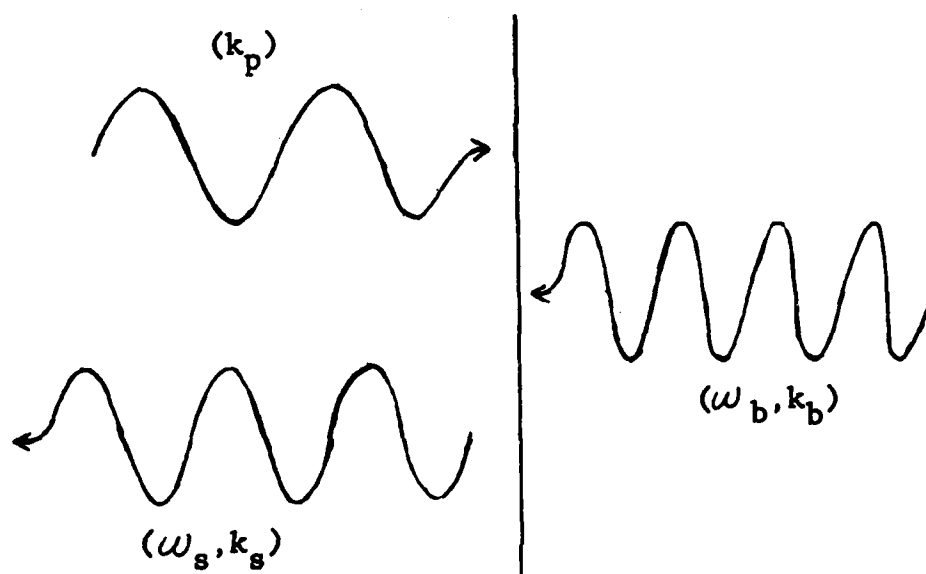
FIGURE 3.2 THE RELATIONSHIPS AMONG THE PUMP, BEAM, AND SCATTERED WAVES.

$$\phi_b = \phi_s + s(j) \, \phi_p \qquad\qquad (3.36D)$$

Since all perturbations vary as $e^{i(kz-\omega t)}$, equations (3.36) are needed to keep the proper phasing among the beam, pump, and scattered waves. Referring to the second order current densities as defined in equations (3.34), the conjugations are chosen such that the proper phasing is retained.

It should be noted that equations (3.16) are still valid to calculate second order quantities. The terms left out have frequencies and wavenumbers of the second harmonic and we are interested only in terms at the fundamental harmonics, $k_p z$, $k_b z - \omega_b t$, and $k_s z - \omega_s t$.

3.4 THE CALCULATION OF THE FIRST ORDER VELOCITY PERTURBATIONS

In the laboratory frame of reference, the calculation of the first order velocity perturbations is simple because all velocity perturbations are much smaller than the electron beam velocity, v_0. Reviewing equations (3.16) once again, we find that they are all similar to one another, except that the z component has a γ_0^3 factor whereas the r and θ components have a γ_0 factor.

Starting with the pump wave, we find from (3.16):

$$\frac{\partial v_r^p}{\partial t} + V_0 \frac{\partial v_r^p}{\partial z} = -\frac{e}{\gamma_0 m}\left(\frac{v_\theta^p}{c}B_0\right)$$

$$(3.37A)$$

$$\frac{\partial v_\theta^p}{\partial t} + V_0 \frac{\partial v_\theta^p}{\partial z} = -\frac{e}{\gamma_0 m}\left(\frac{V_0}{c}B_r^p - \frac{v_r^p}{c}B_0\right)$$

$$(3.37B)$$

$$\frac{\partial v_z^p}{\partial t} + V_0 \frac{\partial v_z^p}{\partial z} = 0$$

$$(3.37C)$$

The factor $e^{i(k_p z + \phi)}$ has been dropped since it appears on both sides of the equations above. The pump fields are given by (3.24) and (3.25). Fourier analysing and noting that $\omega_p = 0$, we find that

$$v_r^p = \frac{i}{k_p}\left(\frac{e}{\gamma_0 mc}\right)\frac{v_\theta^p}{V_0}B_0$$

$$(3.38A)$$

$$v_\theta^p = \frac{i}{k_p}\left(\frac{e}{\gamma_0 mc}\right)\left(B_r^p - \frac{v_r^p}{V_0}B_0\right)$$

$$(3.38B)$$

$$v_z^p = 0$$

$$(3.38C)$$

We see that v_θ^p and v_r^p are coupled together. Substituting for v_r^p in (3.38B), we find:

$$v_\theta^p = \frac{i}{k_p}\left(\frac{e}{\gamma_0 mc}\right)B_r^p + \left(\frac{1}{k_p}\right)^2\left(\frac{e}{\gamma_0 mc}\right)^2\frac{B_0^2}{V_0^2}v_\theta^p$$

$$(3.39)$$

Let

$$\Omega = \frac{eB_0}{\gamma_0 mc}$$

$$(3.40)$$

Rearranging terms, we find:

$$V_\theta^p = i V_0 \frac{(k_p v_0) \Omega}{(k_p v_0)^2 - \Omega^2} \left(\frac{B_r^p}{B_0} \right)$$

(3.41A)

Substituting for v_θ^p in (3.38A),

$$V_r^p = -V_0 \frac{\Omega^2}{(k_p v_0)^2 - \Omega^2} \left(\frac{B_r^p}{B_0} \right)$$

(3.41B)

Inspecting the denominators of (3.40A) and (3.40B), a first order resonance occurs if

$$\left(\frac{1}{k_p v_0} \right)^2 \left(\frac{e B_0}{\gamma_0 m c} \right)^2 = 1$$

(3.42)

or

$$\frac{\lambda_p B_0}{\gamma_0 v_0} \approx 3.5 \times 10^{-7} \left(\frac{gm \; cm}{(stat \; coul) \; sec} \right)^{1/2}$$

Choosing the experimental parameters of :

λ_p = 1/3 centimeters

v_0 = c/2 = 1.5 X 10^{10} centimeters per second

γ_0 = 1.155,

the required magnetic field for resonance is :

$$B_0 = 1.8 \times 10^4 \text{ gauss}$$

Our typical guiding magnetic field strengths are approximately a factor of three lower than this value. Therefore, we are far from resonance, and the electron beam velocity does not change appreciably from v_0 as the beam passes through the interaction region.

Next we consider the beam mode. From (3.17), we have assumed only a z component for the electric field. This electric field will be related to electron beam bunching. Referring to (3.16C),

$$\frac{\partial v_z^b}{\partial t} + v_0 \frac{\partial v_z^b}{\partial z} = - \frac{e}{\gamma_0^3 m} E_z^b \tag{3.43}$$

By Fourier analysing and regrouping terms, we find:

$$v_z^b = - \left(\frac{ie}{\gamma_0^3 m} \right) \left(\frac{1}{\omega_b - k_b v_0} \right) E_z^b \tag{3.44A}$$

There are no other velocity perturbations, to first order, due to beam bunching. We choose:

$$v_r^b \neq 0 \tag{3.44B}$$

$$v_\theta^b \neq 0 \tag{3.44C}$$

Referring to (3.16), we see that (3.44B) and (3.44C) lead to

the dispersion of an electron cyclotron wave.

$$\omega_b = k_b V_0 \pm \Omega \tag{3.45}$$

The final wave to consider is the scattered wave. Referring to (3.16) and (3.27), we find

$$\frac{\partial v_r^s}{\partial t} + V_0 \frac{\partial v_r^s}{\partial z} = -\frac{e}{\gamma_0 m}\left(\frac{v_\theta^s}{c} B_0\right) \tag{3.46A}$$

$$\frac{\partial v_\theta^s}{\partial t} + V_0 \frac{\partial v_\theta^s}{\partial z} = -\frac{e}{\gamma_0 m}\left(E_\theta^s + \frac{V_0}{c} B_r^s - \frac{v_r^s}{c} B_0\right) \tag{3.46B}$$

$$\frac{\partial v_z^s}{\partial t} + V_0 \frac{\partial v_z^s}{\partial z} = 0 \tag{3.46C}$$

Fourier analysing and regrouping terms, we find:

$$v_r^s = -i\left(\frac{e}{\gamma_0 mc}\right)\frac{v_\theta^s B_0}{(\omega_s - k_s V_0)} \tag{3.47A}$$

$$v_\theta^s = -i\left(\frac{e}{\gamma_0 mc}\right)\frac{1}{(\omega_s - k_s V_0)}\left(cE_\theta^s + V_0 B_r^s - v_r^s B_0\right) \tag{3.47B}$$

$$v_z^s = 0 \tag{3.47C}$$

Substituting (3.47A) for v_r^s into (3.47B), we find:

$$v_\theta^s = -i\frac{\left(\frac{e}{\gamma_0 mc}\right)\frac{1}{(\omega_s - k_s V_0)}}{1 - \frac{\Omega^2}{(\omega_s - k_s V_0)^2}}\left(cE_\theta^s + V_0 B_r^s\right) \tag{3.48A}$$

$$V_r^S = - \frac{\left(\frac{e}{\gamma_0 mc}\right)^2 \frac{B_0}{(\omega_s - k_s v_0)^2}}{1 - \frac{\Lambda^2}{(\omega_s - k_s v_0)^2}} \left(cE_\theta^S + v_0 B_r^S\right) \tag{3.48B}$$

From (3.28B), we know that

$$B_r^S = - \frac{ck_s}{\omega_s} E_\theta^S \tag{3.28B}$$

Substituting into (3.48A) and (3.48B), we find:

$$V_r^S = - \left(\frac{\Lambda^2}{(\omega_s - k_s v_0)^2 - \Lambda^2}\right)\left(\frac{\omega_s - k_s v_0}{\omega_s}\right)\left(\frac{cE_\theta^S}{B_0}\right) \tag{3.49A}$$

$$V_\theta^S = -i \left(\frac{(\omega_s - k_s v_0)^2}{(\omega_s - k_s v_0)^2 - \Lambda^2}\right)\left(\frac{\Lambda}{\omega_s}\right)\left(\frac{cE_\theta^S}{B_0}\right) \tag{3.49B}$$

As expected, for energy to be transfered from the electron beam to the scattered wave, or vice versa, it is necessary for the electron beam velocity, v_0, to be different from the scattered wave phase velocity, ω_s/k_s. Note that there is, again, a first order resonance for

$$\omega_s = k_s v_0 \pm \Lambda \tag{3.50}$$

This resonance must also be avoided because we are interested only in a second order interaction. This first order interaction is a Cerenkov-like interaction.

This concludes the calculation of the first order velocity perturbations due to the pump, beam, and scattered waves.

3.5 THE SECOND ORDER VELOCITY PERTURBATIONS.

The second order velocity perturbations come about from the mixing of first order velocity perturbations of one wave with the magnetic field components of a second wave, resulting in a velocity perturbation at the frequency and wavenumber of the third wave. Also the second order velocity perturbations may interact with the guiding magnetic field to redirect the second order motion. Recall that the relations (3.16) are still valid for second order calculations since we are interested in perturbations at the fundamental frequencies and wavenumbers only. For ease of notation, s(j) will be defined as the sign of j.

Starting with the pump wave, the second order equations of motion are:

$$\frac{\partial (v_r^p)^{(2)}}{\partial t} + v_0 \frac{\partial (v_r^p)^{(2)}}{\partial z} = -\left(\frac{e}{\gamma_0 m}\right)\left[\frac{(v_\theta^b)^{(j)}}{c}(iB_z^s)^{(j)} + \frac{(v_\theta^p)^{(2)}}{c}B_0\right] \tag{3.51A}$$

$$\frac{\partial (V_\theta^\rho)^{(2)}}{\partial t} + V_0 \frac{\partial (V_\theta^\rho)^{(2)}}{\partial z} = -\left(\frac{e}{\gamma_0 m}\right)\left[-\frac{(V_r^b)^{(j)}}{c}(iB_z^s)^{(-j)} + \frac{(V_z^b)^{(j)}}{c}(B_r^s)^{(-j)}\right. \quad \text{(3.51B)}$$

$$\left. - \frac{(V_r^\rho)^{(2)}}{c}B_0\right]$$

$$\frac{\partial (V_z^\rho)^{(2)}}{\partial t} + V_0 \frac{\partial (V_z^\rho)^{(2)}}{\partial z} = -\left(\frac{e}{\gamma_0^3 m}\right)\left[-\frac{(V_\theta^b)^{(j)}}{c}(B_r^s)^{(-j)}\right] \qquad \text{(3.51C)}$$

The superscript j's result from the resonance conditions (3.36). Noting that there are cross terms in (3.51A) and (3.51B), the solution of each component is:

$$(V_r^\rho)^{(2)} = -s(j)\left(\frac{e}{\gamma_0 m c}\right)\left[\frac{k_\rho V_0}{\Omega^2 - (k_\rho V_0)^2}\right](V_\theta^b)^{(j)}(B_z^s)^{(-j)}$$

$$+i\left(\frac{e}{\gamma_0 m c}\right)\left[\frac{\Omega}{\Omega^2 - (k_\rho V_0)^2}\right]\left[s(j)(V_r^b)^{(j)}(B_z^s)^{(-j)} - i(V_z^b)^{(j)}(B_r^s)^{(-j)}\right] \quad \text{(3.52A)}$$

$$(V_\theta^\rho)^{(2)} = \left(\frac{1}{\Omega^2 - (k_\rho V_0)^2}\right)\left(\frac{e}{\gamma_0 m c}\right)\left[s(j)(k_\rho V_0)(V_r^b)^{(j)}(B_z^s)^{(-j)}\right.$$

$$\left. + i s(j)\Omega(V_\theta^b)^{(j)}(B_z^s)^{(-j)} - i(k_\rho V_0)(V_z^b)^{(j)}(B_r^s)^{(-j)}\right] \qquad \text{(3.52B)}$$

$$(V_z^\rho)^{(2)} = -\frac{i}{k_\rho V_0}\left(\frac{e}{\gamma_0^3 m c}\right)(V_\theta^b)^{(j)}(B_r^s)^{(-j)} \qquad \text{(3.52C)}$$

The expressions for the velocity perturbations and the magnetic field components are given in previous sections of this chapter. For ease of manipulation, the substitution for

these expressions will not be made yet.

The second order equations of motion for the electron beam mode are:

$$\frac{\partial (v_r^b)^{(2)}}{\partial t} + v_0 \frac{\partial (v_r^b)^{(2)}}{\partial z} = -\left(\frac{e}{\gamma_0 m}\right)\left[\frac{(v_\theta^p)^{(j)}}{c}(iB_z^s) + \frac{(v_\theta^s)}{c}(iB_z^p)^{(j)} + \frac{(v_\theta^b)^{(2)}}{c}B_0\right] \quad (3.53A)$$

$$\frac{\partial (v_\theta^b)^{(2)}}{\partial t} + v_0 \frac{\partial (v_\theta^b)^{(2)}}{\partial z} = +\left(\frac{e}{\gamma_0 m}\right)\left[\frac{(v_r^p)^{(j)}}{c}(iB_z^s) + \frac{(v_r^s)}{c}(iB_z^p)^{(j)} + \frac{(v_r^b)^{(2)}}{c}B_0\right] \quad (3.53B)$$

$$\frac{\partial (v_z^b)^{(2)}}{\partial t} + v_0 \frac{\partial (v_z^b)^{(2)}}{\partial z} = +\left(\frac{e}{\gamma_0^3 m}\right)\left[\frac{(v_\theta^p)^{(j)}}{c}(B_r^s) + \frac{(v_\theta^s)}{c}(B_r^p)^{(j)}\right] \quad (3.53C)$$

The (iB_z)'s are due to the B_z components being out of phase with the B_r components. Solving equations (3.53) in the usual manner, we find:

$$(v_r^b)^{(2)} = \left(\frac{1}{(\omega_b - k_b v_0)^2 - \Lambda^2}\right)\left(\frac{e}{\gamma_0 mc}\right)\Big\{(\omega_b - k_b v_0)\left[s(j)(v_\theta^s)(B_z^p)^{(j)} + (v_\theta^p)^{(j)}(B_z^s)\right]$$
$$+ i\Lambda\left[(v_r^p)^{(j)}(B_r^s) + s(j)(v_r^s)(B_z^p)^{(j)}\right]\Big\} \quad (3.54A)$$

$$(v_\theta^b)^{(2)} = \left(\frac{1}{(\omega_b - k_b v_0)^2 - \Lambda^2}\right)\left(\frac{e}{\gamma_0 mc}\right)\Big\{-(\omega_b - k_b v_0)\left[(v_r^p)^{(j)}(B_z^s) + s(j)(v_r^s)(B_z^p)^{(j)}\right]$$
$$+ i\Lambda\left[s(j)(v_\theta^s)(B_z^p)^{(j)} + (v_\theta^p)^{(j)}(B_z^s)\right]\Big\} \quad (3.54B)$$

$$(V_z^b)^{(2)} = \frac{i}{(\omega_b - k_b V_0)} \left(\frac{e}{\gamma_0^3 mc}\right)\left[(V_\theta^p)^{(j)}(B_r^s) + (V_\theta^s)(B_r^p)^{(j)}\right] \tag{3.54C}$$

Finally, the second order equations of motion for the scattered wave are:

$$\frac{\partial (V_r^s)^{(2)}}{\partial t} + V_0 \frac{\partial (V_r^s)^{(2)}}{\partial z} = -\left(\frac{e}{\gamma_0 m}\right)\left[\frac{(V_\theta^b)}{c}(iB_z^p)^{(-j)} + \frac{(V_\theta^s)^{(2)}}{c}B_0\right] \tag{3.55A}$$

$$\frac{\partial (V_\theta^s)^{(2)}}{\partial t} + V_0 \frac{\partial (V_\theta^s)^{(2)}}{\partial z} = +\left(\frac{e}{\gamma_0 m}\right)\left[\frac{(V_r^b)}{c}(iB_z^p)^{(-j)} + \frac{(V_r^s)}{c}B_0\right] \tag{3.55B}$$

$$\frac{\partial (V_z^s)^{(2)}}{\partial t} + V_0 \frac{\partial (V_z^s)^{(2)}}{\partial z} = +\left(\frac{e}{\gamma_0^3 m}\right)\left[\frac{(V_\theta^b)}{c}(B_r^p)^{(-j)}\right] \tag{3.55C}$$

Solving equations (3.55), we find

$$(V_r^s)^{(2)} = -\left(\frac{\omega_s - k_s V_0}{(\omega_s - k_s V_0)^2 - \Omega^2}\right)s(j)\left(\frac{e}{\gamma_0 mc}\right)\left[(V_\theta^b)(B_z^p)^{(-j)} \right.$$
$$\left. + i\frac{\Omega}{(\omega_s - k_s V_0)}(V_r^b)(B_z^p)^{(-j)}\right] \tag{3.56A}$$

$$(V_\theta^s)^{(2)} = \left(\frac{\omega_s - k_s V_0}{(\omega_s - k_s V_0)^2 - \Omega^2}\right)s(j)\left(\frac{e}{\gamma_0 mc}\right)\left[(V_r^b)(B_z^p)^{(-j)} \right.$$
$$\left. - i\frac{\Omega}{(\omega_s - k_s V_0)}(V_\theta^b)(B_z^p)^{(-j)}\right] \tag{3.56B}$$

$$(V_z^s)^{(2)} = \frac{i}{(\omega_s - k_s V_0)}\left(\frac{e}{\gamma_0^3 mc}\right)(V_\theta^b)(B_r^p)^{(-j)} \tag{3.56C}$$

As seen from (3.54C), there will be longitudinal bunching of
the electron beam due to the interaction of the magnetic
wiggler wave and the scattered wave.

3.6 THE CALCULATION OF THE ELECTRON DENSITY PERTURBATIONS

The electron density perturbations are calculated
through the use of the continuity equation[33]:

$$\frac{\partial n}{\partial t} + \nabla \cdot (n \underset{\sim}{v}) = 0 \tag{3.57}$$

where n is the total density and v is the electron velocity.
To first order, without the mixture of terms from different
waves, (3.57) reduces to

$$\frac{\partial n_i}{\partial t} + n_0 \underset{\sim}{\nabla} \cdot \underset{\sim}{v_i} + \underset{\sim}{v_0} \cdot \underset{\sim}{\nabla} n_i = 0 \quad i = p, b, s \tag{3.58}$$

n_0 is the constant, unperturbed, initial electron beam
density, $\underset{\sim}{v_0}$ is the constant unperturbed, initial electron
velocity, n_i is a first order electron density perturbation,
and $\underset{\sim}{v_i}$ is a first order velocity perturbation. Throughout
this calculation, there are radial and longitudinal (r,z)
dependences, but there is no asimuthal (θ) dependence.

Again, it is necessary to Fourier transform (3.58) for
each wave. For the pump wave, (3.58) reduces to:

$$n_0 \underset{\sim}{\nabla} \cdot \underset{\sim}{V}_p + \underset{\sim}{V}_0 \cdot \underset{\sim}{\nabla} n_p = 0 \tag{3.59}$$

Recall that $\omega_p = 0$. Noting that there are only r and z dependences, (3.59) becomes:

$$n_0 \nabla_r V_r^p + i k_p n_0 V_z^p + i k_p V_0 n_p = 0 \tag{3.60}$$

where[34]

$$\nabla_r = \frac{1}{r} \frac{\partial}{\partial r} r \tag{3.61}$$

From (3.38C), we see that $v_z^p = 0$. Thus:

$$n_p = i n_0 \frac{\nabla_r V_r^p}{k_p V_0} \tag{3.62}$$

Following the same procedure for the beam mode, we find:

$$\frac{\partial n_b}{\partial t} + n_0 \underset{\sim}{\nabla} \cdot \underset{\sim}{V}_b + \underset{\sim}{V}_0 \cdot \underset{\sim}{\nabla} n_b = 0 \tag{3.63}$$

Fourier transforming, we find:

$$-i \omega_b n_b + n_0 \nabla_r V_r^b + i k_b n_0 V_z^b + i k_b V_0 n_b = 0 \tag{3.64}$$

Collecting terms, we find:

$$n_b = -\frac{i n_0}{(\omega_b - k_b v_0)} \left(\nabla_r v_r^b + i k_b v_z^b \right) \tag{3.65}$$

From (3.44B), v_r^b was chosen to be nonzero to allow for transverse electron motion. v_r^b is small and it does vary with the magnetic field. The magnetic field, itself, does vary with the radius. The pump magnetic field magnitude is approximately 15% of the guiding magnetic field amplitude. Therefore, a good approximation is to set

$$\nabla_r v_r^b = 0 \tag{3.66}$$

and, thus,

$$n_b = n_0 \frac{k_b v_z^b}{(\omega_b - k_b v_0)} \tag{3.67}$$

For the scattered wave, the continuity equation is:

$$\frac{\partial n_s}{\partial t} + n_0 \nabla \cdot \underset{\sim}{v}_s + \underset{\sim}{v}_0 \cdot \nabla n_s = 0 \tag{3.68}$$

Fourier transforming, we find:

$$-i \omega_s n_s + n_0 \nabla_r v_r^s + i k_s n_0 v_z^s + i k_s v_0 n_s = 0 \tag{3.69}$$

From (3.47C), we know that $v_z^s = 0$. Therefore, (3.69) becomes:

$$n_s = -i n_0 \frac{\nabla_r V_r{}^s}{(\omega_s - k_s V_0)} \tag{3.70}$$

The next order of business is to calculate the second order electron density perturbations. Referring to (3.57), we find that the appropriate equation for this calculation is:

$$\frac{\partial (n_i)^{(2)}}{\partial t} + n_0 \underset{\sim}{\nabla} \cdot (V_i)^{(2)} + V_0 \cdot \underset{\sim}{\nabla} (n_i)^{(2)} + \sum_{\substack{j,k \\ (i \neq j \neq k)}} \underset{\sim}{\nabla} \cdot (n_j V_k) = 0 \tag{3.71}$$

i, j, and k represent any permutation of the pump, beam, and scattered waves. In the term with the summation over j and k, the jth and kth terms are assumed to have the proper conjugation to maintain the proper phasing with the ith term.

For the pump wave, (3.71) reduces to

$$n_0 \underset{\sim}{\nabla} \cdot (V_p)^{(2)} + i k_p V_0 (n_p)^{(2)} + \underset{\sim}{\nabla} \cdot \left((n_b)^{(j)} (V_s)^{(-j)} + (n_s)^{(-j)} (V_b)^{(j)} \right) \tag{3.72}$$
$$= 0$$

Solving for $(n_p)^{(2)}$,

$$(n_p)^{(2)} = \frac{i}{k_p V_0} \left[n_0 \underset{\sim}{\nabla} \cdot (V_p)^{(2)} + \underset{\sim}{\nabla} \cdot \left((n_b)^{(j)} (V_s)^{(-j)} + (n_s)^{(-j)} (V_b)^{(j)} \right) \right] \tag{3.73}$$

For the beam mode, (3.71) becomes

$$-i \omega_b (n_b)^{(2)} + n_0 \underset{\sim}{\nabla} \cdot (V_b)^{(2)} + i k_b V_0 (n_b)^{(2)}$$
$$+ \underset{\sim}{\nabla} \cdot \left((n_p)^{(j)} (V_s) + (n_s)(V_p)^{(j)} \right) = 0 \tag{3.74}$$

Solving for $(n_b)^{(2)}$,

$$(n_b)^{(2)} = -\frac{i}{(\omega_b - k_b v_0)}\left[n_0 \nabla \cdot (\underset{\sim}{v}_b)^{(2)} + \nabla \cdot \left((n_p)^{(j)}(\underset{\sim}{v}_s) + (n_s)(\underset{\sim}{v}_p)^{(s)}\right)\right] \quad (3.75)$$

For the scattered wave, (3.71) reduces to:

$$-i\omega_s (n_s)^{(2)} + n_0 \nabla \cdot (\underset{\sim}{v}_s)^{(2)} + i k_s v_0 (n_s)^{(2)}$$
$$+ \nabla \cdot \left((n_p)^{(-j)}(\underset{\sim}{v}_b) + (n_b)(\underset{\sim}{v}_p)^{(-j)}\right) = 0 \quad (3.76)$$

Solving for $(n_s)^{(2)}$,

$$(n_s)^{(2)} = -\frac{i}{(\omega_s - k_s v_0)}\left[n_0 \nabla \cdot (\underset{\sim}{v}_s)^{(2)} + \nabla \cdot \left((n_p)^{(-j)}(\underset{\sim}{v}_b) + (n_b)(\underset{\sim}{v}_p)^{(-j)}\right)\right] \quad (3.77)$$

In equations (3.73), (3.75), and (3.77), the ∇'s have both a radial component and a longitudinal component. We will find that the radial components are difficult terms to deal with in the gain calculations.

3.7 THE ELECTRON CURRENT DENSITIES

Only the three most important current densities will be considered in this section. The first is the unperturbed electron beam current density,

$$J_z^0 = -e n_0 v_0 \quad (3.78)$$

This current density will be used to calculate the electron beam's self magnetic field to show that it is insignificant compared to the magnetic wiggler pump wave.

The second current density is that which drives E_z^b, which is related to the electron beam bunching. This current density is:

$$(J_z^b)_{total} = -n_0 e v_z^b - n_b e v_0 - n_0 e (v_z^b)^{(2)} - (n_b)^{(2)} e v_0$$
$$- (n_p)^{(j)} e (v_z^s) - (n_s) e (v_z^p)^{(j)} \tag{3.79}$$

From (3.38C) and (3.47C), both v_z^p and v_z^s are zero. Then (3.79) reduces to:

$$(J_z^b)_{total} = -n_0 e v_z^b - n_b e v_0 - n_0 e (v_z^b)^{(2)} - (n_b)^{(2)} e v_0 \tag{3.80}$$

The substitution for each term will be delayed until a later section.

The third electron current density will be that which drives the scattered wave electric field, E_θ^s. The appropriate current density is:

$$(J_\theta^s)_{total} = -n_0 e v_\theta^s - n_0 e (v_\theta^s)^{(2)} - (n_p)^{(j)} e (v_\theta^b) - (n_b) e (v_\theta^p)^{(-j)} \tag{3.81}$$

Again, the substitution for each term will be delayed until a later section in this chapter.

3.8   THE   CALCULATION   OF THE AMPLITUDE GAIN   FOR THE   PUMP
WAVE.

From Jackson[35], it is easy to derive the wave equation
for a magnetic field propagating in a medium.

$$\nabla^2 \underset{\sim}{B} - \frac{\epsilon\mu}{c^2} \frac{\partial^2 \underset{\sim}{B}}{\partial t^2} = -\frac{4\pi}{c}\mu \underset{\sim}{\nabla} \times \underset{\sim}{J}$$

(3.82)

ϵ is the dielectric constant of the medium, μ is the
permeability, and $\underset{\sim}{J}$ is the current density to all   orders.
Recalling that the pump wave is a zero frequency wave, the
term with the second time derivitive drops out of (3.82).
For the moment, if we disregard all electron current
densities, we find:

$$\nabla^2 \underset{\sim}{B} = 0$$

(3.83)

The magnetic wiggler field, which is given by equations
(3.24) and (3.25), satisfies (3.83).

The largest perturbation to the magnetic wiggler field
is due to the electron beam's self magnetic field, induced
by $J_0 = -n_0 e v_0$. To calculate the amplitude of this self
magnetic field, we shall use Ampere's Law[36]:

$$\underset{\sim}{\nabla} \times \underset{\sim}{H} = \frac{4\pi}{c} \underset{\sim}{J}$$

(3.84A)

or, in integral form[37],

$$\oint_C \underset{\sim}{H} \cdot d\underset{\sim}{\ell} = \frac{4\pi}{c} \int_S \underset{\sim}{J} \cdot d\underset{\sim}{S} \tag{3.84B}$$

where C is the closed line contour around the surface S. Since

$$\underset{\sim}{B} = \mu_0 \underset{\sim}{H} \tag{3.85}$$

and, for our case,

$$\mu_0 = 1, \tag{3.86}$$

we find from (3.84B) that:

$$(B_\theta^p)_{perturb} = \frac{2\pi}{c} J_z^0 r, \quad r \le R_0 \tag{3.87}$$

An infinite cylindrical surface has been assumed, R_0 is the outer radius of the electron beam, and J_z^0 is independent of r.

To estimate the amplitude of this perturbed magnetic field at the electron beam perimeter, let:

$$n_0 = 10^{10} \, cm^{-3} \tag{3.88A}$$

$$V_0 = \frac{c}{2} \tag{3.88B}$$

$$p = 0.5 \; cm. \tag{3.88C}$$

We know that

$$e = 4.8 \times 10^{-10} \; statcoulombs \tag{3.88D}$$

Then,

$$\left| (B_\theta^p)_{perturb} \right| = 7.5 \; gauss \tag{3.89}$$

This is much smaller than the magnetic wiggler field which is of the order of one hundred gauss. Therefore, $(B_\theta^p)_{perturb}$ is discarded.

All first and second order contributions to J_p are much smaller than J_0 and are discarded also. (3.83) remains as the master equation for the pump field.

Since

$$B_p \propto e^{ik_p z}, \tag{3.90}$$

let

$$k_p \rightarrow k_p - i \, k_p^I \tag{3.91}$$

Then,

$$\underset{\sim}{B}_p \propto \left(e^{k_p^I z}\right) e^{ik_p z} \tag{3.92}$$

k_p^I is proportional to the amplitude gain or loss per unit distance. Letting:

$$k_p^I \longrightarrow \frac{\partial}{\partial z}, \tag{3.93}$$

(3.83) becomes:

$$
\begin{aligned}
\nabla^2 \underset{\sim}{B}_p &= \left(\nabla_t^2 - (k_p - ik_p^I)^2\right) \underset{\sim}{B}_p \\
&\approx \left(\nabla_t^2 - k_p^2\right) \underset{\sim}{B}_p + 2ik_p \frac{\partial}{\partial z} \underset{\sim}{B}_p \\
&= 0
\end{aligned} \tag{3.94}
$$

$(k_p^I)^2$ has been dropped since $k_p^I \ll k_p$.

Since the magnetic wiggler fields, given by equations (3.24) and (3.25), satisfy:

$$\left(\nabla_t^2 - k_p^2\right) \underset{\sim}{B}_p = 0 \tag{3.95}$$

then,

$$\frac{\partial \underset{\sim}{B}_p}{\partial z} = 0 \tag{3.96}$$

for any component of the pump field. (3.96) is equivalent to (3.1B) with $A_2 = 0$.

3.9 THE CALCULATION OF THE AMPLITUDE GAIN FOR THE BEAM MODE.

The wave equation for a propagating electric field in a medium of dielectric constant ϵ is[38]:

$$\nabla^2 \underset{\sim}{E} - \frac{\mu\epsilon}{c^2}\frac{\partial^2 \underset{\sim}{E}}{\partial t^2} = -\frac{4\pi e}{\epsilon}\nabla(n)_{total} + \frac{4\pi\mu}{c^2}\frac{\partial(J)_{total}}{\partial t} \quad (3.97)$$

$(n)_{total}$ and $(J)_{total}$ are the electron beam density and the electron beam current density to all orders, respectively. Since we will deal only with the z component of the electric field of the beam mode, (3.97) reduces to

$$\nabla^2 E_z^b - \frac{\epsilon}{c^2}\frac{\partial^2 E_z^b}{\partial t^2} = -\frac{4\pi e}{\epsilon}\frac{\partial}{\partial z}\left(n_b + (n_b)^{(2)}\right)$$
$$+ \frac{4\pi\mu}{c^2}\frac{\partial}{\partial t}\left(J_z^b + (J_z^b)^{(2)}\right) \quad (3.98)$$

where

$$(n_b)_{total} \approx n_b + (n_b)^{(2)} \quad (3.99A)$$

and

$$(J_z^b)_{total} \approx J_z^b + (J_z^b)^{(2)} \quad (3.99B)$$

Also

$$\epsilon = 1 \tag{3.100A}$$

$$\mu = 1 \tag{3.100B}$$

since the electron beam is located within a vacuum region. Referring to (3.80) for the expression of $(J_z^b)_{total}$, the Fourier transformation of (3.98) is:

$$\left(\nabla_t^2 - k_b^2 + \frac{\omega_b^2}{c^2}\right)E_z^b = -i4\pi e\left(k_b - \frac{\omega_b V_o}{c^2}\right)(n_b + (n_b)^{(2)})$$
$$+ i4\pi e n_o \frac{\omega_b}{c^2}(V_z^b + (V_z^b)^{(2)}) \tag{3.101}$$

Substituting for n_b from (3.65), we find:

$$\left(\nabla_t^2 - k_b^2 + \frac{\omega_b^2}{c^2}\right)E_z^b = -i4\pi e n_o\left[\frac{k_b\left(k_b - \frac{\omega_b V_o}{c^2}\right)}{(\omega_b - k_b V_o)} - \frac{\omega_b}{c^2}\right]V_z^b$$
$$+ \frac{4\pi e n_o}{(\omega_b - k_b V_o)}\left(\frac{\omega_b V_o}{c^2} - k_b\right)\nabla_r V_r^b$$
$$+ i4\pi e\left(\frac{\omega_b V_o}{c^2} - k_b\right)(n_b)^{(2)} \tag{3.102}$$
$$+ i4\pi e n_o \frac{\omega_b}{c^2}(V_z^b)^{(2)}$$

Referring to (3.44A) and substituting for v_z^b, (3.101) becomes:

$$\left(\nabla_t^2 - k_b^2 + \frac{\omega_b^2}{c^2} + \frac{\omega_{plasma}^2}{(\omega_b - k_b v_0)^2}\left(k_b^2 - \frac{\omega_b^2}{c^2}\right)\right)E_z^{-b}$$

$$= \frac{4\pi n_0 e}{(\omega_b - k_b v_0)}\left(\frac{\omega_b v_0}{c^2} - k_b\right)\nabla_t V_t^b$$

$$+ i4\pi e\left(\frac{\omega_b v_0}{c^2} - k_b\right)(n_b)^{(2)} \qquad (3.103)$$

$$+ i4\pi e n_0 \frac{\omega_b}{c^2}(V_z^b)^{(2)}$$

where

$$-\omega_{plasma}^2 = \frac{4\pi n_0 e^2}{\gamma_0^3 m} \qquad (3.104)$$

We can no longer delay dealing with the second order terms. As a shorthand notation, RHS will stand for the right hand side of equation (3.103). Substituting the expressions from (3.75), (3.54C), (3.38C), and (3.47C) into (3.103),

$$RHS = \frac{4\pi e}{(\omega_b - k_b v_0)}\left(\frac{\omega_b v_0}{c^2} - k_b\right)\nabla_t\left[n_0 V_t^b + n_0(V_t^b)^{(2)}\right.$$

$$\left. + \left((n_p)^{(j)}(V_t^s) + (n_s)(V_t^p)^{(j)}\right)\right] \qquad (3.106)$$

$$- \frac{\omega_{plasma}^2}{c^3(\omega_b - k_b v_0)^2}(\omega_b^2 - k_b^2 c^2)\left[(V_\theta^p)^{(j)}(B_t^s) + (V_\theta^s)(B_t^p)^{(j)}\right]$$

If we keep the electron beam diameter at least four times smaller than the diameter of the magnetic wiggler, the pump field gradients will not be large in the interaction

region. Therefore, the ∇_r term will be of the same magnitude or smaller than the second term of (3.106). We will drop the first term of (3.106), realizing that the gain calculations to follow may be too optimistic.

If we substitute (3.41A), (3.28B), and (3.49B) into the remaining term of (3.106), we find:

$$RHS = i\,\frac{\omega_{plasma}^2}{c^2}\left(\frac{\omega_b^2-k_b^2c^2}{(\omega_b-k_bv_0)^2}\right)\left(\frac{\Lambda}{\omega_s}\right)\left[S^{(j)}\frac{(k_pv_0)(k_sv_0)}{(k_pv_0)^2-\Lambda^2}\right.$$
$$\left.+\frac{(\omega_s-k_sv_0)^2}{(\omega_s-k_sv_0)^2-\Lambda^2}\right]\left(\frac{B_r^p}{B_0}\right)^{(j)}E_\theta^s \qquad (3.107)$$

If we let:

$$k_b \longrightarrow k_b - ik_b^I \qquad (3.108A)$$

where

$$k_b^I v_0 \ll |\omega_b - k_b v_0| \qquad (3.108B)$$

and

$$k_b^I \longrightarrow \frac{\partial}{\partial z}, \qquad (3.108C)$$

and, if we substitute these equations into the LHS of (3.103), we find:

$$LHS = \left(\nabla_t^2 - \left(1 - \frac{\omega_{plasma}^2}{(\omega_b - k_b V_0)^2} \right) \left(k_b^2 - \frac{\omega_b^2}{c^2} \right) \right) E_z^b$$

$$- 2i k_b^I \left(\frac{\omega_{plasma}^2 V_0}{(\omega_b - k_b V_0)^3} \left(k_b^2 - \frac{\omega_b^2}{c^2} \right) \right.$$

$$\left. - k_b \left(1 - \frac{\omega_{plasma}^2}{(\omega_b - k_b V_0)^2} \right) \right) E_z^b \qquad (3.109)$$

Noting that (3.107) is imaginary, we equate (3.109) and (3.107), and we find:

$$\left(\nabla_t^2 - \left(1 - \frac{\omega_{plasma}^2}{(\omega_b - k_b V_0)^2} \right) \left(k_b^2 - \frac{\omega_b^2}{c^2} \right) \right) E_z^b = 0 \qquad (3.110A)$$

and

$$-2k_b^I \left(\frac{\omega_{plasma}^2 V_0}{(\omega_b - k_b V_0)^3} \left(k_b^2 - \frac{\omega_b^2}{c^2} \right) - k_b \left(1 - \frac{\omega_{plasma}^2}{(\omega_b - k_b V_0)^2} \right) \right) E_z^b$$

$$= \frac{\omega_{plasma}^2}{c^2} \left(\frac{\omega_b^2 - k_b^2 c^2}{(\omega_b - k_b V_0)^2} \right) \left(\frac{\Lambda}{\omega_s} \right) \left[s(j) \frac{(k_p V_0)(k_s V_0)}{(k_p V_0)^2 - \Lambda^2} \right. \qquad (3.110B)$$

$$\left. + \frac{(\omega_s - k_s V_0)^2}{(\omega_s - k_s V_0)^2 - \Lambda^2} \right] \left(\frac{B_h^p}{B_0} \right)^{(j)} E_\theta^s$$

Since we have assumed an electron plasma mode

$$\left| \omega_b - k_b V_0 \right| = \omega_{plasma}$$

(3.110A) and (3.110B) reduce to:

$$\nabla_t^2 E_z^b = 0 \qquad (3.111A)$$

$$\frac{\partial}{\partial z} E_z^b = \pm \frac{\omega_{plasma}}{2 V_0} \left(\frac{\Omega}{\omega_s} \right) \left[s_{(j)} \frac{(k_p V_0)(k_s V_0)}{(k_p V_0)^2 - \Omega^2} \right.$$

$$\left. + \frac{(\omega_s - k_s V_0)^2}{(\omega_s - k_s V_0)^2 - \Omega^2} \right] \left(\frac{B_t^p}{B_0} \right) E_\theta^s \qquad (3.111B)$$

(3.111B) gives the expression for A_1 of (3.1A)

3.10 THE CALCULATION OF THE AMPLITUDE GAIN FOR THE SCATTERED WAVE.

The wave equation appropriate for the scattered wave is given by (3.97). We are interested in the amplitude gain for E_θ^s. Reducing (3.97), subject to the requirements for our particular case, we find:

$$\nabla^2 E_\theta^s - \frac{1}{c^2} \frac{\partial^2 E_\theta^s}{\partial t^2} = \frac{4\pi}{c^2} \frac{\partial}{\partial t} \left(J_\theta^s \right)_{total} \qquad (3.112)$$

There is no θ dependence and within the area of the electron beam, where the scattered wave is driven by currents, $\epsilon = 1$, and $\mu = 1$. $(J^s)_{total}$ is given by (3.81). Doing the usual Fourier transforms, (3.112) becomes:

$$\left(\nabla_t^2 - k_s^2 + \frac{\omega_s^2}{c^2} \right) E_\theta^s = i \frac{4\pi e}{c^2} \left[n_0 v_\theta^s + n_0 (v_\theta^s)^{(2)} \right.$$

$$\left. + (n_p)^{(-j)}(v_\theta^b) + (n_b)(v_\theta^p)^{(-j)} \right] \omega_s \qquad (3.113)$$

Referring to equations (3.49B), (3.56B), (3.61), (3.65), (3.44C), and (3.41A), (3.113) reduces to:

$$\left(\nabla_t^2 - \left(k_s^2 - \frac{\omega_s^2}{c^2} + \frac{\gamma_0^2 \omega_{plasma}^2}{c^2}\left(\frac{(\omega_s - k_s v_0)^2}{(\omega_s - k_s v_0)^2 - \Omega^2}\right)\right)\right)E_\theta^s$$

$$= \frac{4\pi n_0 e}{c^2}\left\{\left(\frac{e}{\gamma_0 mc}\right)\left(\frac{(\omega_s - k_s v_0)\omega_s}{(\omega_s - k_s v_0)^2 - \Omega^2}\right)S(j)\left[i(v_r^b) + \frac{\Omega}{(\omega_s - k_s v_0)}(v_\theta^b)\right](B_z^p)^{(j)}\right.$$

$$- S(j)\left(\frac{1}{k_p B_0}\right)\left(\frac{\Omega^2}{(k_p v_0)^2 - \Omega^2}\right)^{(-j)}(\nabla_r B_r^p)^{(-j)}(v_\theta^b)\omega_s$$

$$- i\, S(j)\frac{v_0 \omega_s}{(\omega_b - k_b v_0)}\left(\frac{(k_p v_0)\Omega}{(k_p v_0)^2 - \Omega^2}\right)\frac{(B_r^p)^{(-j)}}{B_0}\nabla_r v_r^b\right\}$$

$$- i\, S(j)\frac{\omega_{plasma}^2}{c^2}\left(\frac{(k_b v_0)\omega_s}{(\omega_b - k_b v_0)^2}\right)\left(\frac{(k_b v_0)\Omega}{(k_p v_0)^2 - \Omega^2}\right)E_z^b\left(\frac{B_r^p}{B_0}\right)^{(-j)} \tag{3.114}$$

We find that (3.114) has a complex collection of terms that depend on v_r^b and v^b. v_r^b and v^b were included because they allow for the motion due to a cyclotron mode in the electron beam. Let us assume they are small and may be dropped. Dropping the conjugations from the field quantities, we have:

$$\left(\nabla_t^2 - \left(k_s^2 - \frac{\omega_s^2}{c^2} + \frac{\gamma_0^2 \omega_{plasma}^2}{c^2}\left(\frac{(\omega_s - k_s v_0)^2}{(\omega_s - k_s v_0)^2 - \Omega^2}\right)\right)\right)E_\theta^s$$

$$= -i\, S(j)\frac{\omega_{plasma}^2}{c^2}\left(\frac{(k_b v_0)\omega_s}{(\omega_b - k_s v_0)^2}\right)\left(\frac{(k_p v_0)\Omega}{(k_p v_0)^2 - \Omega^2}\right)E_z^b\left(\frac{B_r^p}{B_0}\right) \tag{3.115}$$

Using the same procedure as in previous sections, we let:

$$k_s \rightarrow k_s - i k_s^I, \quad k_s^I << k_s \tag{3.116A}$$

and

$$k_s^I \rightarrow \frac{\partial}{\partial z} \tag{3.116B}$$

(3.115) becomes:

$$\left(\nabla_t^2 - \left(k_s^2 - \frac{\omega_s^2}{c^2} + \frac{\gamma_0^2 \omega_{plasma}^2}{c^2} \left(\frac{(\omega_s - k_s v_0)^2}{(\omega_s - k_s v_0)^2 - \Omega^2} \right) \right) \right) E_\theta^s$$
$$= 0 \tag{3.117A}$$

$$\frac{\partial}{\partial z} E_\theta^s = - \frac{s(j)}{2} \left(\frac{\omega_s}{k_s} \right) \left(\frac{k_p v_0}{c^2} \right) \left(\frac{(k_p v_0) \Omega}{(k_p v_0)^2 - \Omega^2} \right) E_z^b \left(\frac{b_r^\rho}{B_0} \right) \tag{3.117B}$$

The plasma frequency, $\omega_{plasma}/2\pi$ is much smaller than either the scattered frequency, $\omega_s/2\pi$, or the cyclotron frequency, $\Omega/2\pi$. Thus, the scattered wave dispersion is:

$$\omega_s^2 = \omega_{co}^2 + k_s^2 c^2 \tag{3.118}$$

where ω_{co} is a waveguide cutoff frequency. The coefficient A_3 in (3.1C) can be obtained from (3.117B).

3.11   THE CALCULATION OF GAIN

In sections 3.8,   3.9, and   3.10, we   have obtained the coefficients A_1, A_2, and A_3 to be used in equations (3.1). Solving these   equations   for   the   scattered   wave electric field, and assuming $A_2 = 0$, we obtained (3.2) where

$$\chi = \sqrt{A_1 A_3}\ B_\rho$$

The average power gain per   unit   distance for the scattered wave is defined as:

$$Gain = (20 \log e^{\chi z})/z \quad decibels/cm. \tag{3.119}$$

where z is the total magnetic wiggler length in centimeters.

From equations (3.96), (3.111B), and (3.117B), we have:

$$A_1 = \pm \frac{\omega_{plasma}}{2v_0\,\omega_s}\left(\frac{e}{\gamma_0 mc}\right)\left[S(j)\,\frac{(k_p v_0)(k_s v_0)}{(k_p v_0)^2 - \Omega^2}\right.$$
$$\left. + \frac{(\omega_s - k_s v_0)^2}{(\omega_s - k_s v_0)^2 - \Omega^2}\right] \tag{3.120A}$$

$$A_2 = 0 \tag{3.120B}$$

$$A_3 = -\frac{s(j)}{2}\left(\frac{e}{\gamma_0 mc}\right)\left(\frac{\omega_s}{k_s}\right)\left(\frac{k_b v_0}{c^2}\right)\left(\frac{k_p v_0}{(k_p v_0)^2 - \Omega^2}\right) \tag{3.120C}$$

Therefore,

$$Gain = 8.69\,(\omega_{plasma})^{1/2}\left(\frac{e}{2\gamma_0 mc^2}\right)\Big|\left(\frac{k_b}{k_s}\right)\left(\frac{k_p v_0}{(k_p v_0)^2 - \Omega^2}\right)$$
$$\times \left(\frac{(k_p v_0)(k_s v_0)}{(k_p v_0)^2 - \Omega^2} + s(j)\frac{(\omega_s - k_s v_0)^2}{(\omega_s - k_s v_0)^2 - \Omega^2}\right)\Big|^{1/2}\beta_r^p \tag{3.121}$$

3.12 CONCLUSION

Given the dispersion for any annularly filled waveguide and knowing the pump wavelength and the plasma density, (3.121) can be used to calculate the gain as a function of the frequency. If the interaction frequency is near the waveguide cutoff ($k_s{\sim}0$), we have:

$$Gain = 8.69\,(\omega_{plasma})^{1/2}\left(\frac{e}{2\gamma_0 mc^2}\right)\Big|\left(\frac{k_p v_0}{(k_p v_0)^2 - \Omega^2}\right)(k_b v_0)$$
$$+ s(j)\frac{k_b}{k_s}\left(\frac{k_p v_0}{(k_p v_0)^2 - \Omega^2}\right)\left(\frac{\omega_s^2}{\omega_s^2 - \Omega^2}\right)\Big|^{1/2}\beta_r^p \tag{3.122}$$

We expect that the (ω_s/k term would soon dominate, and the gain would become large. In the previous analysis, we assumed that the growth, k^I, is much smaller than the

wavenumber, k. The analysis could be used for a high growth regime if the terms of order $(k^I)^2$ were included.

At high frequency where $\omega_s - k_s v_0 \sim 0$, we find that:

$$\text{Gain} = 8.69 \, (\omega_{plasma})^{1/2} \left(\frac{e}{2\gamma_0 m c^2}\right)\left(\frac{(k_p v_0)^{3/2}}{(k_p v_0)^2 - \Omega^2}\right) B_r^P \quad ; \quad V_0 \sim \frac{c}{n} \quad (3.123)$$

In order to maximize the gain, we find that we need to increase both $k_p v_0$ and Ω such that $k_p v_0 > \Omega$.

CHAPTER 4

THE EXPERIMENTAL APPARATUS

The experimental apparatus can be divided up into four basic components: the high voltage network, the electron gun, the resonator, and the microwave diagnostics. In practice, the electron gun is the most difficult component to keep working well. The largest challenges in the future will be in the development of the resonator structure and the microwave diagnostics. In the following, the experimental system is described, and the reasons behind the choice of certain experimental parameters are given.

4.1 The High Voltage Network

The design of the high voltage network, as shown in figure 4.1[39,40]. A 30 kilovolt, 200 milliampere power supply is used to charge up the capacitor in the pulse forming network. A capacitor and a single inductor form the pulse forming network. A 150 kilo-ohm charging resistor is used prevent the power supply from an overload during a pulse.

The 50 kilovolt hydrogen thyratron is a high voltage, high current switch. At zero bias, a grid in the thyratron
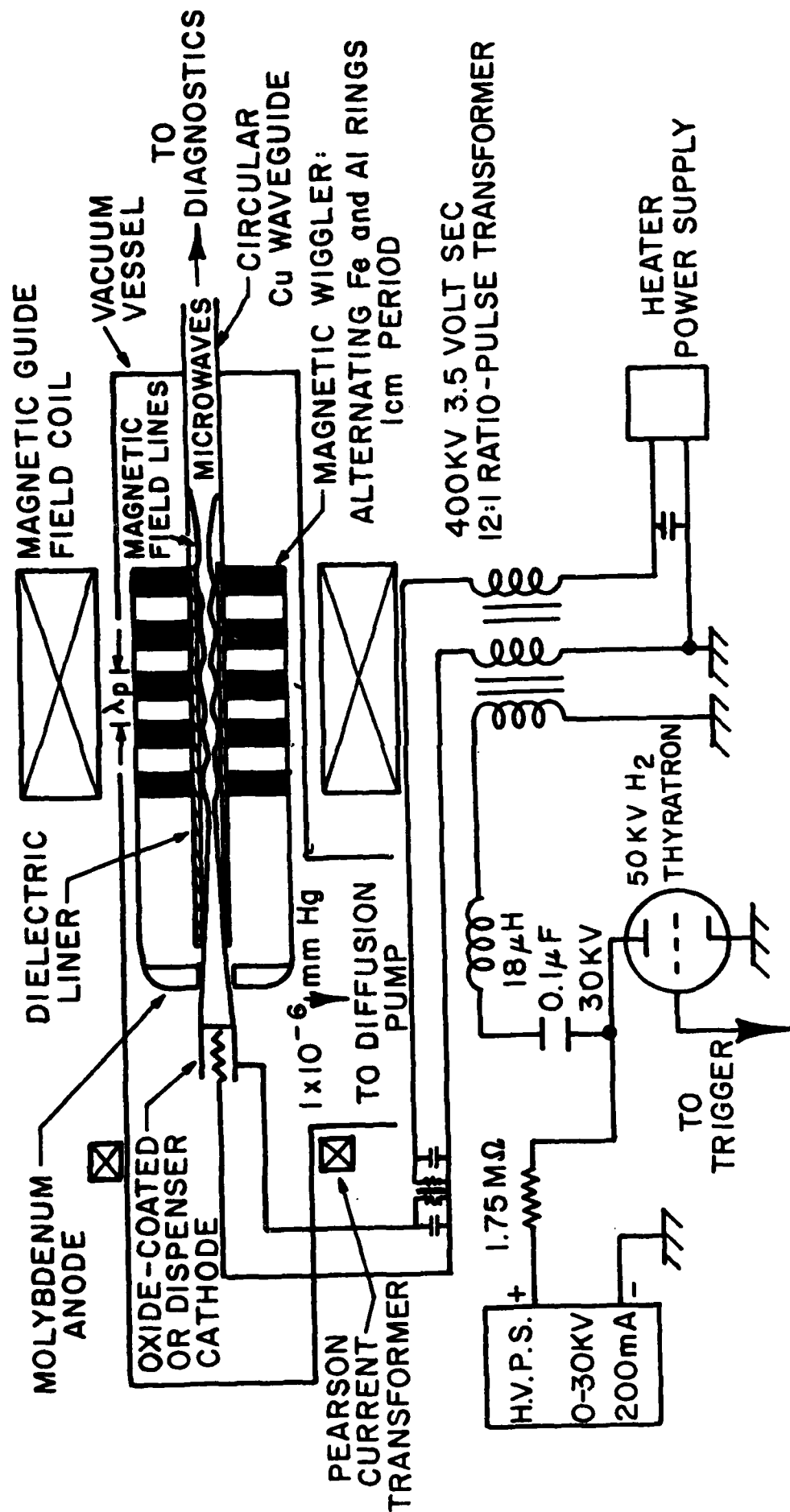
FIGURE 4.1   THE HIGH VOLTAGE NETWORK [26]

prevents the formation of a plasma that would allow a conducting path between the anode and the cathode. When given a positive voltage pulse by the 5C22 thyratron, the grid allows a plasma to form, and, thus a conducting path is established for current to flow[41]. The 5C22 thyratron is controlled by a multivibrator pulser.

While being charged, one side of the 0.1 microfarad capacitor is grounded through the 18 microhenry inductor to the primary windings of the pulse transformer. After the charging cycle is completed, the 50 kilovolt hydrogen thyratron grounds the high voltage side of the capacitor, and a negative pulse is directed into the pulse transformer. The maximum charging and discharging repetition rate is ten hertz. Usually, we set the repetition rate at one hertz.

The resonant frequency of the capacitor and the inductor is:

$$\omega = \frac{1}{\sqrt{LC}} = 7.45 \times 10^5 \; radians/second \qquad (4.1)$$

Resulting in a pulse width time:

$$\tau_{pulse} = \left(\frac{2\pi}{\omega}\right)\left(\frac{1}{2}\right) = 4.2 \times 10^{-6} \; seconds \qquad (4.2)$$

The extra factor of 1/2 is needed because a pulse to the

electron gun is one half a cycle of a sine wave.

The effective impedance of the pulse forming network is:

$$Z = \sqrt{\frac{L}{C}} = 13.4 \ ohms \tag{4.3}$$

The pulse forming network is not impedance matched to the electron gun. Typical electron gun parameters are 100 to 250 kilovolts at 20 to 30 amperes. Including the 10 kilo-ohm bypass resistor, a typical electron gun impedance is roughly 5 kilo-ohms. Because the pulse transformer ratio is 12 to 1, the pulse forming network sees an effective impedance of:

$$R \approx 420 \ ohms \tag{4.4}$$

It turned out that impedance matching was not important to the operation of the electron gun.

The pulse transformer is a 400 kilovolt, 200 ampere, 0.5 microsecond rise time transformer originally used to power an electron gun for a microwave klystron in the Stanford Linear Accelerator. It is a bifilar transformer and it can be pulsed at a repetition rate as high as 300 pulses per second. The maximum pulse length is ten microseconds and the maximum magnetic flux at transformer saturation is 3.5

volt – seconds. Although not needed for our experiments, a core bias power supply is available to obtain the peak power characteristics.

The heater power supply for the dispenser or the barium oxide coated cathode is a variac controlled, alternating current power supply in series with an isolation transformer. The power is directed through the secondary windings of the bifilar transformer, and through the step down voltage transformers. Typically, at an operating temperature of 1150 $^\circ$C, there are 10 amperes at 10 volts delivered to the thermionic cathode.

Throughout the heater supply circuit, there are small filter capacitors placed to prevent voltage transients. The pulse transformer, the filament transformers, the core bias inductor, and the filter capacitors are located within a transformer oil tank. From the interface flange at the top of the transformer oil tank to the electron gun assembly, the high voltage line is insulated by sulfur hexafluoride within a four inch PVC pipe.

4.2 THE ELECTRON GUN

The electron gun and the high voltage network are the most difficult parts of the apparatus to keep working properly. A great many problems were encountered in the construction of the high voltage interfaces between the sulfur hexafluoride container and the vacuum system. In addition, the vacuum system is barely large enough for good high voltage holdoff.

To accelerate the electrons, the cathode structure, in which the heated cathode is housed, has its potential lowered with respect to ground. The anode is at ground potential. The anode-cathode gap can be varied from 0.95 to two centimeters or more. A .550 inch diameter hole is drilled through the anode to allow the electrons to pass through. A magnetic guide field parallel to the z direction is provided. If the magnetic guide field were not present, most of the electron beam would hit the anode.

The cathode support structure is of the re-entrant variety. On the inside, the vacuum is the electrical insulator, and, on the outside, sulfur hexafluoride is the insulator.

An aluminum pipe lines the inside of the vacuum container in the vicinity of the cathode support. Without the liner, charge builds up on the pyrex vacuum vessel and arcing occurs.

The remainder of the machine in the resonator section and the diagnostics is at ground potential. The only fields to accelerate the electrons there are the magnetic pump field (to be described in the next section) and the microwave fields.

A grounding plane consisting of a wide copper strip running from the transformer tank, and beneath the pyrex vacuum system, to the resonator area is used to provide a common ground for the entire system. The ground plane effectively helps to eliminate the noise problem in the diagnostics. The ground plane, itself, is grounded to overhead water pipes, which lead to the earth outside.

4.3 THE RESONATOR STRUCTURE

The resonator structure includes the waveguide with its dielectric loading and the magnetic wiggler. This is the region where the electron beam couples to the waveguide modes.

Figure 4.2 is a general schematic of the resonator structure. The waveguide is a standard circular copper pipe. The waveguides used in the experiment had an inside diameter of either .495 inch or .373 inch. Occasionally, long waveguides were not used. The experimental set-ups for these situations are shown in figure 4.3.
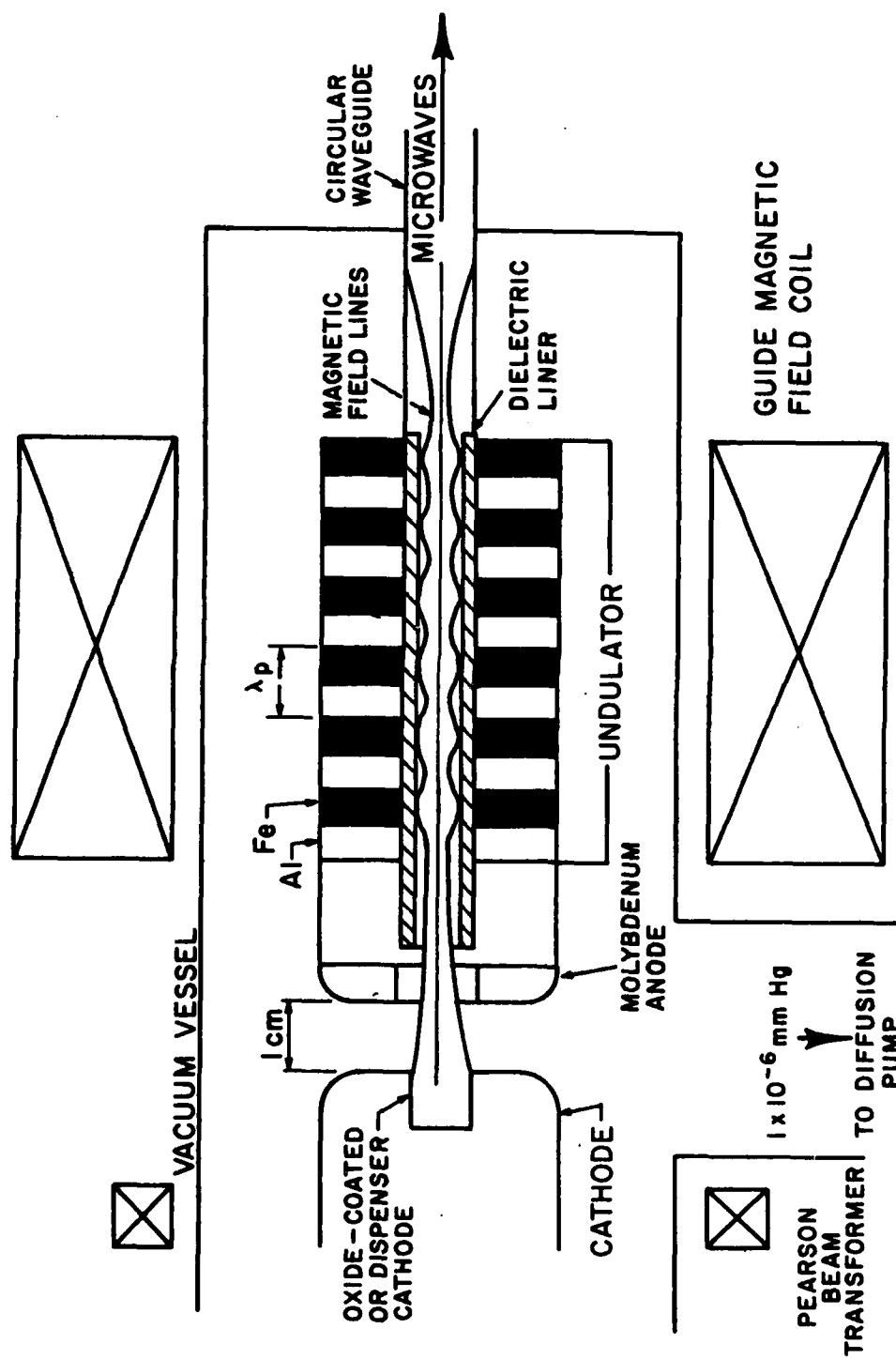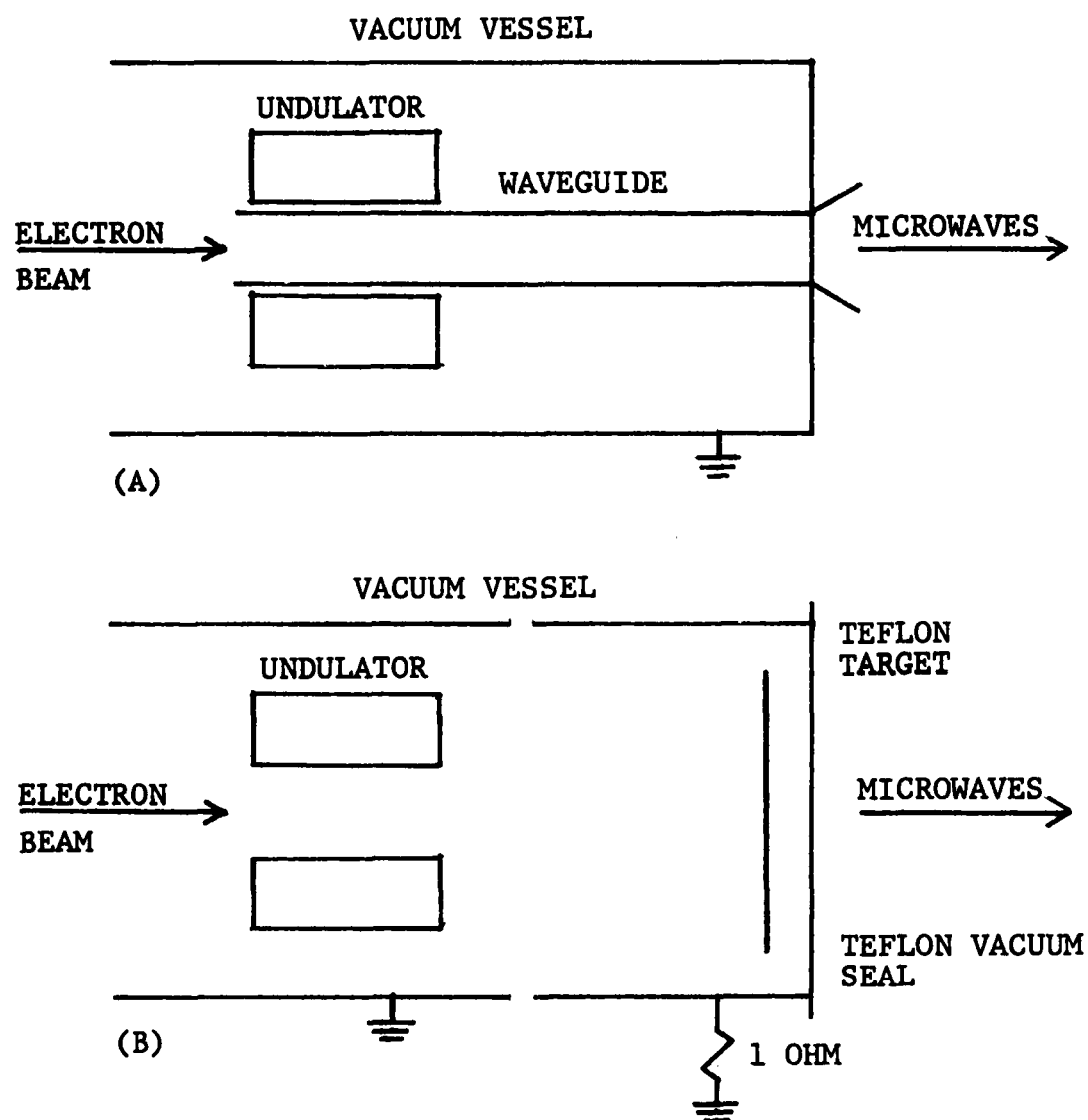
74

FIGURE 4.2 THE RESONATOR STRUCTURE [26]

FIGURES 4.3 A AND B.
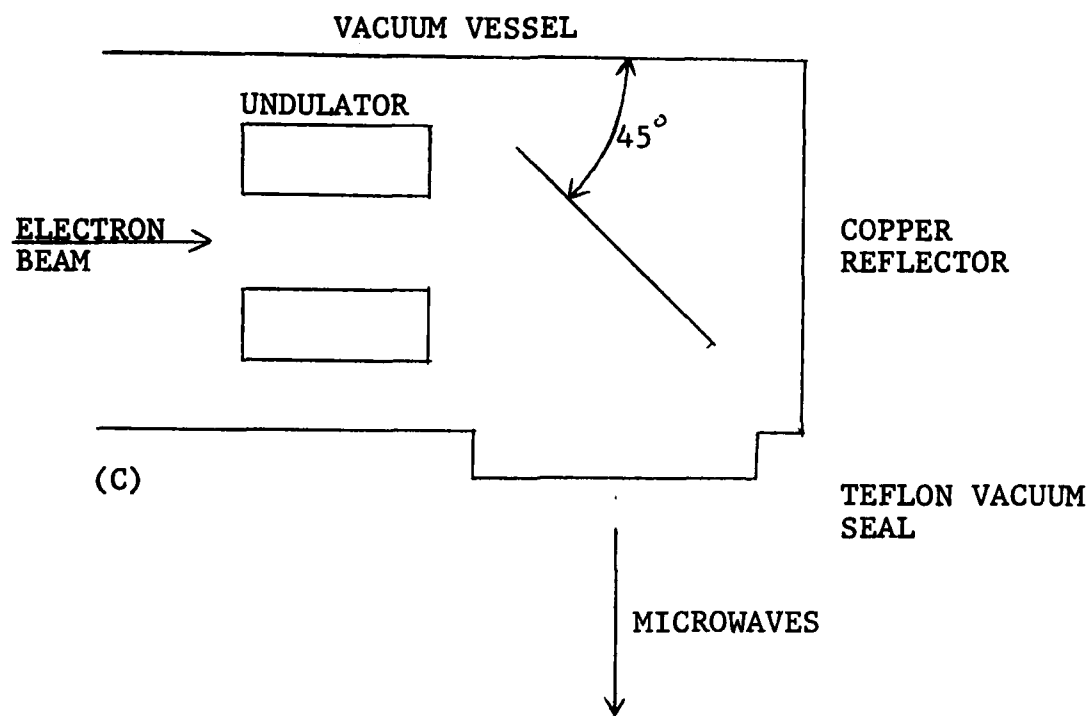
FIGURE 4.3 THE EXPERIMENTAL CONFIGURATIONS FOR THE
INTERFEROMETER EXPERIMENTS. (A) WAS USED FOR 0.495 INCH
DIAMETER AND SMALLER WAVEGUIDES. EITHER THE (B) OR (C)
CONFIGURATION WAS REQUIRED WHEN THE INSIDE OF THE UNDULATOR
WAS THE EFFECTIVE WAVEGUIDE.

On the front of the waveguide, a molybdenum electron beam mask was sometimes used to protect the annular filler within the waveguide. The annular filler was usually quartz, but plastics with low losses at microwave frequencies, such as polyethylene or polypropylene were used. Quartz is a better material than plastics because it is less easily damaged by an electron beam. For the vacuum Raman experiment no liner was used.

The magnetic wiggler or undulator is a set of alternating aluminum and iron rings located in a strong longitudinal magnetic field. The iron rings are magnetic and pull the magnetic field lines towards themselves. Inside the magnetic wiggler, rippled field lines result, as shown in figure 4.2. This is the zero frequency pump wave.

Well beyond the undulator, the field lines from the guiding magnetic longitudinal magnetic field diverge outwardly. The electrons follow these field lines into the inside wall of the waveguide or the liner. A few electrons on or near the magnetic axis will not hit the waveguide walls and may travel into the diagnostic area. To eliminate this problem, either the microwaves are guided around an H-bend and the electrons hit the metal walls or the diagnostics are located far downstream. The microwave diagnostics are outside the vacuum system. A thin teflon sheet is the vacuum seal separating the maser and the diagnostics.

4.4 THE DIAGNOSTICS

The diagnostics for the Raman and the Cerenkov-Raman experiments are simple and reliable. We can measure the electron beam accelerating voltage and current and the frequency, power, and time evolution of the scattered microwaves.

The accelerating voltage between the anode and the cathode is measured at the top of the pulse transformer by a capacitive voltage divider. The voltage divider is a model VD 500A, made by Pearson Electronics, Incorporated. Its division ratio is 10,330 to 1, and its maximum voltage capability is 500 kilovolts. The voltage divider is located in the transformer tank and is immersed in transformer oil. The output of the voltage divider leads to a BNC connection on the exterior of the transformer tank. A BNC cable then leads the output signal into an oscilloscope where the output voltage versus time is displayed.

The electron beam current is measured with a model 1010 Pearson Current Monitor Transformer. Its placement is around the electron gun, as shown in figure 4.1. The Pearson Transformer is essentially a Rogowski belt with an iron core. A signal output of 0.1 volt is equivalent to 1.0 ampere of electron beam current. The Pearson transformer and a Faraday cup, placed downstream, have good agreement in the measurement of current.

The microwave detection system consists of standard microwave detectors, attenuators, and waveguide transitions. Most of the waveguide transitions and all of the waveguide bends, attenuators, and detectors use rectangular waveguide. Transitions were used to avoid undesired reflections because we wanted the maser to operate in a superradiant mode.

The particular type of microwave detectors used were 1N26 and 1N53 diodes. The detectors are square law detectors, and, at power levels less than a few tens of milliwatts, the video output is proportional to the microwave power.

For some of our frequency measurements, we used high pass frequency filters. They are made by drilling circular holes into a brass block. Microwaves that pass through the holes must have a frequency greater than the fundamental frequency cutoff of the holes. The length of the filters was at least five free space wavelengths of the fundamental frequency cutoff to assure large attenuation of any microwaves with frequencies lower than the filter cutoff.

Some detectors were equipped with tunable micrometer stubs suitable for interferometry. The stubs are near perfect reflectors of microwaves and the amplitude of the video signal from the detectors varied with stub position. The distance between two signal maxima or minima is one-half a guide wavelength, λ_g.

A second microwave diagnostic is the Fabry-Perot interferometer shown in figure 4.4. A second moveable screen, with attached detector, is placed behind the first screen. Since each screen is only partially reflecting, a microwave resonance can be set up by adjusting the relative positions of the two screens. As the moveable screen is translated further downstream, the detector signal will be a series of maxima and minima, corresponding to resonances and anti-resonances, respectively. The distance between two maxima or minima is one half a free space wavelength. This diagnostic has proven useful to measure the wavelengths of two or more modes that exist concurrently in the microwave output.

This concludes the discussion of the experimental apparatus. The experimental results are presented in chapter five.

MICROWAVES

FIXED SCREEN   MOVEABLE SCREEN WITH DETECTOR
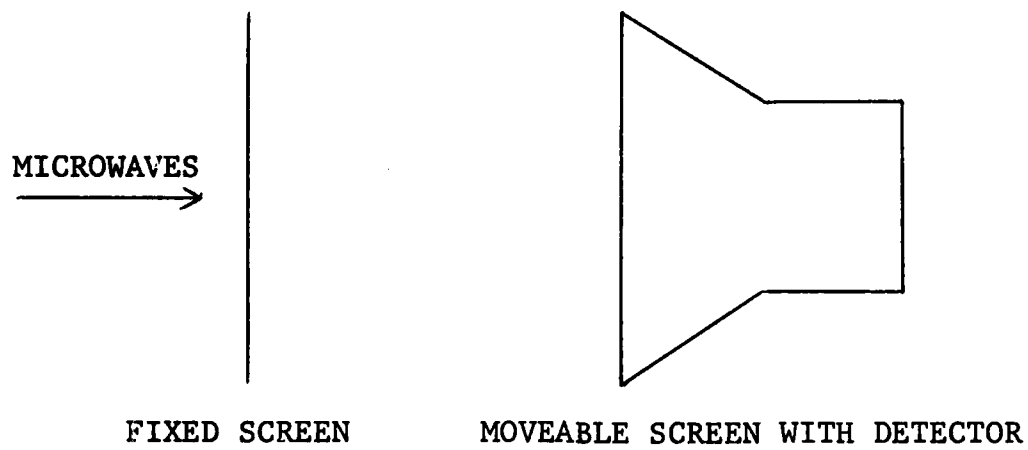
FIGURE 4.4   THE FABRY-PEROT INTERFEROMETER

CHAPTER 5

THE EXPERIMENTAL RESULTS

In this chapter, we will discuss and analyse the experimental data. We have detected vacuum Raman radiation due to both electron cyclotron and electron plasma waves and Cerenkov-Raman radiation due to electron cyclotron waves. In the first section, we review our preliminary data, which verifies the existence of the lower branch of vacuum Raman scattering by means of an in-guide interferometer. The data of the observation of the upper branch of this interaction are presented in the following section. The free space interferometer results are listed in the third section. With this interferometer, we measured the output frequency spectrum as a function of the electron energy and the magnetic field.

Next, the problems inherent in obtaing Cerenkov-Raman radiation are discussed in the fourth section. The data for the lower and the upper branches of this interaction are discussed in the fifth and sixth sections. In the final section, the scattered microwave turn-on voltage is measured as a function of the magnetic field. This data is consistent with the Cerenkov-Raman theory.

The conclusions of this research are stated in chapter
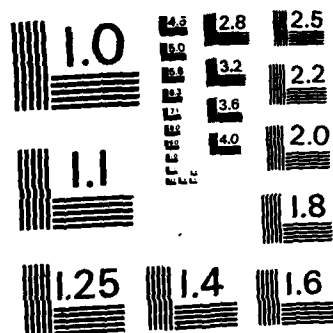
MICROCOPY RESOLUTION TEST CHART

NATIONAL BUREAU OF STANDARDS-1963-A

six. Interesting experimental observations are presented in the appendices.

First, we will briefly discuss the diagnostics. Our diagnostics for microwave detection and electron beam parameter measurement are simple and accurate. To calculate the microwave frequency, we measured either a free space wavelength or a waveguide wavelength with an interferometer located outside in the laboratory room or inside a rectangular waveguide detector mount, respectively. We have not developed the technique of measuring the waveguide wavelength inside of the cylindrical resonator where the microwaves are produced, but this technique would have little advantage over the above mentioned interferometry. The free space wavelength measurement is accurate to $\pm.1$ millimeters, and the waveguide wavelength measurement is accurate to $\pm.003$ inches.

The advantage of the in-guide interferometer is that it is easier to obtain consistent data and that the timing of the microwave pulse can be correlated with the electron beam voltage and current. Its disadvantage is that it does not have good discrimination at frequencies above the recommended waveband. Higher order modes can result and it is difficult to tell which modes are present.

Since the dominate microwave output was within the recommended waveband, this interferometer gave consistent measurements. For the vacuum Raman experiments using a .495

inch diameter waveguide, the mean measured frequency was about 28 gigahertz. The range of frequencies was from 27.5 gigahertz to 28.8 gigahertz, measured during six different runs performed during a one month period. These frequencies correspond to the $TE_{01}{}^{42}$ mode cutoff.

Similar vacuum Raman experiments were done with a .373 inch diameter waveguide. For two runs, the frequency range of the dominate mode was from 37.0 to 37.2 gigahertz. These frequencies correspond to the TE_{01} mode cutoff also.

The advantage of the free space interferometer is that it measures the wavelength of plane waves. One need not worry about higher order mode problems. The microwaves pass out of the circular waveguide, with or without a horn, and into the laboratory. Between each pulse of the Raman maser, the etalon spacing in the interferometer changes. The microwave pulse height and the etalon spacing, via a potentiometer voltage, is recorded on an oscilloscope. The maximum microwave signal occurs when the microwave frequency is the resonance frequency of the etalon.

The main disadvantage of this technique is that each interferogram requires one hundred shots. The Raman maser must work consistently well throughout the interferogram. If the electron beam parameters or the magnetic field should drift, the microwave frequency could vary. The relative timing between the microwave output and the voltage and current pulse must be determined separately before or after

the interferometer scan. These interferometer measurements will be presented later in this chapter.

The electron beam mode frequency and wavenumber cannot be measured directly. The electron cyclotron frequency can be determined by measuring the magnitude of the guiding magnetic field. The electron plasma frequency can be calculated knowing the electron beam current and velocity. The fundamental wavelength of the magnetic wiggler is the period between the magnetic disks. The magnitude of the magnetic undulations is measured by a magnetic probe.

The electron beam velocity can be calculated from the electron beam accelerating voltage. This voltage is that at the output of of the pulse transformer, as measured by a capacitive voltage divider. I estimate that the actual electron beam kinetic energy is well within ten percent of that recorded by the capacitive voltage divider.

The electron beam current measured by the Pearson Transformer is within five percent of the actual electron beam current. A Faraday cup, which is an electron beam collector, placed downstream behind the anode recorded the same magnitude of electron beam current as did the Pearson transformer.

DISTANCE FROM MAGNET COIL TO MIDPLANE (CENTIMETERS)

FIGURE 5.1 A THE LONGITUDINAL MAGNETIC FIELD PROFILE OF THE SEVEN UNDULATION, ONE CENTIMETER PERIOD MAGNETIC WIGGLER AS A FUNCTION OF DISTANCE ALONG THE MAGNET COIL AXIS. THE MEAN OF THE MAGNETIC FIELD MAXIMUMS AND MINIMUMS IS 3.63 GAUSS/AMPERE. THE MEAN PEAK TO PEAK UNDULATION IS 0.91 GAUSS/AMPERE, RESULTING IN A MEAN MODULATION OF 25 PERCENT.

87

DISTANCE FROM THE MAGNET COIL MIDPLANE (CENTIMETERS)
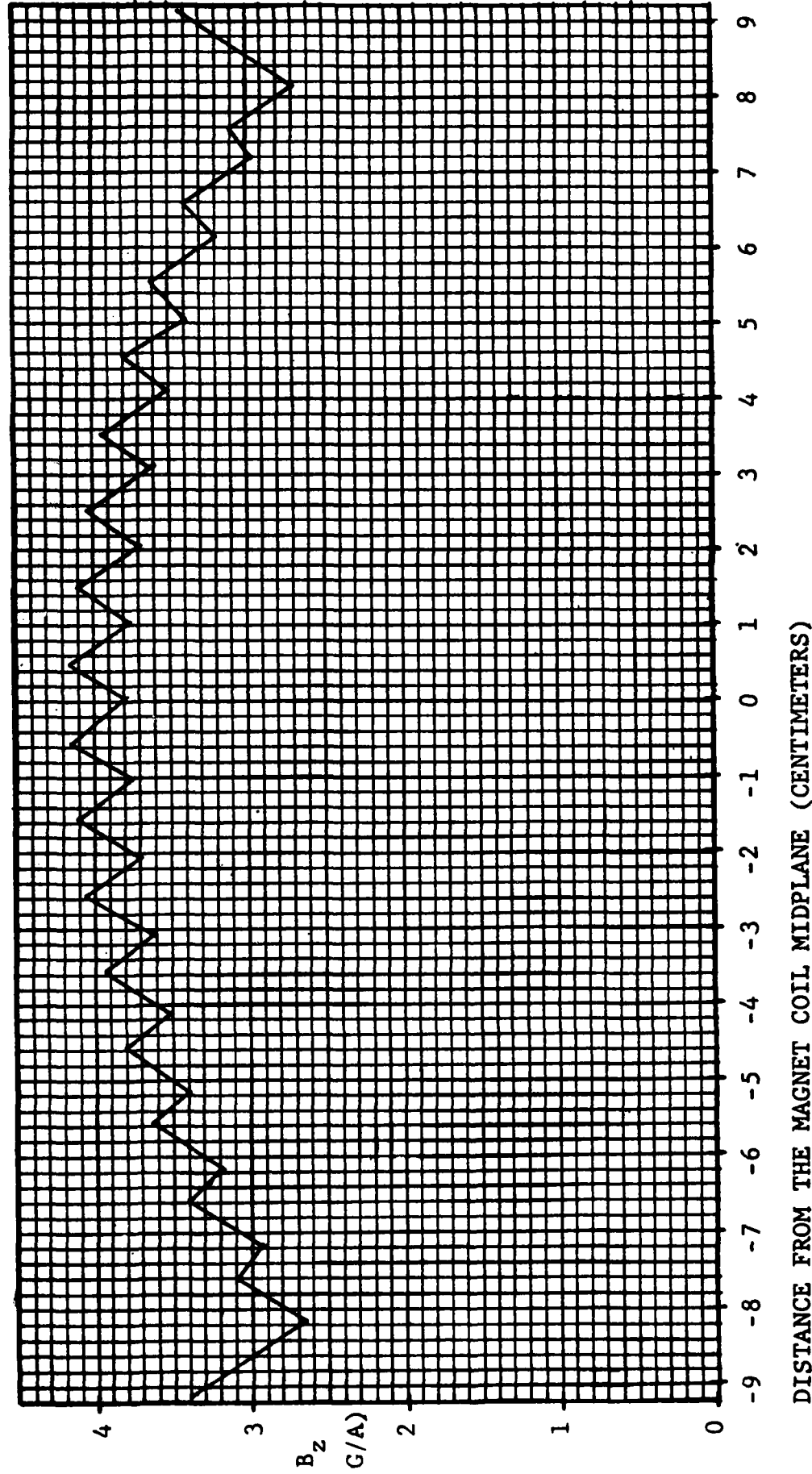
FIGURE 5.1 B THE LONGITUDINAL MAGNETIC FIELD PROFILE OF THE SEVENTEEN UNDULATION, ONE CENTI-
METER PERIOD MAGNETIC WIGGLER AS A FUNCTION OF DISTANCE ALONG THE MAGNET COIL AXIS. THE MEAN
OF THE MAGNETIC FIELD MAXIMUMS AND MINIMUMS IS 3.56 GAUSS/AMPERE. THE MEAN PEAK TO PEAK UNDU-
LATION IS 0.37 GAUSS/AMPERE, RESULTING IN A MEAN MODULATION OF 10 PERCENT.
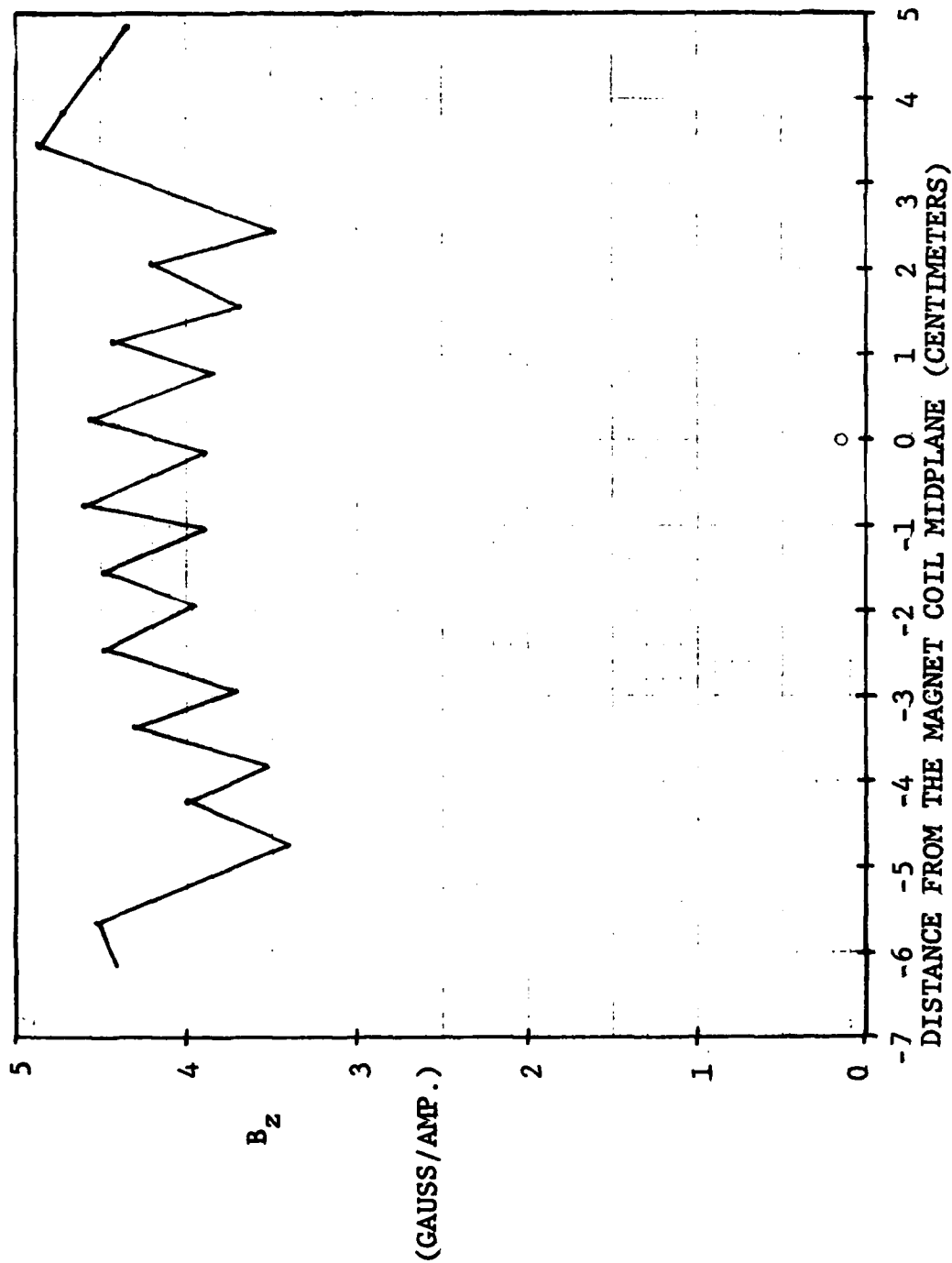
FIGURE 5.1C THE LONGITUDINAL MAGNETIC FIELD PROFILE OF THE NINE UNDULATION, 0.91 CENTIMETER PERIOD MAGNETIC WIGGLER AS A FUNCTION OF DISTANCE ALONG THE MAGNET COIL AXIS. THE MEAN OF THE MAGNETIC FIELD MAXIMUMS AND MINIMUMS IS 4.10 GAUSS/AMPERE. THE MEAN PEAK TO PEAK UNDULATION IS 0.69 GAUSS/AMPERE, RESULTING IN A MEAN MODULATION OF 17 PERCENT.
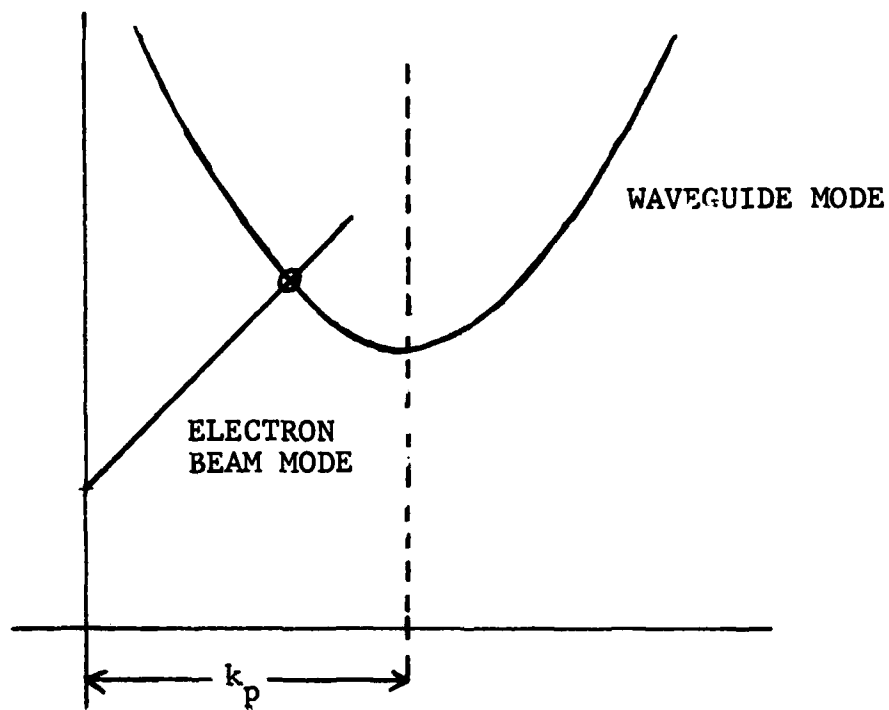
FIGURE 5.2 THE DISPERSION RELATIONS OF THE ELECTRON BEAM
MODE, THE PUMP WAVE, AND THE WAVEGUIDE MODE FOR THE RAMAN
INTERACTION.

FIGURE 5.3 THE MICROWAVE FREQUENCY VS. ACCELERATING VOLTAGE FOR THE VACUUM RAMAN INTERACTION. THE FAST ELECTRON CYCLOTRON BEAM MODE AND THE TE_{01} WAVEGUIDE MODE SOLUTION IS SHOWN.

λ_p = 1.01 CENTIMETERS

B = 5720 GAUSS

ν_{co} = 29.1 GIGAHERTZ

Identical vacuum Raman experiments were performed with a seventeen period, 1.01 centimeter wavelength undulator. As shown in figure 5.1B, its peak to peak undulation is ten percent of the guiding magnetic field. The output microwave frequencies ranged from 27.5 gigahertz to 28.8 gigahertz. The microwave frequencies were the same whether the guiding magnetic field was parallel or antiparallel to the electron beam velocity.

Additional experiments were conducted with the same undulator, but with a .373 inch diameter waveguide. The observed microwave frequencies then ranged from 37.0 gigahertz to 37.2 gigahertz over electron kinetic energies from 71 KeV to 95 KeV. The electron beam currents were from six to seven amperes. Once again, the microwave frequencies are comparable to the TE_{01} waveguide cutoff of 38.9 gigahertz. The instability is due to fast electron cyclotron waves. We will discuss the observation of higher frequencies in the next section

5.2 HIGHER FREQUENCY BRANCHES OF THE VACUUM RAMAN INTERACTION

With the use of high pass frequency filters, we have determined the existence of microwaves with frequencies in excess of the waveguide cutoff. These frequencies are due

to an electron cyclotron beam mode interacting with the third harmonic of the pump wave. The Frequency vs Accelerating Voltage graph for this interaction is shown in figure 5.4. Since the data points represent the lowest possible observed frequencies, the fast ele' 'on cyclotron solution is adequate for the explanation o 'he data. The lower branch of the interaction for the idamental pump wavelength is at a lower frequency than t ic of the data. The data points at 49.3 gigahertz are probably due to an interaction of the fifth harmonic of the pump wave.

5.3 VACUUM RAMAN INTERFEROMETER DATA

There have been several sets of runs with a free space interferometer as the microwave diagnostic. All these runs have been with the 0.91 centimeter wavelength, nine period magnetic rippler, whose magnetic field profile is shown in figure 5.1C. The accelerating voltage and the magnetic field strength were the parameters that were varied. The electron beam current also varied.

The main trends in the data to follow are that the strongest interactions are between a fast electron cyclotron beam mode or an electron plasma mode driving a scattered wave near the cutoff frequency region of the waveguide mode.

The data and the analysis will be presented in tabular

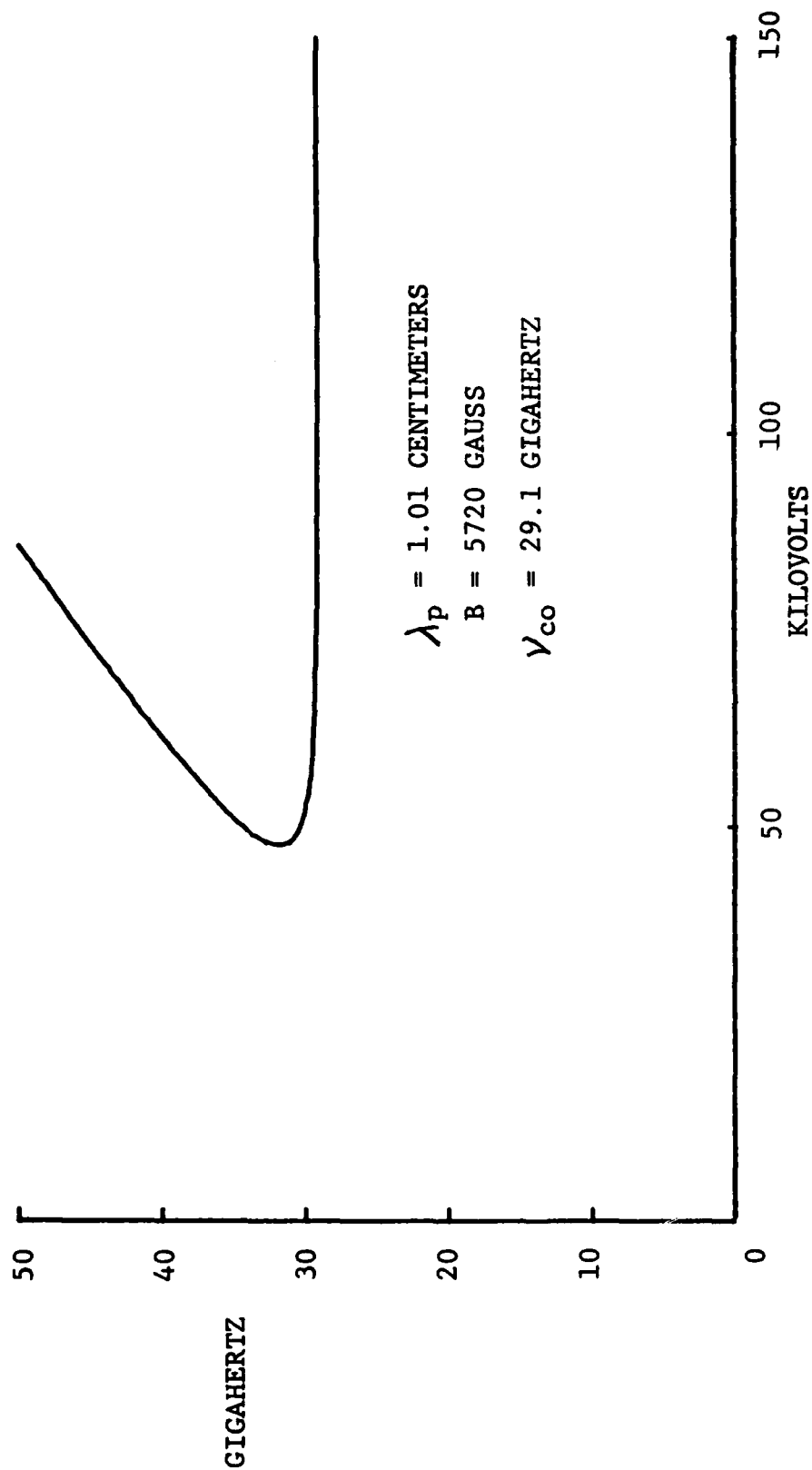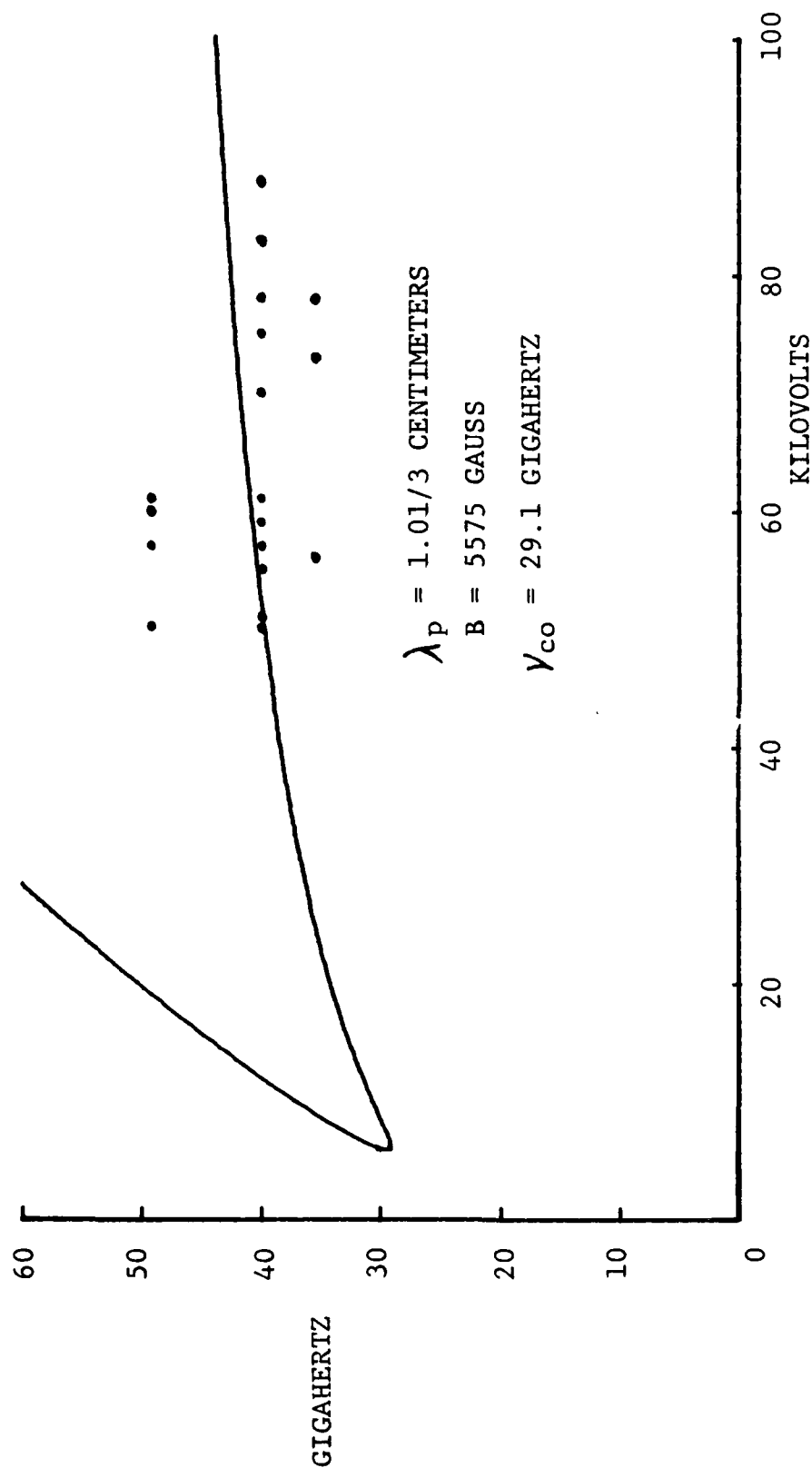FIGURE 5.4 THE MICROWAVE FREQUENCY VS. ACCELERATING VOLTAGE FOR THE VACUUM RAMAN INTERACTION. THE FAST ELECTRON CYCLOTRON BEAM MODE AND THE TE_{01} WAVEGUIDE MODE SOLUTION IS SHOWN. THE HIGH PASS FREQUENCY DATA IS FROM 3/11/79 - 4/11/79.

form. We were not always able to hold all but one parameter constant and determine the microwave frequency as a function of this one parameter.

The general equation for the frequency at synchronism is:

$$\omega = \frac{1}{(1-\epsilon\beta_o^2)}\left[(k_p v_o - W) \pm \sqrt{\epsilon}\beta_o\sqrt{(k_p v_o - W)^2 - \frac{\omega_{k_o}^2}{\epsilon}(1-\epsilon\beta_o^2)}\right] \quad (5.1)$$

where

$$W = \pm\frac{eB_o}{\gamma_o m c}$$

or

$$W = \pm\left(\frac{4\pi n_o e^2}{\gamma_o^3 m}\right)$$

For notational simplicity, I will define +, - interactions as those frequencies calculated using the +, - sign in (5.1), respectively.

The first interferometer data is shown in figure 5.5. The large peaks correspond to a frequency of 36 gigahertz, whereas the smaller peaks correspond to a frequency of 42 gigahertz. With an experimental peak accelerating voltage of 73 kilovolts and a peak current of 10 amperes, table 5.1 lists the possible interactions for the frequencies observed. The frequencies listed in table 5.1 are those calculated from the synchronism condition, (5.1)

VACUUM RAMAN SCATTERING

ACCELERATING
VOLTAGE   50 KV/DIV.

ELECTRON BEAM
CURRENT   6 A/DIV.
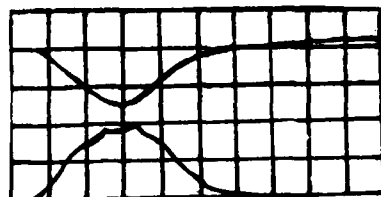
1 MICROSECOND/DIV.

INTERFEROMETER

MICROWAVES   50 mV/DIV.

0 mm ——————————————— 17.5 mm
3.4 mm ——————————————— 16.7 mm
5.4 mm ——————————————— 14.2 mm
6.9 mm ——————————————— 12.7 mm
8.8 mm ——————————————— 10.6 mm
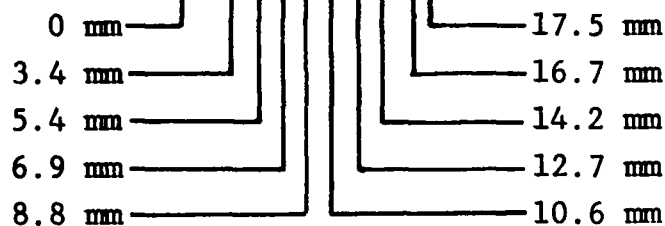
B = 6360 GAUSS

FIGURE 5.5   INTERFEROMETER DATA OF 12/3/79,#4C,D.
VACUUM RAMAN SCATTERING IN A 9 PERIOD, 0.9 CENTI-
METER WAVELENGTH MAGNETIC WIGGLER AND A .495 INCH
DIAMETER CIRCULAR WAVEGUIDE.

TABLE 5.1 POSSIBLE INTERACTIONS FOR THE DATA OF 12/3/79,#4C,D.

OBSERVED FREQUENCIES: 36, 42 GIGAHERTZ

73 KILOVOLTS, 10 AMPERES, 6360 GAUSS

λ_p = .303 CENTIMETERS, - INTERACTION

WAVEGUIDE MODE	FAST CYCLOTRON WAVE (GHZ)	FAST PLASMA WAVE (GHZ)	SLOW PLASMA WAVE (GHZ)
TE_{11}	43.5	33.6	33.0
TM_{01}	44.0	34.3	33.7
TE_{21}	44.9	35.4	34.8
TM_{11} OR TE_{01}	46.1	37.2	36.6
TE_{31}	46.8	38.2	37.6
TM_{21}	49.1	41.6	41.2

The microwave production is due to the interaction of several waveguide modes. The plasma frequency is less than one gigahertz, and the separation between the fast and slow plasma mode frequencies is smaller than the experimental error. Fom table 5.1, we know that plasma waves are present. Since the cyclotron frequency is about 15 gigahertz, the separation between the fast and slow cyclotron mode frequencies is large enough so that we can experimentally distinguish · two modes. From table 5.1, we see that a fast cyclo is present.

Three s ent runs are shown in figures 5.6, 5.7, and 5.8, and the prominant $\lambda/2$'s are 4.3 mm, 4.6[+] mm, and 4.3 mm, respectively; corresponding to frequencies of 35, 32, and 35 gigahertz, respectively. The peak accelerating voltages and currents were held nearly constant throughout

VACUUM RAMAN SCATTERING

ACCELERATING
VOLTAGE

ELECTRON BEAM
CURRENT
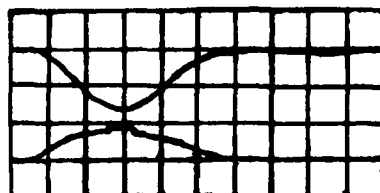
50 KV/DIV.

6 A/DIV.

1 MICROSECOND/DIV.

INTERFEROMETER

MICROWAVES
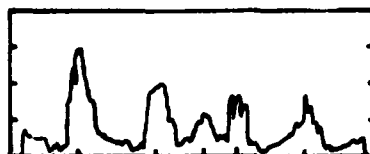
5 mV/DIV.

0 mm ———————————— 12.4 mm
4.3 mm ———————————— 8.6 mm
6.8 mm ————————————

B = 6970 GAUSS

FIGURE 5.6   INTERFEROMETER DATA OF 12/3/79,#5A,B.
VACUUM RAMAN SCATTERING IN A 9 PERIOD, 0.9 CENTI-
METER WAVELENGTH MAGNETIC WIGGLER AND A .495 INCH
DIAMETER CIRCULAR WAVEGUIDE.

VACUUM RAMAN SCATTERING

INTERFEROMETER

MICROWAVES   5 mV/DIV.

0 mm ——————13.9 mm
3.5 mm —————10.4 mm
7.8 mm —————7.3 mm
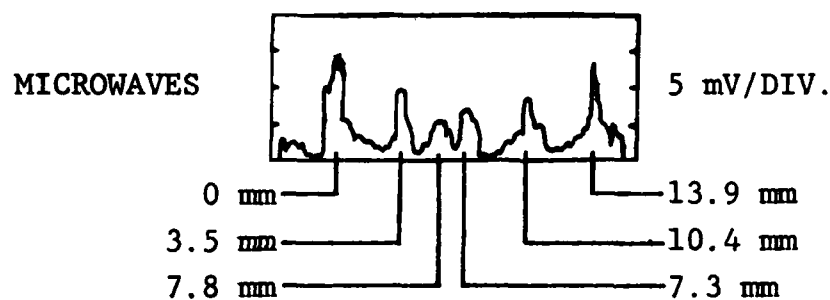
B = 6830 GAUSS

FIGURE 5.7   INTERFEROMETER DATA OF 12/3/79,#5C.
VACUUM RAMAN SCATTERING IN A 9 PERIOD, 0.9 CENTI-
METER WAVELENGTH MAGNETIC WIGGLER AND A .495 INCH
DIAMETER CIRCULAR WAVEGUIDE.

VACUUM RAMAN SCATTERING

ACCELERATING
VOLTAGE

ELECTRON BEAM
CURRENT

50 KV/DIV.

6 A/DIV.

1 MICROSECOND/DIV.

INTERFEROMETER

MICROWAVES

5 mV/DIV.

0 mm — 16.4 mm

4.3 mm — 12.8 mm

6.7 mm — 8.7 mm
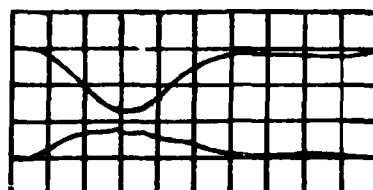
B = 6680 GAUSS

FIGURE 5.8   INTERFEROMETER DATA OF 12/3/79,#5D,E.
VACUUM RAMAN SCATTERING IN A 9 PERIOD, 0.9 CENTI-
METER WAVELENGTH MAGNETIC WIGGLER AND A .495 INCH
DIAMETER CIRCULAR WAVEGUIDE.

these three runs. Only the magnetic field was varied. It should be noted from the bumps on the current trace, in figure 5.8, that microwaves were emitted at two different times. Both occurances will be analysed. Tables 5.2, 5.3, and 5.4 list the interactions.

TABLE 5.2 POSSIBLE INTERACTIONS FOR THE DATA OF 12/3/79,#5A,B.

OBSERVED FREQUENCY: 35 GIGAHERTZ

80 KILOVOLTS, 4 AMPERES, 6970 GAUSS

λ_p = .303 CENTIMETERS, - INTERACTION

WAVEGUIDE MODE	FAST PLASMA WAVE (GHZ)	SLOW PLASMA WAVE (GHZ)
TE_{11}	34.3	33.9
TM_{01}	35.0	34.6
TE_{21}	36.1	35.7
TM_{11} OR TE_{01}	37.8	37.5
TE_{31}	38.8	38.5

Once again, it appears that there is either a fast or a slow plasma mode is coupling to the Raman interaction. This time the fast cyclotron mode would occur at approximately 45 gigahertz, but it was not observed.

TABLE 5.3 POSSIBLE INTERACTIONS FOR THE DATA OF 12/3/79,#5C.

OBSERVED FREQUENCY: 32 GIGAHERTZ

81 KILOVOLTS, 4 AMPERES, 6830 GAUSS

λ_p = .303 CENTIMETERS, - INTERACTION

WAVEGUIDE MODE	FAST PLASMA WAVE (GHZ)	SLOW PLASMA WAVE (GHZ)	SLOW CYCLOTRON WAVE (GHZ)
TE_{11}	34.4	34.0	
TM_{01}	35.1	34.7	
TE_{21}	36.2	35.8	
TM_{11} OR TE_{01}	37.9	37.6	
TE_{31}	38.9	38.6	31.9

λ_p = .91 CENTIMETERS, - INTERACTION

WAVEGUIDE MODE	FAST CYCLOTRON WAVE (GHZ)
TM_{11} OR TE_{01}	29.8
TE_{31}	31.9

The plasma wave interaction may still be present. Now, fast and slow cyclotron waves result in frequencies consistent with the data.

TABLE 5.4 POSSIBLE INTERACTIONS FOR THE DATA OF 12/3/79,#5D,E.

OBSERVED FREQUENCY: 35 GIGAHERTZ

81 KILOVOLTS,4 AMPERES, 6680 GAUSS

λ_p = .303 CENTIMETERS, - INTERACTION

WAVEGUIDE MODE	FAST PLASMA WAVE (GHZ)	SLOW PLASMA WAVE (GHZ)	SLOW CYCLOTRON WAVE (GHZ)
TE_{11}	34.4	34.0	
TM_{01}	35.1	34.7	
TE_{21}	36.2	35.8	
TM_{11} OR TE_{01}	37.9	37.6	
TE_{31}	38.9	38.6	32.0

λ_p = .91 CENTIMETERS, - INTERACTION

WAVEGUIDE MODE	FAST CYCLOTRON WAVE (GHZ)
TE_{31}	31.9

73 KILOVOLTS, 4 AMPERES, 6680 GAUSS

λ_p = .303 CENTIMETERS, - INTERACTION

WAVEGUIDE MODE	FAST PLASMA WAVE (GHZ)	SLOW PLASMA WAVE (GHZ)
TE_{11}	33.5	33.1
TM_{01}	34.2	33.8
TE_{21}	35.3	34.9
TM_{11} OR TE_{01}	37.1	36.7
TE_{31}	38.1	37.7

λ_p = .91 CENTIMETERS, - INTERACTION

WAVEGUIDE MODE	FAST CYCLOTRON WAVE (GHZ)
TE_{31}	31.8

As throughout the previous data of 12/3/79, it appears that plasma waves are responsible for the bulk of the microwaves observed. From figure 5.5, there is definite evidence of fast cyclotron waves contributing radiation in the 45 gigahertz frequency range.

On 12/19/79, we continued the vacuum Raman experiments as a confirmation of our earlier work in 12/3/79. Although the interferograms of figures 5.9, 5.10, and 5.11 appear to be more complex, they are no more difficult to analyse than the previous interferograms.

From figure 5.9, tne two dominate $\lambda/2$'s are 4.9 mm and 3.15 mm, corresponding to 31 and 48 gigahertz, respectively. From figure 5.10, the single dominate $\lambda/2$ is 5.3 mm, corresponding to 28 gigahertz. The interferogram of figure 5.11 gives the most complicated spectrum. The frequencies that appear are 21, 26, 28, and 42 gigahertz. 26 and 28 gigahertz are close together, yet each is distinguishable on the interferogram ($\lambda/2$ = 5.7 and 5.4 mm, respectively). 42 gigahertz could be a harmonic of 21 gigahertz and not an independent frequency. But we will not exclude either frequency . Tables 5.5, 5.6, and 5.7 list the possible interactions for the data of figures 5.9, 5.10, and 5.11, respectively.

VACUUM RAMAN SCATTERING

ACCELERATING
VOLTAGE   20 KV/DIV.

ELECTRON
BEAM   6 A/DIV.
CURRENT

WR-28
MICROWAVES   115 mV/DIV.

1 MICROSECOND/DIV.

INTERFEROMETER

MICROWAVES   115 mV/DIV.

```
    0 mm                                       20.8 mm
  1.1 mm                                       19.4 mm
  1.9 mm                                       17.3 mm
  4.7 mm                                       16.5 mm
  6.8 mm                                       14.5 mm
  7.8 mm            9.6 mm                     11.6 mm
                                               10.9 mm
```

B = 6150 GAUSS
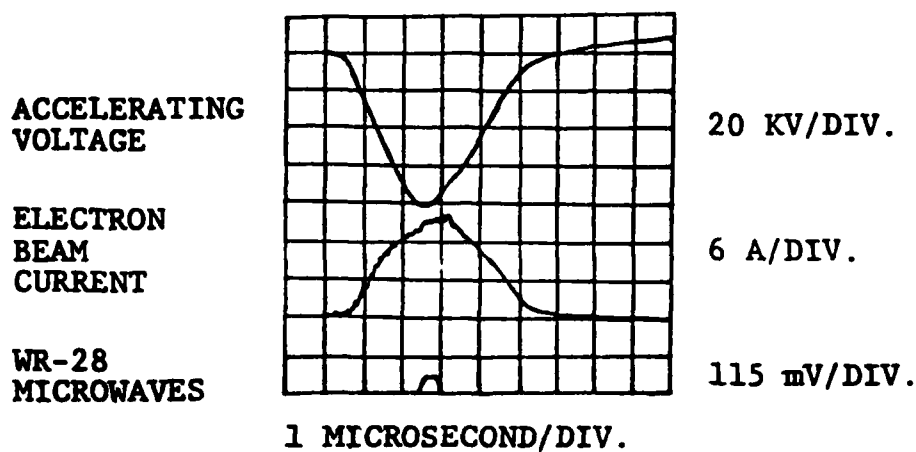
FIGURE 5.9   INTERFEROMETER DATA OF 12/19/79,
#7,8 AND RUN 4. VACUUM RAMAN SCATTERING IN A
9 PERIOD, 0.9 CENTIMETER WAVELENGTH MAGNETIC
WIGGLER AND A .495 INCH DIAMETER CIRCULAR
WAVEGUIDE.

VACUUM RAMAN SCATTERING

ACCELERATING VOLTAGE — 50 KV/DIV.

ELECTRON BEAM CURRENT — 6 A/DIV.

WR-28 MICROWAVES — 115 mV/DIV.

1 MICROSECOND/DIV.

INTERFEROMETER

MICROWAVES — 115 mV/DIV.

0 mm — 21.1 mm
1.9 mm — 17.5 mm
5.2 mm — 15.8 mm
10.3 mm — 12.2 mm

B = 6520 GAUSS

FIGURE 5.10 INTERFEROMETER DATA OF 12/19/79, #15,17, AND RUN 9. VACUUM RAMAN SCATTERING IN A 9 PERIOD, 0.9 CENTIMETER WAVELENGTH MAGNETIC WIGGLER AND A .495 INCH DIAMETER CIRCULAR WAVEGUIDE.

VACUUM RAMAN SCATTERING

ACCELERATING
VOLTAGE   20 KV/DIV.

ELECTRON
BEAM   6 A/DIV.
CURRENT

1 MICROSECOND/DIV.

INTERFEROMETER

MICROWAVES   11 mV/DIV.

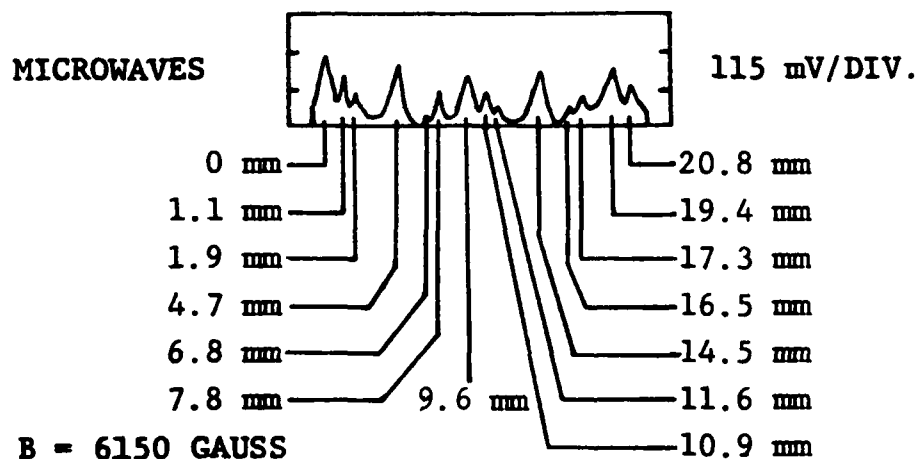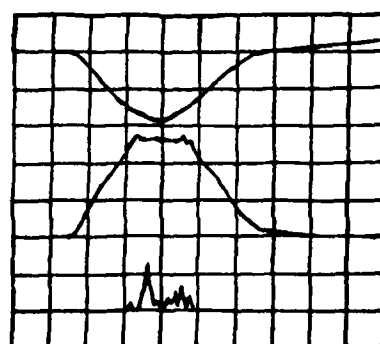| 0 mm | | 23.1 mm |
1.7 mm		21.6 mm
2.3 mm		19.5 mm
5.3 mm		16.1 mm
8.8 mm		12.3 mm
10.8 mm		
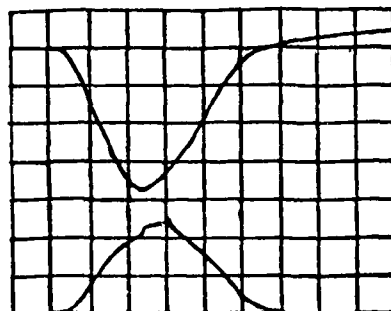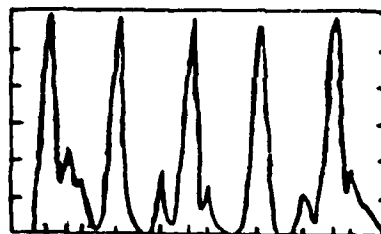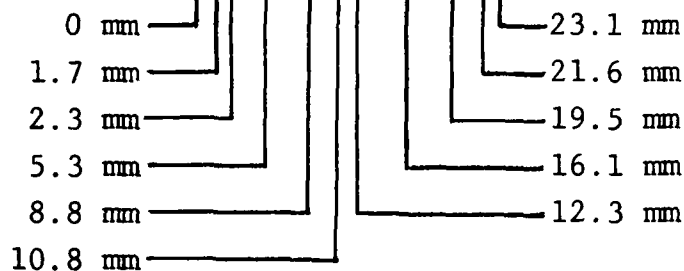
B = 5970 GAUSS

FIGURE 5.11 INTERFEROMETER DATA OF 12/19/79,
#21 AND RUN 11. VACUUM RAMAN SCATTERING IN A
9 PERIOD, 0.9 CENTIMETER WAVELENGTH MAGNETIC
WIGGLER AND A .495 INCH DIAMETER CIRCULAR
WAVEGUIDE.

TABLE 5.5 POSSIBLE INTERACTIONS FOR THE DATA OF 12/19/79, RUN 4.

79 KILOVOLTS, 14 AMPERES, 6150 GAUSS

OBSERVED FREQUENCIES: 31, 48 GIGAHERTZ

λ_p = .91 CENTIMETERS, - INTERACTION

TE_{11} WAVEGUIDE MODE	SLOW PLASMA WAVE	28.1 GHZ	
TE_{01} WAVEGUIDE MODE	FAST CYCLOTRON WAVE	29.4 GHZ	

λ_p = .303 CENTIMETERS, - INTERACTION

WAVEGUIDE MODE	FAST CYCLOTRON WAVE (GHZ)	FAST PLASMA WAVE (GHZ)	SLOW PLASMA WAVE (GHZ)	SLOW CYCLOTRON WAVE (GHZ)
TE_{11}	43.7	34.3	33.6	
TM_{01}	44.2	35.0	34.3	
TE_{21}	45.0	36.1	35.5	
TM_{11} OR TE_{01}	46.3			30.3
TE_{31}	47.0			32.2
TM_{21}	49.3			

This time, it appears that the data is due to fast and slow cyclotron beam modes interacting with TE_{01} and nearby waveguide modes with an effective λ_p = .303 centimeters.

For the data of figure 5.10, we will consider both the turn-on accelerating voltage for microwave production of 69 kilovolts and the peak voltage of 79 kilovolts.

TABLE 5.6 POSSIBLE INTERACTIONS FOR THE DATA OF 12/19/79, RUN 9.

69 KILOVOLTS, 13 AMPERES, 6520 GAUSS

OBSERVED FREQUENCY: 28 GIGAHERTZ

λ_p = .91 CENTIMETERS, - INTERACTION

WAVEGUIDE MODE	FAST CYCLOTRON WAVE (GHZ)
TE_{11}	23.0
TM_{01}	24.1
TE_{21}	26.0
TM_{11} OR TE_{01}	29.5
TE_{31}	NO INTERACTION

λ_p = .303 CENTIMETERS, - INTERACTION

WAVEGUIDE MODE	FAST CYCLOTRON WAVE (GHZ)
TE_{21}	25.6
TM_{11} OR TE_{01}	29.3
TE_{31}	31.9

79 KILOVOLTS, 13 AMPERES, 6520 GAUSS

λ_p = .91 CENTIMETERS, - INTERACTION

WAVEGUIDE MODE	FAST CYCLOTRON WAVE (GHZ)
TE_{11}	23.1
TM_{01}	24.3
TE_{21}	26.2
TM_{11} OR TE_{01}	29.6
TE_{31}	31.8
TM_{21}	NO INTERACTION

λ_p = .303 CENTIMETERS, - INTERACTION

WAVEGUIDE MODE	SLOW CYCLOTRON WAVE (GHZ)
TE_{11}	23.9
TM_{01}	25.1
TE_{21}	26.9
TM_{11} OR TE_{01}	30.0
TE_{31}	32.0
TM_{21}	NO INTERACTION

Both the fast cyclotron waves and the slow cyclotron waves give the correct range of frequencies. But the fast cyclotron modes occur with the fundamental pump wavelength and, therefore, should dominate.

For the data of run 11, as shown in figure 5.11, we must allow for a broad spectrum of frequencies, ranging from 21 to 42 gigahertz.

TABLE 5.7 POSSIBLE INTERACTIONS FOR THE DATA OF 12/19/79, RUN 11.

76 KILOVOLTS, 13 AMPERES, 5970 GAUSS

OBSERVED FREQUENCIES: 21,26,28,42 GIGAHERTZ

λ_p = .91 CENTIMETERS, - INTERACTION

WAVEGUIDE MODE	FAST CYCLOTRON WAVE (GHZ)
TE_{11}	22.2
TM_{01}	23.5
TE_{21}	25.5
TM_{11} OR TE_{01}	29.3
TE_{31}	NO INTERACTION

λ_p = .91 CENTIMETERS, + INTERACTION

TE_{11} WAVEGUIDE MODE, SLOW PLASMA WAVE   27.1 GHZ

λ_p = .303 CENTIMETERS, - INTERACTION

WAVEGUIDE MODE	FAST CYCLOTRON WAVE (GHZ)	SLOW CYCLOTRON WAVE (GHZ)
TE_{11}	43.1	24.3
TM_{01}	43.7	25.4
TE_{21}	44.5	30.2
TM_{01} OR TE_{01}	45.8	30.2
TE_{31}	46.5	32.1

These results are a little more difficult to compare with the theory. The strongest interaction was at 28 gigahertz, corresponding to λ_p = 0.91 centimeters, a TE_{01} waveguide mode, and a fast electron cyclotron wave. The remaining frequencies were at lower power and correspond to fast cyclotron waves and a slow plasma wave at the fundamental pump wavelength. Fast and slow cyclotron waves could also exist with λ_p = .303 centimeters, but are less likely than

the beam modes described above.

Throughout the runs of 12/19/79, the observed frequencies are predominately due to fast cyclotron waves interacting with the microwave fields via the 0.91 centimeter pump. During the 12/3/79 runs, the observed frequencies were primarily due to plasma waves coupling to the microwave fields via the third harmonic of the 0.91 centimeter pump. The two experiments were similarly conducted. The accelerating voltages were similar in magnitude. The 12/19/79 runs had about twice the electron beam current as the 12/3/79 runs. The anomalous current rises were more pronounced on 12/19/79, indicating a stronger coupling. Between the experiments, the electron gun was cleaned and realigned. Thus, the two experiments could have had different beam qualities.

As another comparison with theory, we did a vacuum Raman scattering experiment within a waveguide of a different diameter. We chose to use the inside of the undulator as the effective waveguide since it is the largest diameter waveguide possible for this undulator. The inside diameter of the 0.91 centimeter wavelength undulator was 0.625 inches.

With a larger waveguide, the Raman interaction should occur at lower frequencies with a lower electron beam velocity. The inside wall of the magnetic wiggler is not as smooth as a normal waveguide since the disks are not

perfectly aligned. Therefore, one should not necessarily expect the sharpness of the interferometry as obtained before.

We performed the Raman scattering in a 0.625 inch diameter waveguide on 1/22/80 and the data are shown in figures 5.12 and 5.13. The observations are to be compared to the theoretical calculations shown in tables 5.8 and 5.9. In figure 5.12, the measured frequencies are 11, 19, and 26 gigahertz, and, in figure 5.13, the dominate frequency is 23 gigahertz.

VACUUM RAMAN SCATTERING

ACCELERATING VOLTAGE — 20 KV/DIV.

ELECTRON BEAM CURRENT — 6 A/DIV.

1 MICROSECOND/DIV.

INTERFEROMETER

MICROWAVES — 6 mV/DIV.

0 mm   5.8 mm   13.5 mm
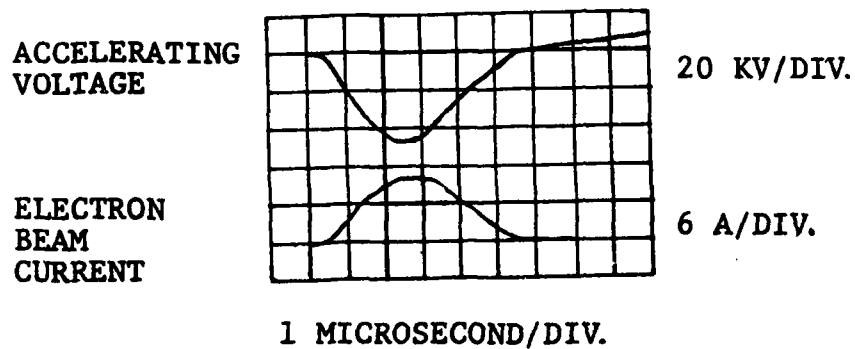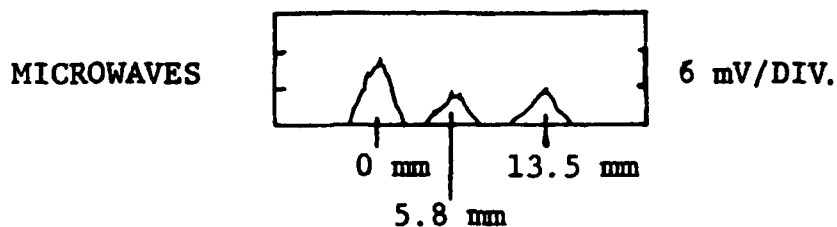
B = 3850 GAUSS

FIGURE 5.12 INTERFEROMETER DATA OF 1/22/80, #2B,C. VACUUM RAMAN SCATTERING IN A 9 PERIOD, 0.9 CENTIMETER WAVELENTH MAGNETIC WIGGLER AND A .625 INCH DIAMETER CIRCULAR WAVEGUIDE.

VACUUM RAMAN SCATTERING

ACCELERATING VOLTAGE — 20 KV/DIV.

ELECTRON BEAM CURRENT — 6 A/DIV.

1 MICROSECOND/DIV.

INTERFEROMETER

MICROWAVES — 10 mV/DIV.

0 mm — 19.3 mm
2.2 mm — 12.5 mm
5.0 mm

B = 5000 GAUSS

FIGURE 5.13 INTERFEROMETER DATA OF 1/22/80,#9B,C.
VACUUM RAMAN SCATTERING IN A 9 PERIOD, 0.9 CENTI-
METER WAVELENGTH MAGNETIC WIGGLER AND A .625 INCH
DIAMETER CIRCULAR WAVEGUIDE.

TABLE 5.8 POSSIBLE INTERACTIONS FOR THE DATA OF 1/22/80,#2B,C.

47 KILOVOLTS, 9 AMPERES, 3850 GAUSS

OBSERVED FREQUENCIES: 11, 19, AND 26 GIGAHERTZ

λ_p = .91 CENTIMETERS, - INTERACTION

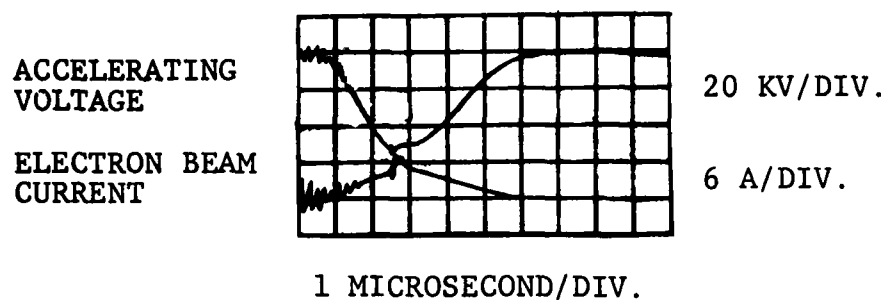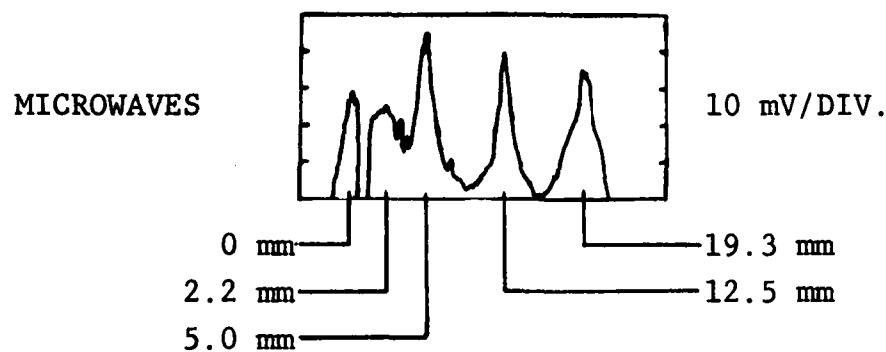| WAVEGUIDE MODE	FAST PLASMA WAVE (GHZ)	SLOW PLASMA WAVE (GHZ)	SLOW CYCLOTRON WAVE (GHZ)
TE_{11}	17.6	12.0	11.5
TM_{01}	18.5	14.7	NO INTERACTION
TE_{21}	19.9	NO INTERACTION	
TM_{11} OR TE_{01}	23.0		
TE_{31}	NO INTERACTION		

λ_p = .91 CENTIMETERS, + INTERACTION

TE_{11} WAVEGUIDE MODE, SLOW PLASMA WAVE   18.8 GHZ

λ_p = .303 CENTIMETERS, - INTERACTION

WAVEGUIDE MODE	FAST PLASMA WAVE (GHZ)	SLOW PLASMA WAVE (GHZ)	SLOW CYCLOTRON WAVE (GHZ)
TE_{11}	29.4	28.6	22.2
TM_{01}	29.8	29.1	22.8
TE_{21}	30.5	29.7	23.8
TM_{11} OR TE_{01}	31.6	30.9	25.5
TE_{31}	32.2	31.6	26.5
TM_{21}	34.3	33.8	31.2

From table 5.8, the fundamental, 0.91 centimeter, pump wavelength interactions are sufficient to explain the observed frequencies. Both slow cyclotron waves and plasma waves are present. If slow plasma waves were present, one would also expect 15 gigahertz microwaves, which were not observed.

TABLE 5.9 POSSIBLE INTERACTIONS FOR THE DATA OF 1/22/80,#9B,C.

30 KILOVOLTS, 5 AMPERES, 5000 GAUSS

OBSERVED FREQUENCIES: 23 GIGAHERTZ

λ_p = .91 CENTIMETERS, - INTERACTION

WAVEGUIDE MODE	FAST CYCLOTRON WAVE (GHZ)
TE_{21}	20.8
TM_{11} OR TE_{01}	23.2
TE_{31}	NO INTERACTION

λ_p = .303 CENTIMETERS, - INTERACTION

WAVEGUIDE MODE	FAST PLASMA WAVE (GHZ)	SLOW PLASMA WAVE (GHZ)
TE_{11}	25.4	24.7
TM_{01}	25.9	25.2
TE_{21}	26.6	26.0
TM_{11} OR TE_{01}	27.8	27.2

λ_p = .303 CENTIMETERS, + INTERACTION

WAVEGUIDE MODE	SLOW CYCLOTRON WAVE (GHZ)
TE_{11}	27.6
TM_{01}	26.6
TE_{21}	24.7
TM_{11} OR TE_{01}	NO INTERACTION

The interaction is due to a fast cyclotron wave coupling to the waveguide modes via the 0.91 centimeter pump. For the TE_{31} mode and above, the electron velocity is too slow for synchronism.

From the data of 1/22/80, we can conclude that the observed frequencies are due to the fundamental, 0.91

centimeter pump wavelengtn and a fast electron cyclotron wave. From the analysis of this section, we can conclude that both fast and slow electron cyclotron waves will drive the Raman backscattering interaction, if kinematically possible. It has been shown that electron plasma waves can drive the Raman instability also.

5.4 THE PROBLEMS INHERENT IN OBTAINING CERENKOV-RAMAN RADIATION

The same experimental techniques are used for the production of Cerenkov-Raman radiation as for vacuum Raman radiation. The only difference is that a dielectric liner is placed inside the waveguide. The problems arise because the dielectric liner reduces the waveguide cutoff frequency and the phase velocity of the waveguide modes. In order to avoid gyrotron-like or Cerenkov-like interactions, we must keep the electron cyclotron frequency less than the waveguide cutoff and the electron velocity slow enough so as not to intersect the unshifted waveguide dispersion, as shown in figure 5.14.

We know that reducing the guiding magnetic field decreases both the electron cyclotron frequency and the pump field, B_p. By lowering the electron velocity, we reduce the magnitude of the source of energy to drive the Raman
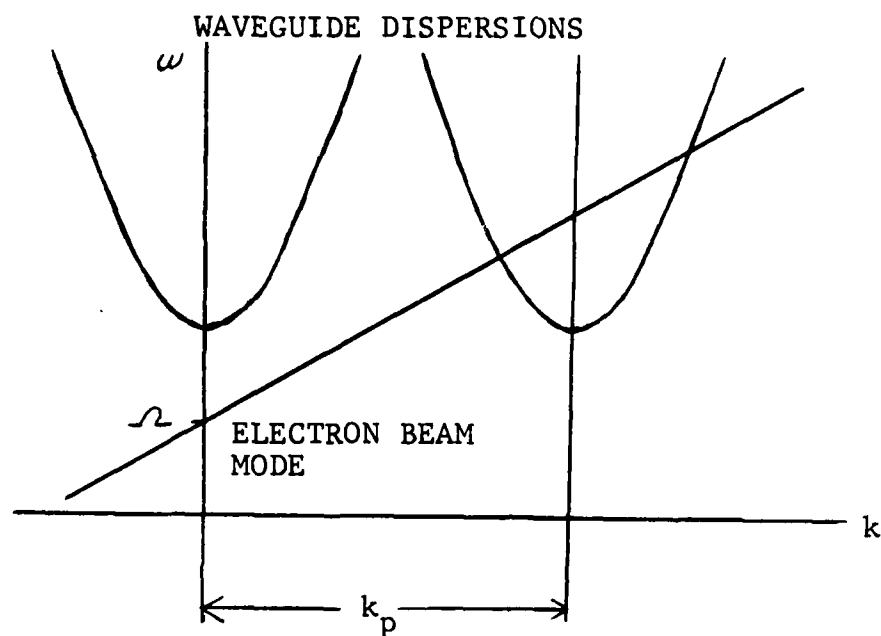
FIGURE 5.14 THE PUMP, BEAM, AND WAVEGUIDE DISPERSIONS
TO BE CONSIDERED FOR CERENKOV-RAMAN SCATTERING.

instability. Referring to the parametric equations, (3.1) and (3.2), we should expect a lower gain for the scattered microwave field, and it is reasonable to expect the Cerenkov-Raman interaction to be more difficult to observe than the vacuum Raman interaction.

5.5 THE OBSERVATION OF CERENKOV-RAMAN RADIATION

The first data of Cerenkov-Raman radiation to be presented is shown in figures 5.15 and 5.16. We used a seven period, 1.01 centimeter wavelength undulator. The 0.495 inch waveguide was lined with a 0.25 inch X 0.495 inch annular tube of polyproplyene inside the magnetic wiggler region. The dielectric constant of polyproplyene is 2.25.

The data presented are for two differnt guiding magnetic field strengths. As shown in figures 5.15 and 5.16, the fast electron cyclotron wave instability is sufficient to explain the data. Since the observations were made with a $wk-2\sigma$ detector, the lowest frequency that could be observed was the $wk-2\sigma$ cutoff frequency of 21.1 gigahertz.

The observed microwaves occurred at voltages much lower than that required for Cerenkov-cyclotron radiation. Straight Cerenkov radiation requires still higher accelerating voltages. The guiding magnetic field strength is too low for a gyrotron-like interaction.

FIGURE 5.15A THE MICROWAVE FREQUENCY VS. ACCELERATING VOLTAGE FOR THE CERENKOV-RAMAN INTERACTION. THE ELECTRON CYCLOTRON BEAM MODE AND THE TE_{01} WAVEGUIDE MODE SOLUTION IS SHOWN. THE HIGH PASS FREQUENCY FILTER DATA IS FROM 3/19/79.[18]

λ_p = 1.01 CENTIMETERS

B = 3470 GAUSS

ϵ = 2.25

I.R. = .318 CENTIMETERS

O.R. = .629 CENTIMETERS

GIGAHERTZ

KILOVOLTS

FIGURE 5.15B THE MICROWAVE FREQUENCY VS. ACCELERATING VOLTAGE FOR THE CERENKOV-RAMAN INTERACTION. THE ELECTRON CYCLOTRON BEAM MODE AND THE TE_{01} WAVEGUIDE MODE SOLUTION IS SHOWN. THE HIGH PASS FREQUENCY FILTER DATA IS FROM 3/19/79.[18]

The following labels appear within the figure:

GIGAHERTZ

λ_p = 1.01/3 CENTIMETERS

B = 3470 GAUSS

ϵ = 2.25

I.R. = .318 CENTIMETERS

O.R. = .629 CENTIMETERS

KILOVOLTS

λ_p = 1.01 CENTIMETERS

B = 5460 GAUSS

ϵ = 2.25

I.R. = .318 CENTIMETERS
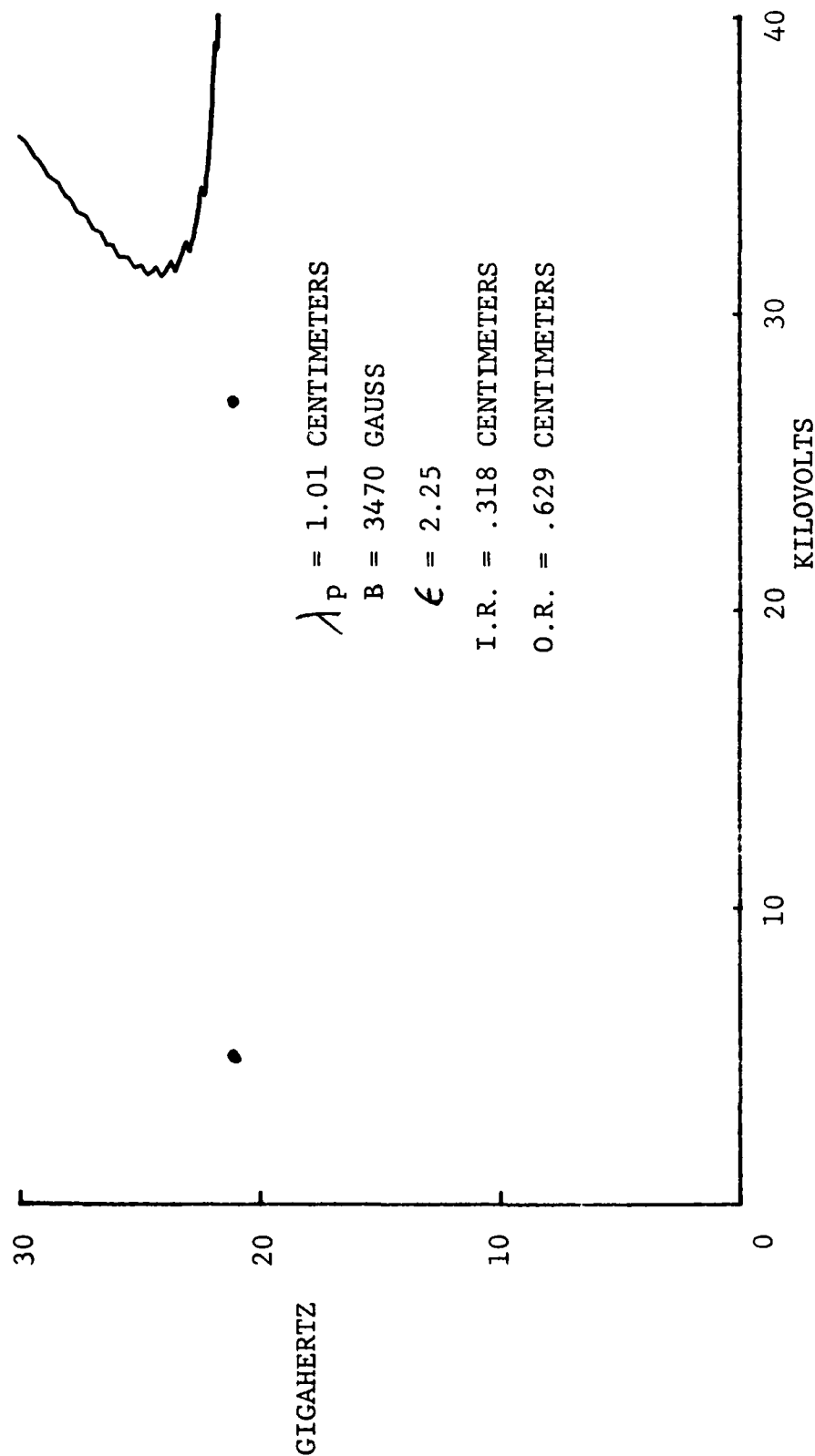
O.R. = .629 CENTIMETERS

FIGURE 5.16A THE MICROWAVE FREQUENCY VS. ACCELERATING VOLTAGE FOR THE CERENKOV-RAMAN INTERACTION. THE ELECTRON CYCLOTRON BEAM MODE AND THE TE_{01} WAVEGUIDE MODE SOLUTION IS SHOWN. THE HIGH PASS FREQUENCY FILTER DATA IS FROM 3/19/79.[8]

FIGURE 5.16B THE MICROWAVE FREQUENCY VS. ACCELERATING VOLTAGE FOR THE CERENKOV-RAMAN INTERACTION. THE ELECTRON CYCLOTRON BEAM MODE AND THE TE_{01} WAVEGUIDE MODE SOLUTION IS SHOWN. THE HIGH PASS FREQUENCY FILTER DATA IS FROM 3/19/79.[8]
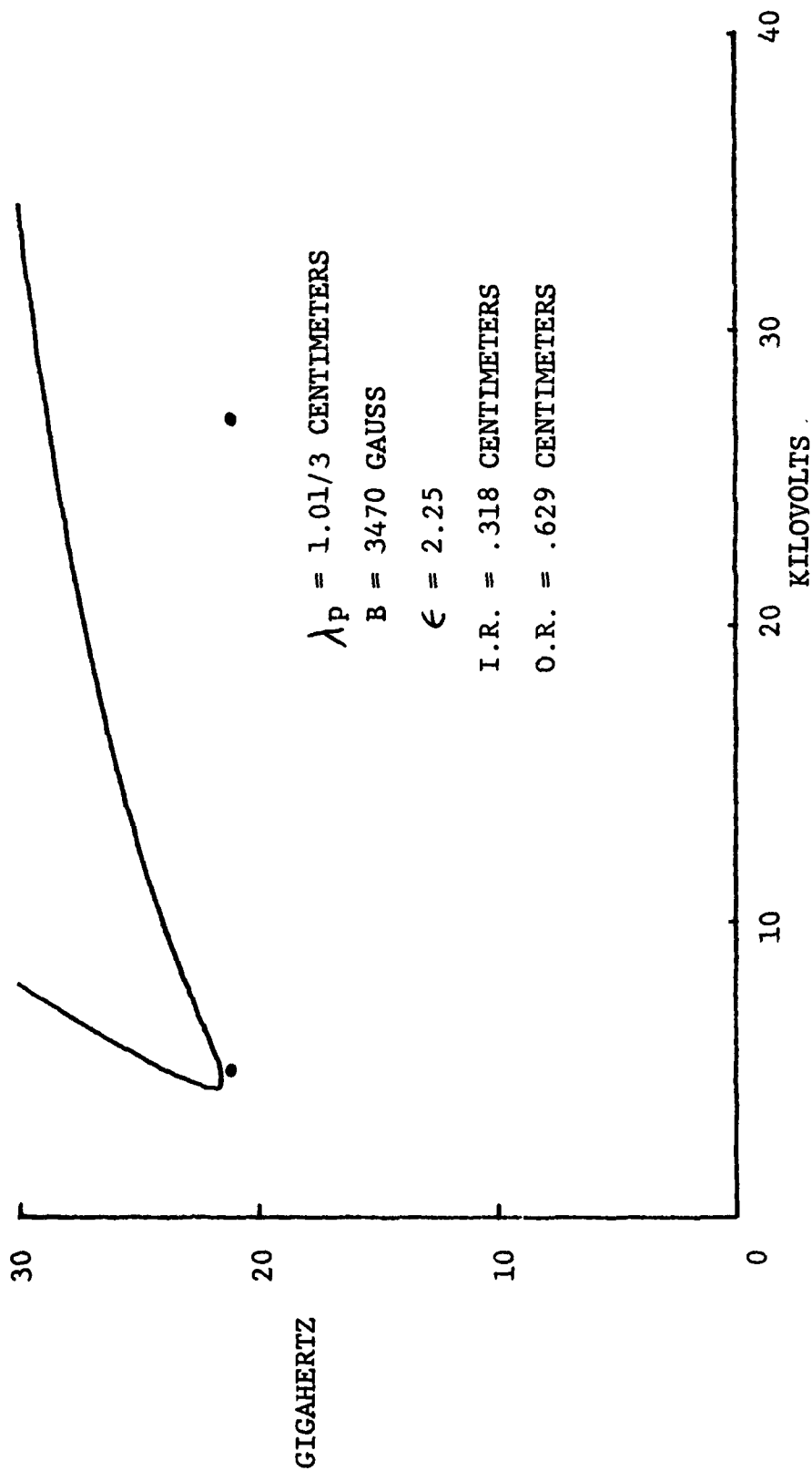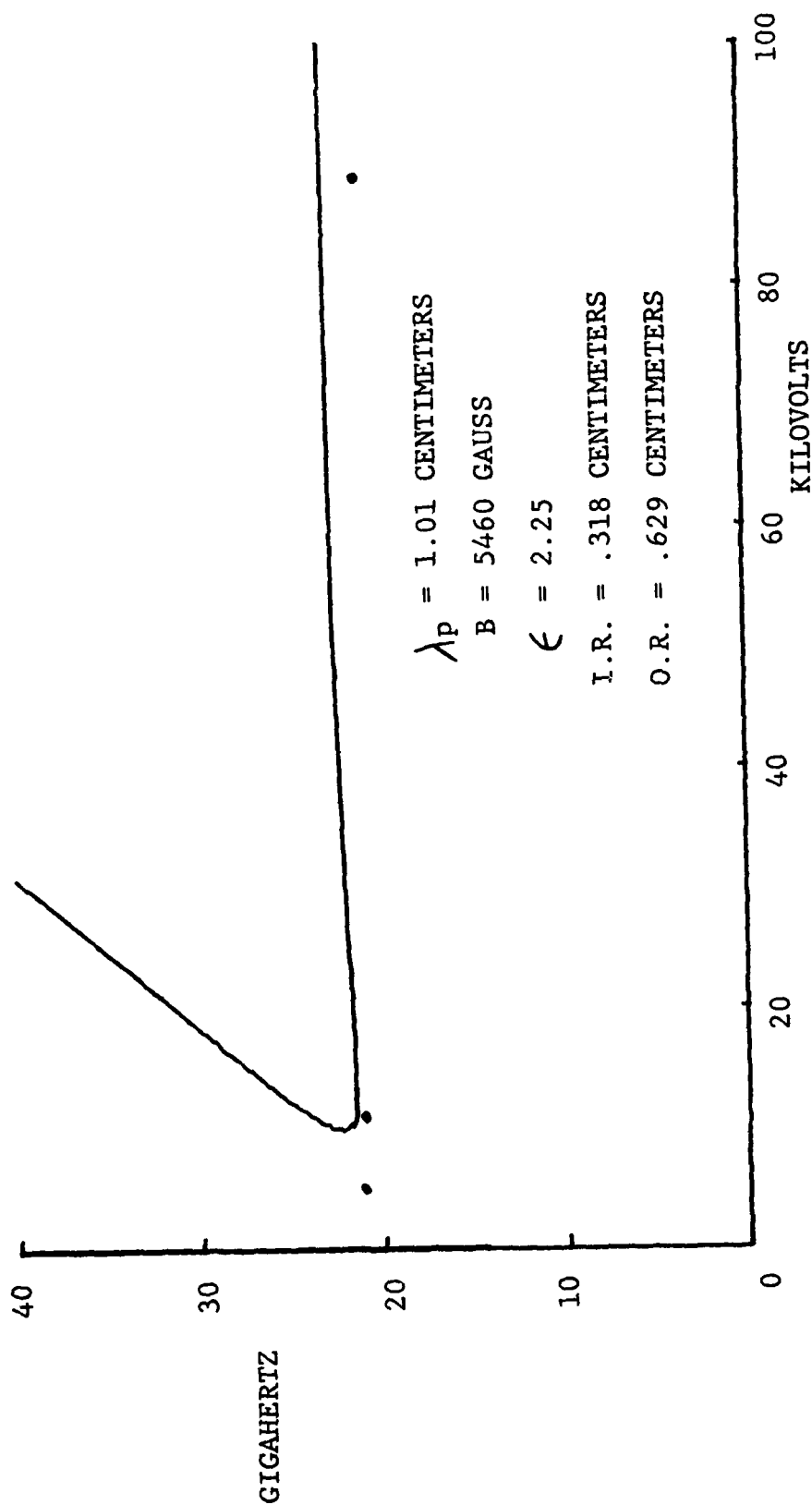
λ_p = 1.01/3 CENTIMETERS

B = 5460 GAUSS

ϵ = 2.25

I.R. = .318 CENTIMETERS

O.R. = .629 CENTIMETERS

KILOVOLTS

GIGAHERTZ

In figure 5.17, free space interferometer data is
presented to verify that the Cerenkov-Raman interaction does
scale with the waveguide diameter and the dielectric filler.
The effective waveguide diameter is .577 inches, and the
filler is quartz. The data is consistent with the fast
electron cyclotron mode.

5.6 THE OBSERVATION OF THE UPPER BRANCHES OF THE CERENKOV-RAMAN BACKSCATTERING INTERACTION

For these observations, we used high pass frequency
filters. The data points are plotted at the cutoff
frequency of the filters. The data is plotted in figures
5.18 and 5.19.

In figure 5.18, the data is for a polyproplyene liner
with an inside diameter of 5/16 inches and an outside
diameter of 0.495 inches. A 0.495 inch diameter waveguide
was used. The data agrees well for Cerenkov-Raman scattering
due to a slow cyclotron wave and the third harmonic of the
pump wave, $k_p = 3(2\pi/1.01)$ cm.$^{-1}$.

At a later date, we observed the data plotted in
figures 5.19A and 5.19B. The high frequency data and the
low frequency data were taken with different guiding
magnetic field strengths. In figure 5.19A, the data is
consistent with a fast electron cyclotron wave and a pump

λ_p = 1.01/3 CENTIMETERS

B = 2610 GAUSS

ϵ = 3.78

I.R. = .635 CENTIMETERS

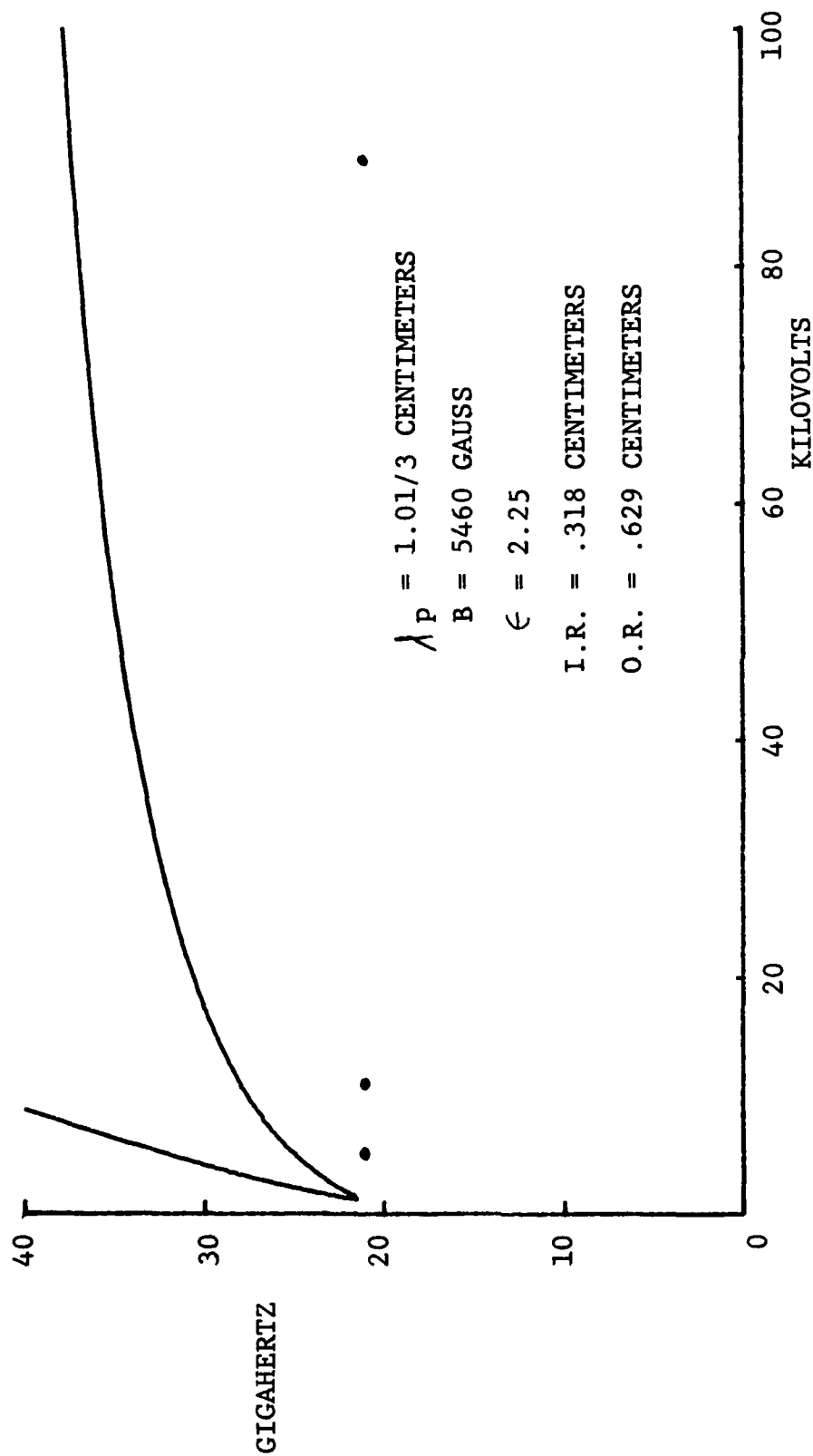O.R. = .733 CENTIMETERS

KILOVOLTS

GIGAHERTZ

FIGURE 5.17 THE MICROWAVE FREQUENCY VS. ACCELERATING VOLTAGE FOR THE CERENKOV-RAMAN INTERACTION. THE ELECTRON CYCLOTRON BEAM MODE AND THE TE_{01} WAVEGUIDE MODE SOLUTION IS SHOWN. THE HIGH PASS FREQUENCY FILTER DATA IS FROM 3/16/80.[18]

GIGAHERTZ

60

50

40

30

20

10

0

10   20   30   40   50

KILOVOLTS

λ_p = 1.01/3 CENTIMETERS

B = 2700 GAUSS

ϵ = 2.25
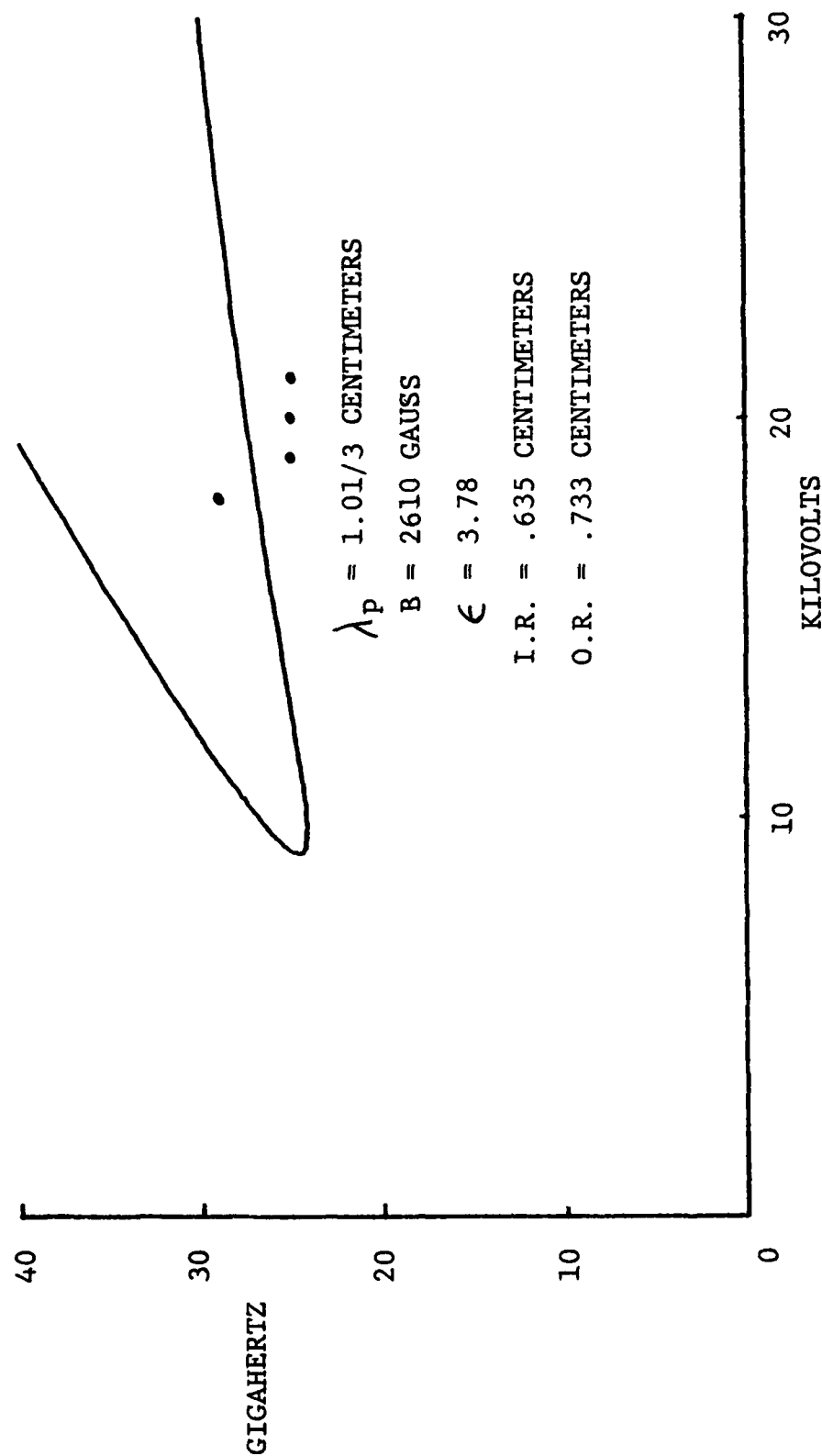
I.R. = .397 CENTIMETERS

O.R. = .629 CENTIMETERS

FIGURE 5.18 THE MICROWAVE FREQUENCY VS. ACCELERATING VOLTAGE FOR THE CERENKOV-RAMAN INTERACTION. THE SLOW ELECTRON CYCLOTRON BEAM MODE AND THE TE_{01} WAVEGUIDE MODE SOLUTION IS SHOWN. THE HIGH PASS FREQUENCY FILTER DATA IS FROM 4/17/79.[8]

FIGURE 5.19A THE MICROWAVE FREQUENCY VS. ACCELERATING VOLTAGE FOR THE CERENKOV-RAMAN INTERACTION. THE FAST ELECTRON CYCLOTRON BEAM MODE AND THE TM_{01} WAVEGUIDE MODE SOLUTION IS SHOWN. THE INTERFEROMETER DATA IS FROM 5/5/79.[8]

Plot axis labels and values:

GIGAHERTZ (vertical axis): 70, 60, 50, 40, 30, 20, 10, 0

KILOVOLTS (horizontal axis): 10, 20, 30, 40, 50, 60

λ_p = 1.01 CENTIMETERS
B = 5320 GAUSS
ϵ = 2.25

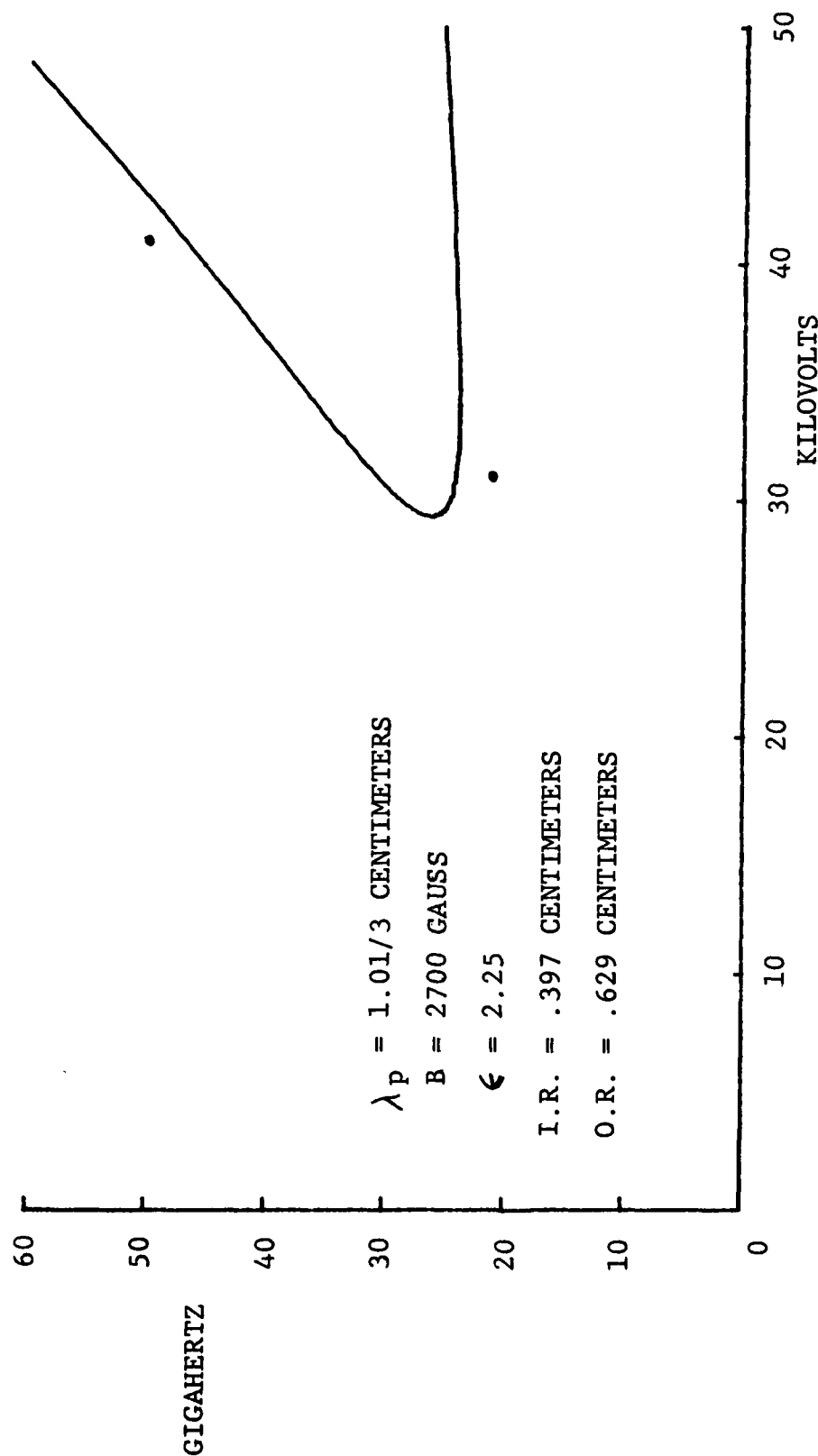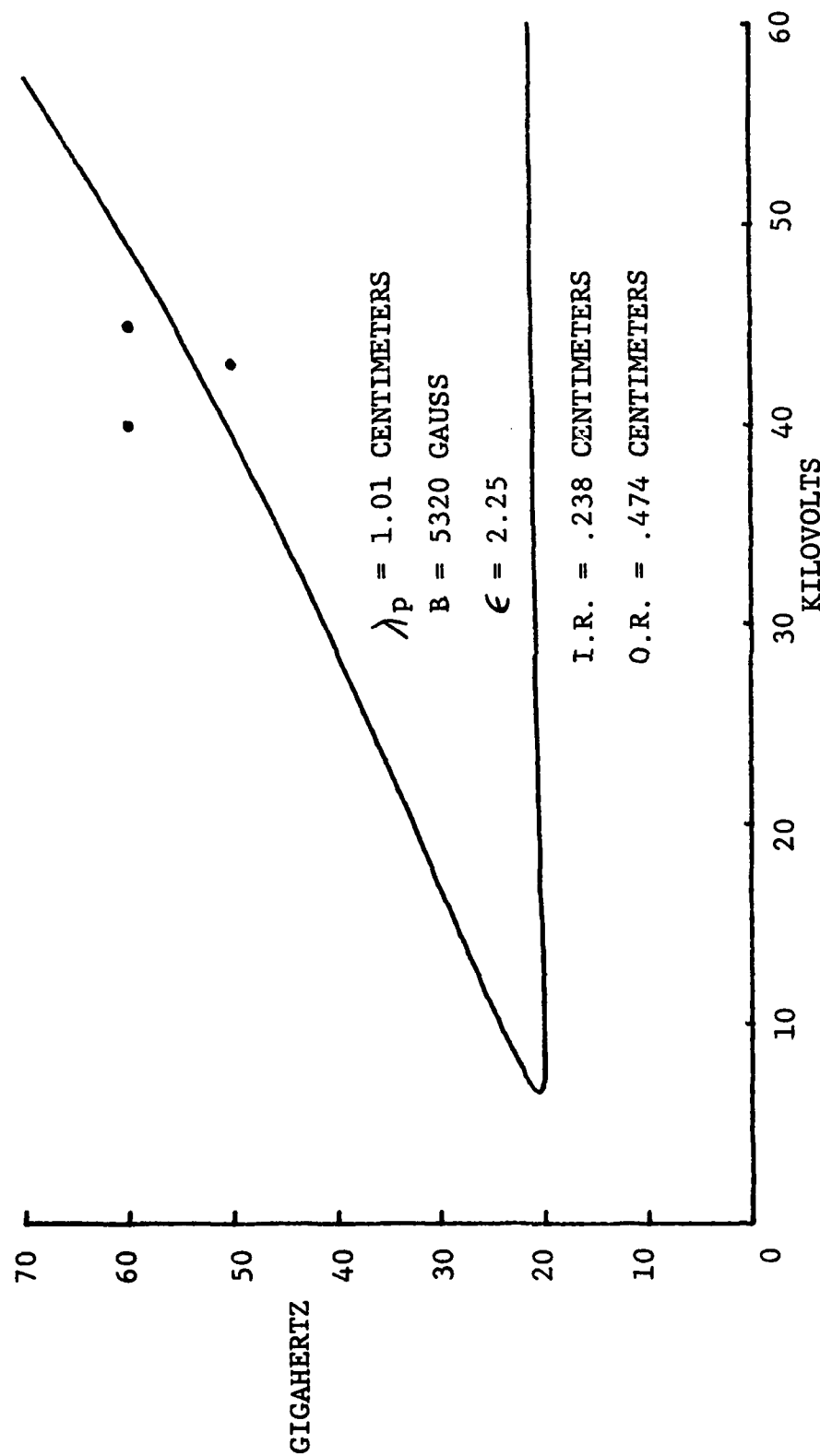I.R. = .238 CENTIMETERS
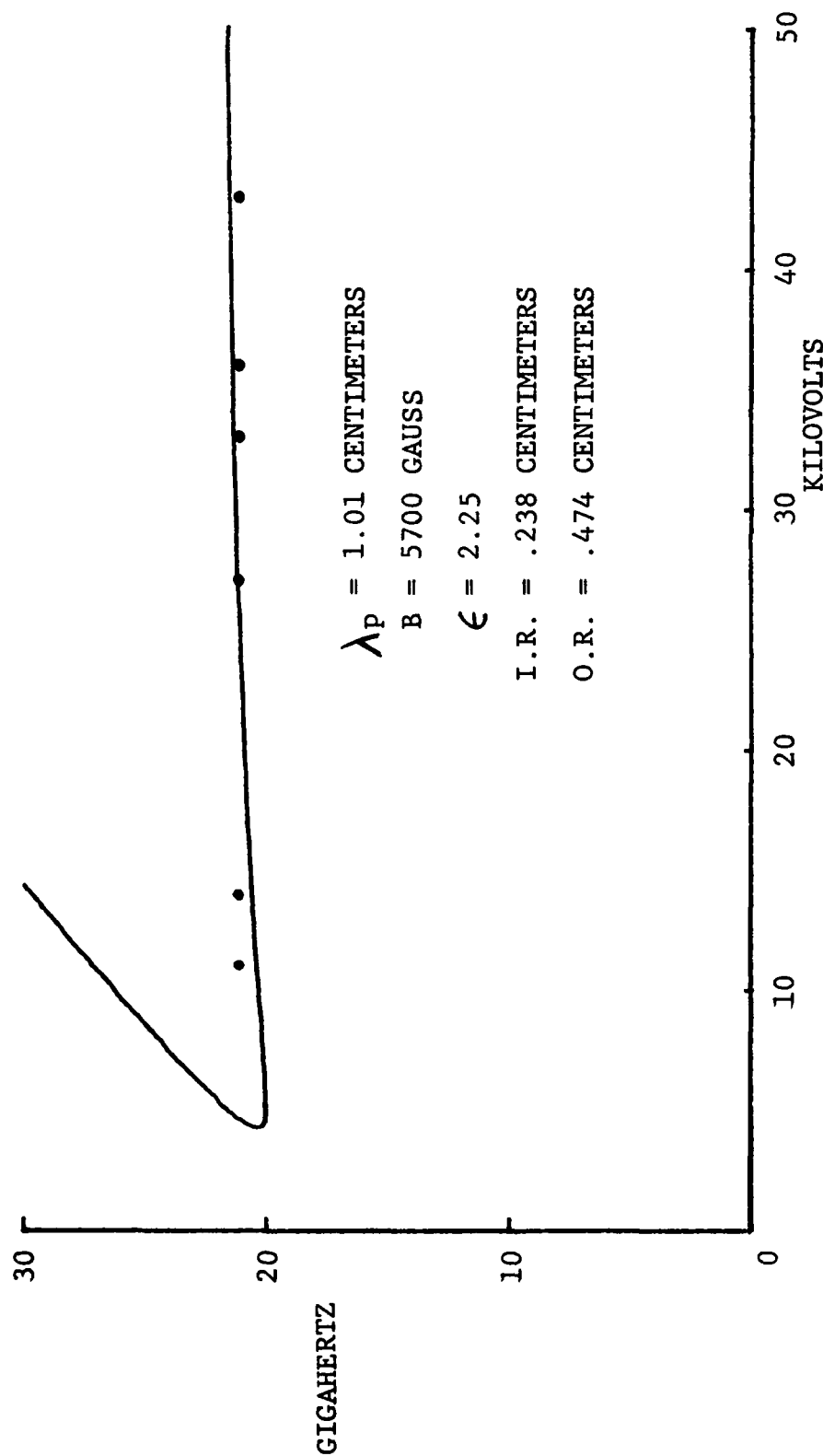O.R. = .474 CENTIMETERS

FIGURE 5.19B THE MICROWAVE FREQUENCY VS. ACCELERATING VOLTAGE FOR THE CERENKOV-RAMAN INTERACTION. THE FAST ELECTRON CYCLOTRON BEAM MODE AND THE TM_{01} WAVEGUIDE MODE SOLUTION IS SHOWN. THE HIGH PASS FREQUENCY FILTER DATA IS FROM 5/5/79.[18]

λ_p = 1.01 CENTIMETERS

B = 5700 GAUSS

ϵ = 2.25

I.R. = .238 CENTIMETERS

O.R. = .474 CENTIMETERS

GIGAHERTZ

KILOVOLTS

wavelength of 1.01 centimeters. A TM_{01} waveguide mode is assumed here for comparison. Some of this data would fit the TE_{11} waveguide dispersion better. The data point at (60GHz, 40 KV) is due to a microwave pulse during the second half of the accelerating voltage pulse. These late microwave pulses correspond to lower order modes, such as the TE_{11} mode.

The data in figure 5.19B are for the lower branch of the interaction. Here too, high pass frequency filters were used. We see that both branches of the Cerenkov-Raman interaction are present simultaneously.

5.7 CONFIRMATION OF CERENKOV-RAMAN RADIATION BY AN ACCELERATING VOLTAGE TURN-ON TECHNIQUE

For this experiment, we used a 1.01 centimeter wavelength, 18.5 period split ring undulator. It consisted of sets of rings which were one-half aluminum and one-half iron. The rings were stacked such that the iron and aluminum one-half rings were alternating. A 0.25 inch inside diameter and a 0.490 inch outside diameter quartz filler was used. The effective diameter of the waveguide was 0.490 inches.

The motivation for this experiment is illustrated by figure 5.20. We see that no interaction is possible until the electron velocity is fast enough to intersect the
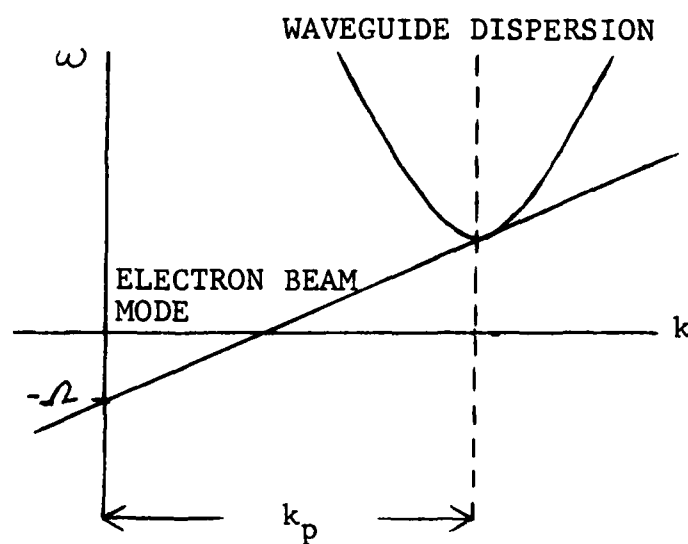
FIGURE 5.20 THE RELATION OF THE PUMP, BEAM, AND WAVEGUIDE DISPERSIONS FOR THE THRESHOLD OF MICROWAVE PRODUCTION.

waveguide dispersion, hence the interaction will turn on approximately at the waveguide cutoff.

The data for this experiment are shown in figure 5.21. A slow electron cyclotron mode and a $k_p = 3(2\pi/1.01)$ cm.$^{-1}$ is assumed. The interaction curves are for the TE_{11} and the TE_{01} waveguide modes. The TE_{11} cutoff frequency is estimated to be 9.5 gigahertz. The TE_{01} cutoff frequency is calculated to be 17.4 gigahertz. The data shows the predicted trend. A WR-90 detector was used because its cutoff frequency is less than either the TE_{01} or the TE_{11} waveguide modes.

We performed a null experiment without the magnetic wiggler. This data shows the correct trend for either a backward wave oscillator or a Cerenkov-gyrotron. Therefore, the microwaves previously observed were due to the Cerenkov-Raman interaction.
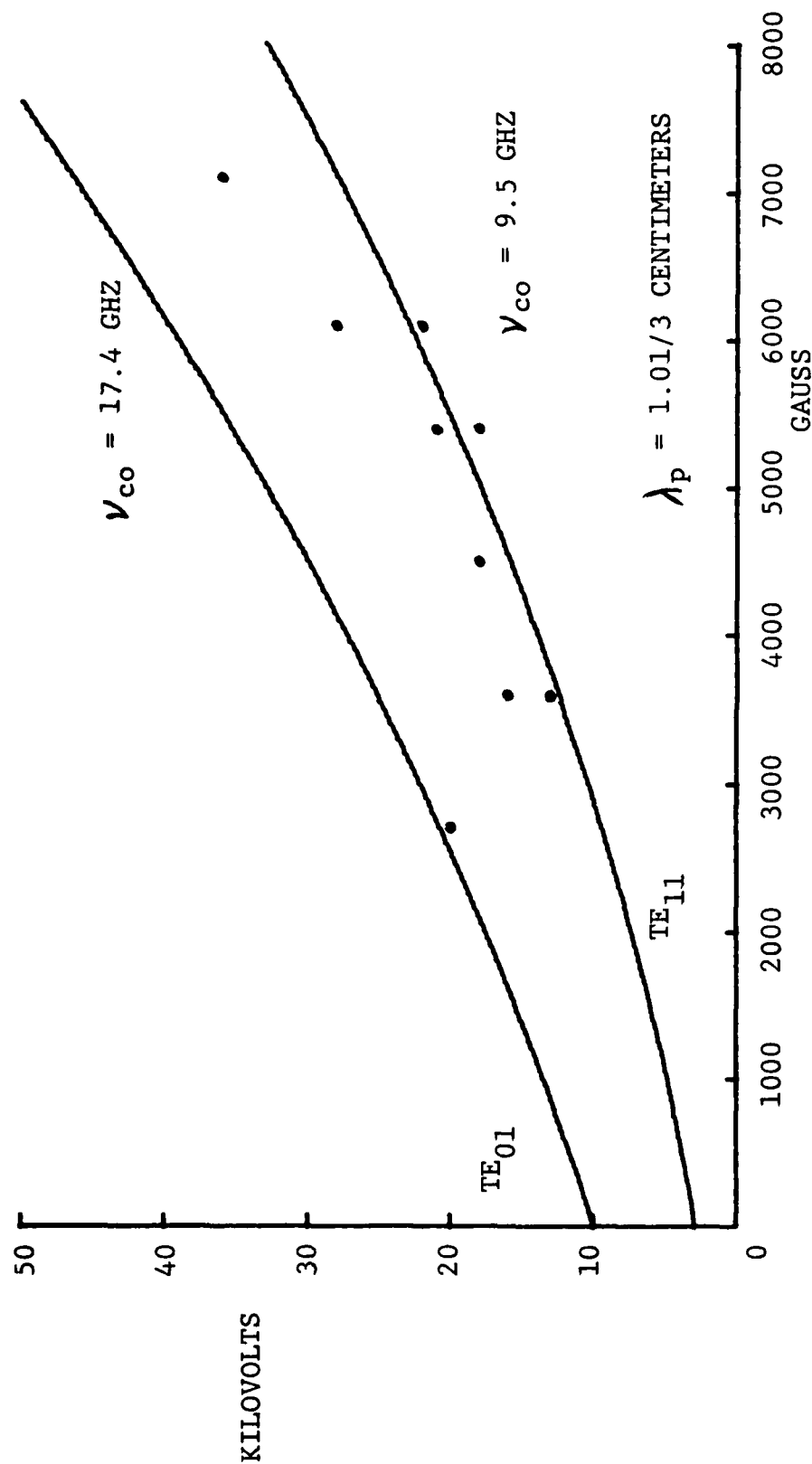
134

FIGURE 5.21 THE ACCELERATING VOLTAGE FOR MICROWAVE TURN-ON VS. THE MAGNETIC FIELD STRENGTH. THE THEORETICAL CALCULATIONS ARE FOR A SLOW ELECTRON CYCLOTRON BEAM MODE. THE HIGH PASS FREQUENCY FILTER DATA IS FROM 10/17/79.

CHAPTER 6

CONCLUSIONS

This thesis documents several advances in both theoretical and experimental physics. The first accomplishment is the theory of chapter three. This is the first time either Raman or Cerenkov-Raman Backscattering has been analysed with the experimental constraints due to the magnetic wiggler and the cylindrical waveguide. The prediction, in section 3.12, of strong microwave coupling near the waveguide cutoff has been experimentally observed.

The second advance is the observation of vacuum Raman scattering due to the third wavelength harmonic of the pump wave. This technique may prove valuable for the production of high frequency radiation. We have also shown that substantial microwave production is possible with electron beam currents on the order of tens of amperes. We estimate the microwave production to be of the order of hundreds of watts to one kilowatt for frequencies near the waveguide cutoff and watts to tens of watts for frequencies above the waveguide cutoff.

The third and most significant contribution of this thesis is the first observation of Cerenkov-Raman radiation. Two different techniques for the verification of the observations are documented in chapter five. The microwave

power is estimated to be from one to ten watts for electron beam energies of 50 KeV and for electron beam currents of a few tens of amperes. Cerenkov-Raman backscattering has the potential for becoming a practical source for the generation of high frequency microwave radiation.

APPENDIX 1 MAGNETIC FIELD SHAPING

An interesting phenomenon is that the magnetic field shape in the electron gun region distinctly affects the coupling between the electron beam and the microwaves. Figures A1 and A2 give the magnetic field profiles with the corresponding microwave output. A seventeen undulation, 1.01 centimeter period magnetic wiggler was present. An iron liner was placed inside the cathode tube to effectively help straighten out the magnetic field lines in the electron gun area. The iron liner did raise the magnetic field at the cathode face by ten percent above that which would be present without the iron liner.

Before the iron was added, an anomalous current rise of zero to ten percent was observed during the microwave pulse, whereas, with the iron, a thirty to fifty percent rise in the current was observed. Typical neutral gas background pressures were $2X10^{-6}$ Torr. Microwave powers were less than one kilowatt per square centimeter inside the waveguide. Under these conditions, back ion bombardment, leading to an observed current rise would not be probable[43].

The anomalous current rise was present only when the microwaves were being produced. When the operating conditions were changed such that the microwaves were no longer present, no anomolous current was observed. A conclusion that can be made is that the positioning of the
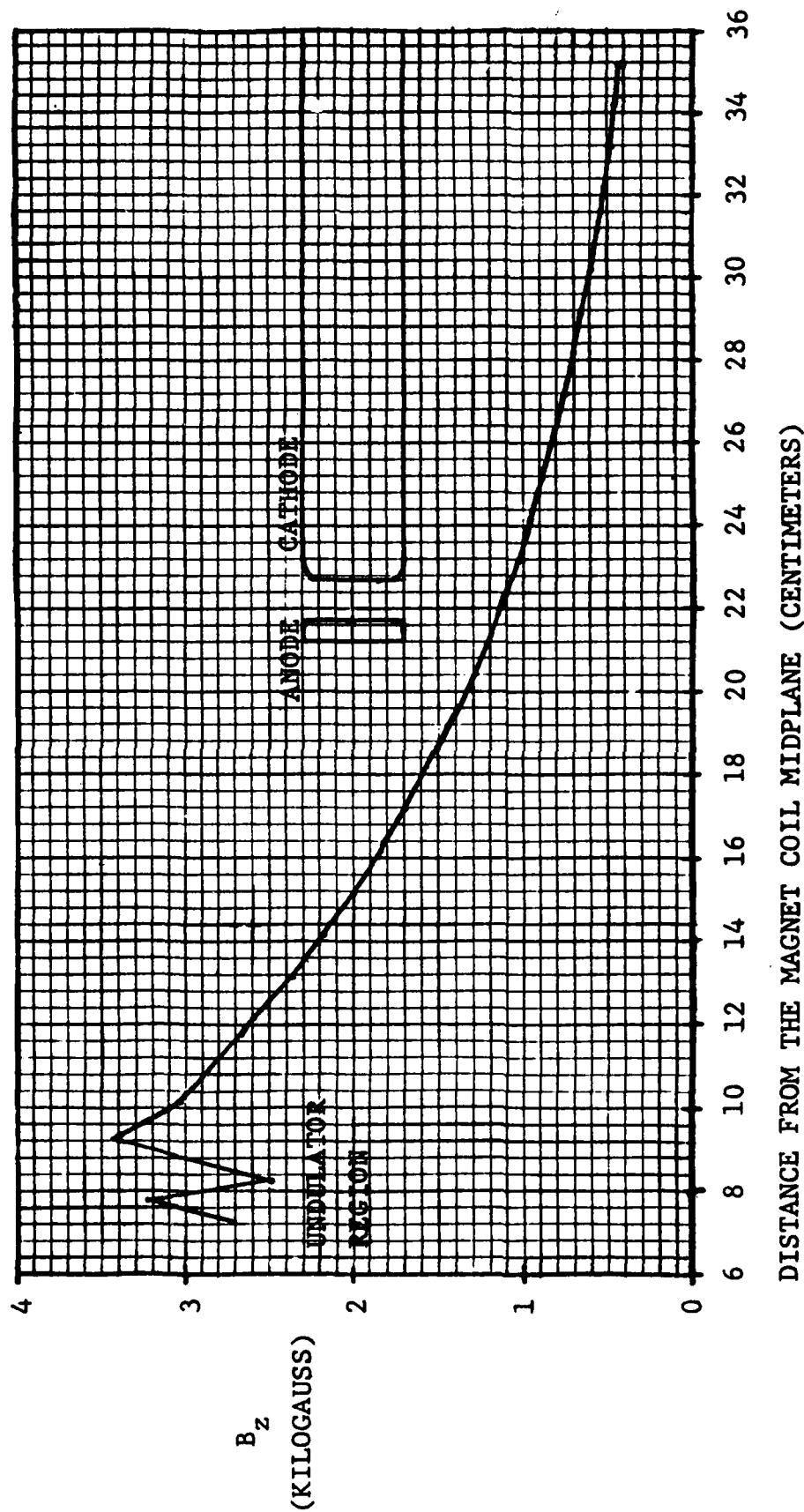
137

FIGURE A1.A   THE LONGITUDINAL MAGNETIC FIELD PROFILE ALONG THE MAGNET COIL AXIS AS A FUNCTION OF DISTANCE FROM THE MAGNET COIL MIDPLANE, WITHOUT THE PRESENCE OF AN IRON LINER.

138

ACCELERATING
VOLTAGE   50 KV/DIV.

WR-28
MICROWAVES   500 mV/DIV.

ELECTRON
BEAM   2 A/DIV.
CURRENT

1 MICROSECOND/DIV.

B = 5680 GAUSS

FIGURE A1.B   ANOMALOUS CURRENT RISE DURING MICROWAVE PRODUCTION
WITH A SEVENTEEN UNDULATION, ONE CENTIMETER PERIOD MAGNETIC WIGGLER
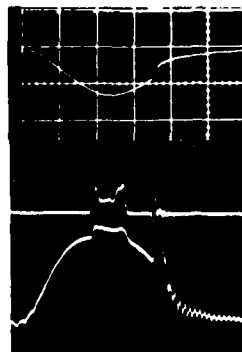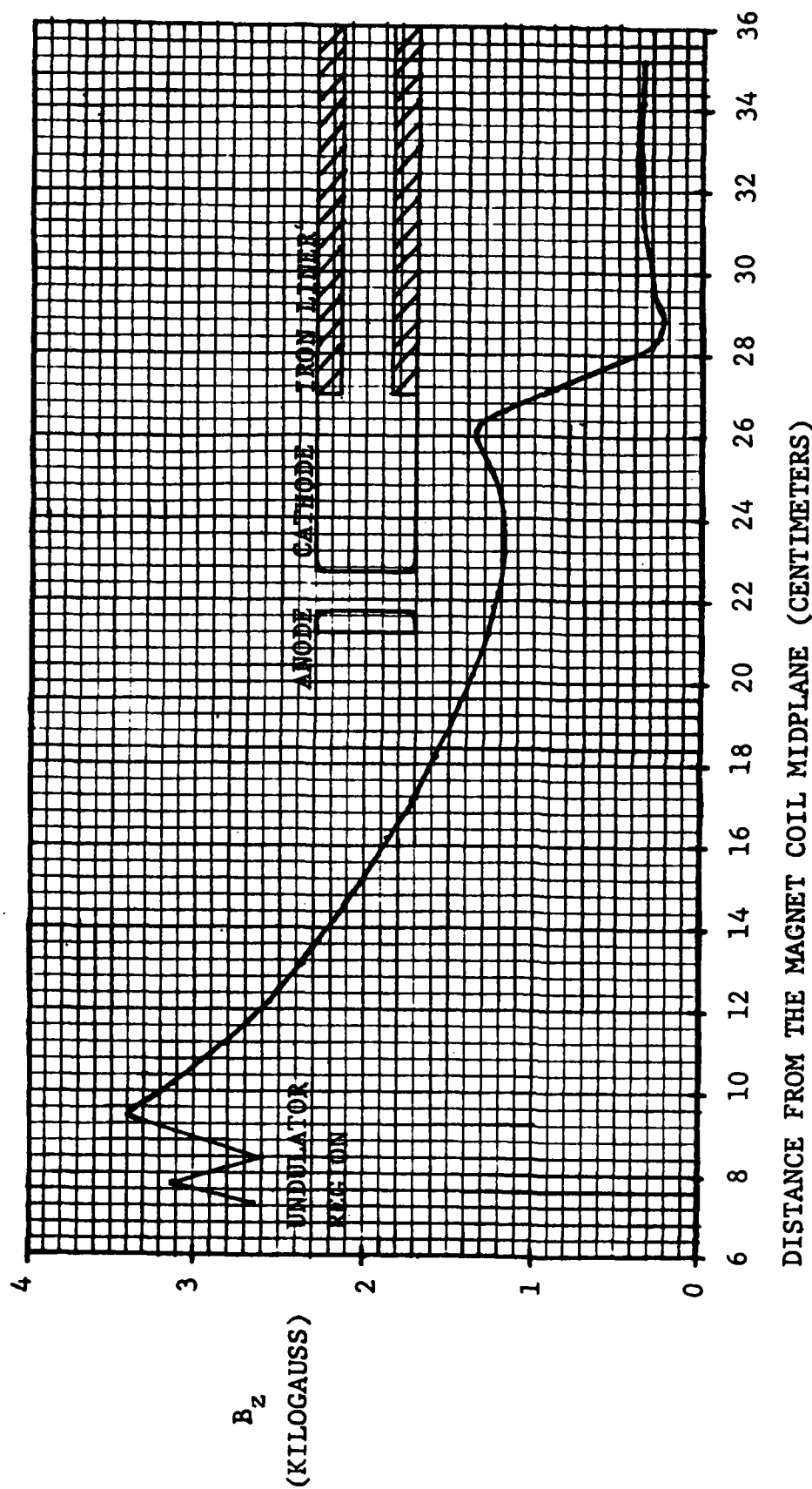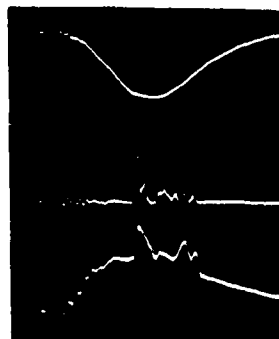AND WITHOUT THE PRESENCE OF AN IRON LINER. DATA OF 4/9/79,#1D,E.

FIGURE A2.A   THE LONGITUDINAL MAGNETIC FIELD PROFILE ALONG THE MAGNET COIL AXIS AS A
FUNCTION OF DISTANCE FROM THE MAGNET COIL MIDPLANE, IN THE PRESENCE OF AN IRON LINER.

FIGURE A2.B   ANOMALOUS CURRENT RISE DURING MICROWAVE PRODUCTION
WITH A SEVENTEEN UNDULATION, ONE CENTIMETER MAGNETIC WIGGLER
AND WITH AN IRON LINER. DATA OF 4/6/79,#8A,B.

cathode-anode gap in a straight magnetic field affects the electron beam quality

The following simple mathematical derivation shows that electron beam acceleration in a magnetic field with a transverse component leads to a warming of the electron beam. Since the Raman interaction is a collective instability, a colder electron beam would lead to a stronger interaction.

Consider an electron gun accelerating gap with E_r, E_z, B_r, an B_z fields present. A similar problem, to follow later, has been considered by Lashinsky[44]. E_z is the accelerating electric field and E_r is a consequence of imperfect electron gun design. E is not present since since the accelerating gap is cylindrically symmetric. B_z, which has a magnitude of B_0, is the guiding magnetic field. Diverging magnetic field lines imply a B_r field, and B is disregarded. I will also disregard relativistc effects since it adds no additional insight, but it does complicate the issue. The equations of motion in the accelerating gap are:

$$\frac{dV_r}{dt} = -\frac{e}{m}\left[E_r + \frac{V_\theta}{r}B_0\right] \tag{A1}$$

$$\frac{dV_\theta}{dt} = -\frac{e}{m}\left[-\frac{V_r}{c}B_0 + \frac{V_z}{c}B_r\right] \tag{A2}$$

$$\frac{dV_z}{dt} = -\frac{e}{m}\left[E_z\right] \tag{A3}$$

A reasonable estimate is that the magnitudes of the radial field quantities are of the order of ten percent of the longitudinal field quantities. These equations are simple enough so that we do not need to use Fourier transforms. Solving for the radial term, we find;

$$\left(\frac{d^2}{dt^2}+\Omega^2\right)v_r = -\frac{e}{m}\frac{dE_r}{dt}+\Omega^2 v_z\left(\frac{B_r}{B_o}\right) \tag{A4}$$

It is easily seen, although not easily calculated, that the (B_r/B_0) term can lead to a significant increase in v_r. Physically, the electrons are accelerating up a magnetic mirror, which directs longitudinal energy into transverse energy, warming the electron beam[45]. Experimentally, when B_r is made small in the accelerating gap, the microwaves couple to the electron beam strongly. Thus, the beam quality is an important factor.

APPENDIX 2   ELECTRON BEAM SCALLOPS

It has been observed that there exists a ripple in the electron beam current, even when no microwave coupling mechanisms exist. Figure A3 gives a typical example. This perturbation is in the ten megahertz frequency range, superimposed upon the usual space charge limited or emission limited current trace. The current ripple does not depend on the diameter of the waveguide through which the electron beam propagates. It even exists if the electron beam propagates through the center of a pyrex vacuum tube. The ripple is not present on the Pearson transformer measurements, which record the total current emitted from the cathode region. Although barely noticeable when measured by a Faraday cup located directly behind the anode, the ripple becomes a ten to fifty percent perturbation further downstream.

The perturbation is strongly dependent upon the accelerating voltage and the magnetic field strength. As either quantity alone is increased, a bump at the peak of the current trace peaks up, then splits in half into two peaks, which move to opposite sides of the current trace. If the accelerating voltage or the magnetic field is increased still further, another bump forms at the peak of the current trace, and the process repeats itself. The process is reversible if either the accelerating voltage or

144

ACCELERATING VOLTAGE — 30 KV/DIV.
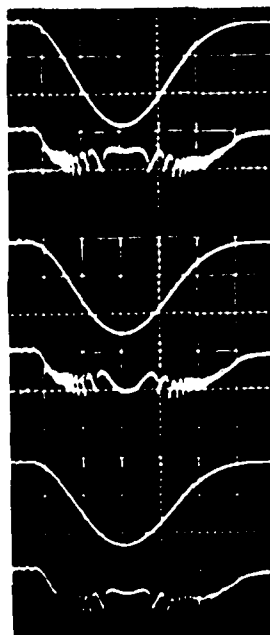
ELECTRON BEAM CURRENT — 1 A/DIV.

1 MICROSECOND/DIV.

FIGURE A3   THE ELECTRON BEAM RIPPLE STRUCTURE AS
A FUNCTION OF THE ELECTRON BEAM ACCELERATING VOLT-
AGE. THERE IS A ONE PERIOD DIFFERENCE BETWEEN THE
TOP AND BOTTOM SETS OF TRACES. DATA OF 10/2/78,
#11.

the magnetic field is turned down.

After a discussion with Herb Lashinsky[46,47], it became apparent that the ripples are due to electron beam scallops. The scallops are due to the radial electric field present in the accelerating gap of the electron gun. Our electron gun has a simple, planar, single stage accelerating gap. The radial electric fields are due to to the finite transverse dimensions of the accelerating gap and to the presence of a hole in the anode for the electron beam to pass through. The electric equipotential surfaces in the hole can have curved shapes.

The electron beam scallops are produced by the radial electric field in the accelerating gap, which induces a wave-like structure into the electron beam. The perturbation is then propagated downstream, as shown in figure A4. The radial electric field perturbs the cyclotron orbits of individual electrons such that the beam is defocused. Once every cyclotron period, the electron beam becomes focused, increasing its current density. The spatial period of the electron density modulation depends upon both the magnetic field, which determines the cyclotron frequency, and the electron velocity, which is the velocity of propagation of the perturbation.

We have two data points to check out the electron beam scallop theory. The first is when the Faraday cup is placed directly behind the anode. This would staighten out the
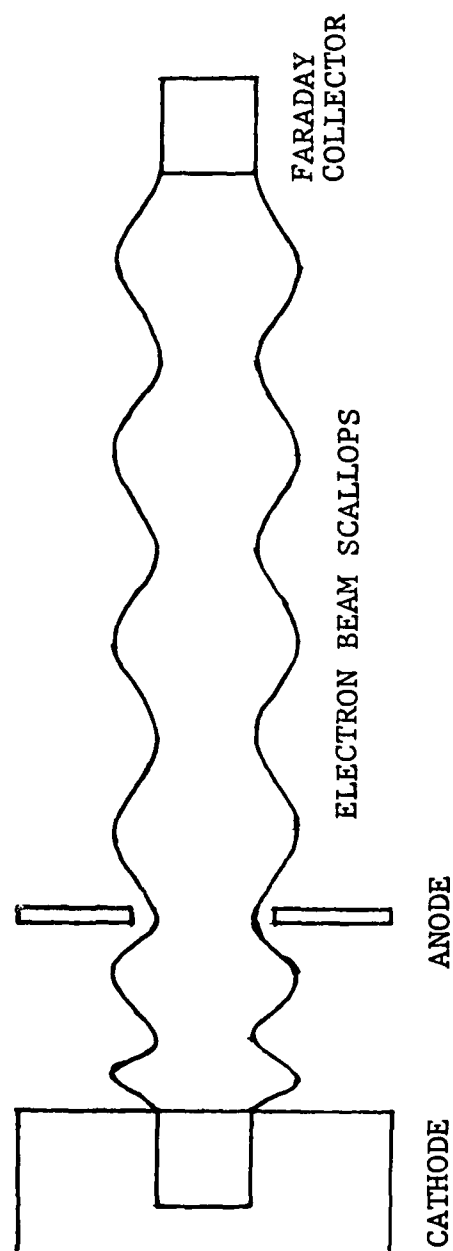
147

CATHODE ANODE ELECTRON BEAM SCALLOPS FARADAY COLLECTOR

FIGURE A4 DIAGRAM OF THE ELECTRON BEAM SCALLOPS, WHICH LEAD TO CURRENT DENSITY MODULATIONS.[44]

potential surfaces in the region of the anode hole. Thus, the radial electric fields would be diminished, and the magnitude of the current ripples would diminish. This has been observed.

The second piece of data is that shown in figure A3. If a Faraday cup, with approximately the same dimensions as the electron beam, is placed at a node of the density modulation of the electron beam, it will collect the maximum electron current. Holding the magnetic field constant and leaving the Faraday cup in the same position, it should be possible to adjust the electron velocity such that there is exactly one more or one less cyclotron period between the cathode and the Faraday cup. When this happens, the electron beam current collected will become a maximum once again.

We performed this experiment, except that we looked for antinodes instead. The mean magnetic field, defined as one quarter of the fields at the cathode and the Faraday cup plus one half the peak field, was 1600 gauss. The effective distance from the cathode to the Faraday cup, defined as the distance from the anode to the Faraday cup plus twice the anode-cathode gap (because the mean gap velocity is $v_0/2$), is 53.6 centimeters. The 1600 gauss magnetic field sets the cyclotron frequency at 3.9 gigahertz. With an electron kinetic energy of 82 KeV, there are 13.5 cyclotron periods between the cathode and the Faraday cup. To increase the number of periods by one requires an accelerating voltage of

67 kilovolts. The theoretical difference in the accelerating voltage is 15 kilovolts. The experimentally measured voltage difference is 15 kilovolts.

Therefore, it appears that electron beam scallops lead to the current ripple downstream. This ripple is probably detrimental to the Raman interaction because it is a current density modulation independent of the Raman interaction. Better electron gun design to eliminate the radial electric fields will alleviate the problem.

APPENDIX 3   COMMENTS ABOUT THE   GYROTRON AND THE CERENKOV-
GYROTRON MASERS

In   addition   to   our   Cerenkov-Raman   experiments,   we
performed   a Cerenkov-gyrotron experiment as   a null run   to
check our results.   This experiment is similar to the
gyrotron experiment conducted by Granatstein and Sprangle[46].
The Cerenkov-gyrotron experiment is set up physically the
same as the Cerenkov-Raman experiment, except that there is
only one large undulation.

From our point of view, the useful fact about gyrotrons
is   that   their   microwave output   turns on   just   above the
waveguide cutoff and approximately at the electron cyclotron
frequency. We fixed the accelerating voltage and   increased
the magnetic field.   When the microwave   power   peaked,   we
could approximate that the electron cyclotron frequency, as
calculated from the magnetic field strength, would be at the
waveguide cutoff frequency.   For the quartz filler of
section 5.7, we found three maxima, corresponding to the
electron cyclotron frequencies of 9.4,   14.9,   and 17.9
giganertz.   The first frequency corresponds to the TE_{11}
mode, the second to the TE_{21} mode, and the third to the TE_{01}
mode.   The calculated cutoff frequencies for the TM_{01} and
the TE_{01} modes are 12.8 and 17.4 gigahertz, respectively.
This gives us more confidence in our calculated waveguide
dispersions.

150

BIBLIOGRAPHY

[1] H. Motz, J. Appl. Phys., 22, 5, pp. 527-535.

[2] Private communication with John Walsh and Kevin Felch, 1979.

[3] P.L. Kapitza and P.A.M. Dirac, Proceedings of the Cambridge Philosophical Society, 1933, pp. 297-300.

[4] V.L. Ginzburg and I.M. Frank, Dok. Akad. Nauk. SSSR, 56(1947), 6, pp. 583-586. Translated by E.R. Hope, Defence Research Board, Canada, February, 1954, pp. 12-17.

[5] V.L. Ginzburg, Dok. Akad. Nauk. SSSR, 56(1947), 3, pp.253-254. Translated by E.R. Hope, Defence Research Board, Canada, February, 1954, pp. 8-11.

[6] Motz, op. cit., pp. 527-535.

[7] W.M. Manheimer and E. Ott, Phys. Fluids, 17, 2, pp. 463-473.

[8] R.H. Pantell, G. Soncini, and H.E. Puthoff, IEEE Quant. Elect., QE-4, 11, pp. 905-907.

[9] A. Hasegawa, The Bell System Technical Journal, 57, 8, pp. 3069-3089.

[10] W.H. Louisell, J.F. Lam, D.A. Copeland, and W.B. Colson, Phys. Rev. A, $\underline{19}$, 1, pp. 288-300.

[11] R.M. Phillips, U.S. Patent 3,259,786, July 5, 1966.

[12] R.E. Shefer, K.D. Jacobs, and G. Bekefi, Bull. Am. Phys. Soc., $\underline{24}$, 8, p. 1067.

[13] V.L. Granatstein and P. Sprangle, IEEE Trans. Micro. Theory and Tech., MTT-25, 6, pp. 545-550.

[14] P.C. Efthimion and S.P. Schlesinger, Phys. Rev. A, $\underline{16}$, 2, pp. 633-639.

[15] H. Boehmer, J. Munch, and M. Zales Caponi, Bull. Am. Phys. Soc., $\underline{24}$, 8, p. 1066.

[16] G. Providakes and J.A. Nation, Laboratory of Plasma Studies, Cornell University, LPS 254, August 1978.

[17] D.A.G. Deacon, L.R. Elias, J.M.J. Madey, G.J. Ramian, H.A. Schwettman, and T.I. Smith, Phys. Rev. Lett., $\underline{38}$, 16, pp. 892-894.

[18] I gratefully acknowledge the use of a computer program written by Kevin Felch. The computer program calculates the partially filled waveguide dispersion relation.

[19]James W. Gewartowski and Hugh A Watson, Introduction to Electron Tubes, Van Nostrand Reinhold Company, New York, 1965, p. 334.

[20]Marcelo Alsonso and Edward J. Finn, Fundamental University Physics I and II, Addison-Wesley Publishing Company, Reading, Mass., 1967.

[21]Kenneth Busby, M.A. Thesis, University of Texas at Austin, December, 1975.

[22]J.A. Beaulieu, Proceedings of the IEEE, 59(4), 1971, pp. 667-674.

[23]Geoff Crewe, Honors Thesis, Dartmouth College, 1978.

[24]Herbert Goldstein, Classical Mechanics, Addison-Wesley Publishing Company, Reading, Mass., p. 20.

[25]David L. Book, Naval Research Laboratory Plasma Formulary, first and revised 1978 editions.

[26]Illustrated by Ed Perkins. Original done by Dartmouth Plasma Laboratory Personnel.

[27]Jackson, op. cit., p. 139.

[28]Murray Spiegel, Mathematical Handbook of Formulas and Tables, Schaum's Outline Series, McGraw-Hill Book Company, New York, 1968, pp. 136-141.

[29]C.R. Wylie, Jr., Advanced Engineering Mathematics, third edition, McGraw-Hill Book company, New York, pp. 161-195.

[30]Spiegel, op. cit., p. 132.

[31]William Case, Private Communication, 1979.

[32]Jackson, op. cit., p. 261.

[33]Krall and Trivelpiece, Principles of Plasma Physics, McGraw-Hill Book Company, 1973, p. 85.

[34]Book, NRL Plasma Formulary, op. cit.

[35]Jackson, op. cit., pp. 176-179.

[36]Jackson, op. cit., p. 177.

[37]Book, NRL Plasma Formulary, op. cit.

[38]Jackson, op. cit., pp. 178-179.

[39]The circuit was designed by Robert Layman and John Walsh.

[40]The high voltage components were made available to us by Bob Rowe and Carl Olsen of the Stanford Linear Accelerator facility.

[41]Tung-Sol Technical Memorandum.

[42]G. Southworth, Principles and Applications of Waveguide Transmission, Van Nostrand Company, New York, 1950.

[43]Private communication with Jay Hirshfield and Mike Reid, 1980.

[44]Herbert Lashinsky, IRE Transactions On Electron Devices, ED-8, 3, 1961, pp. 185-191.

[45]Francis Chen, Introduction To Plasma Physics, Plenum Press, New York, 1974, pp. 27-31.

[46]Herbert Lashinsky, Ph.D. Thesis, "Cerenkov Radiation At Microwave Frequencies", 1961.

[47]J.R. Pierce, The Bell System Technical Journal, 30, 1951, pp. 825-829.

[48]Granatstein and Sprangle, op. cit., pp. 545-550.

[49]K.L. Felch, K.O. Busby, R.W. Layman, and J.E. Walsh, "Cerenkov and Cerenkov-Raman Masers: Experiments," Physics of Quantum Electronics, Vol. 7.

END

FILMED

4-84

DTIC